NASA CONTRACTOR REPORT

NASA CR-2869

NASA CR-2869

FEASIBILITY INVESTIGATION OF INTEGRATED OPTICS FOURIER TRANSFORM DEVICES

C. M. Verber, D. W. Vahey, V. E. Wood,
R. P. Kenan, and N. F. Hartman

Prepared by
BATTELLE COLUMBUS LABORATORIES
Columbus, Ohio 43201
for Langley Research Center

NATIONAL AERONAUTICS AND SPACE ADMINISTRATION • WASHINGTON D. C. • JULY 1977

1. Report No. NASA CR-2869	2. Government Accession No.	3. Recipien 0061665

4. Title and Subtitle FEASIBILITY INVESTIGATION OF INTEGRATED OPTICS FOURIER TRANSFORM DEVICES	5. Report Date July 1977 6. Performing Organization Code
7. Author(s) C. M. Verber, D. W. Vahey, V. E. Wood, R. P. Kenan, and N. F. Hartman	8. Performing Organization Report No. 10. Work Unit No.
9. Performing Organization Name and Address Battelle Columbus Laboratories 505 King Avenue Columbus, Ohio 43201	11. Contract or Grant No. NAS1-13802 13. Type of Report and Period Covered Final Report 2/10/75 to 9/30/76
12. Sponsoring Agency Name and Address National Aeronautics and Space Administration Langley Research Center Hampton, Virginia	14. Sponsoring Agency Code

15. Supplementary Notes

Langley technical monitor: Marvin E. Beatty III

Final report.

16. Abstract

This program had the dual goals of investigating the feasibility of an integrated optics Fourier-transform device and investigating the ways in which some of NASA's current and projected data-handling problems might be solved by integrated optics techniques. Since the key to Fourier-transform processing is the availability of high-quality lenses, much effort was devoted to the lens problem. The key accomplishments of this part of the program were: 1) production of near-diffraction-limited goedesic lenses in glass waveguides, 2) development of grinding and polishing techniques for the production of geodesic lenses in $LiNbO_3$ waveguides, 3) development of a characterization technique for waveguide lenses, and 4) development of a theory for corrected aspheric geodesic lenses. As a result of this work we conclude that the production of high-quality large-aperture, low f/number geodesic waveguide lenses is possible. In addressing the problem of applicability of integrated optics techniques to NASA data handling problems, we devised a holographic subtraction system which should be capable of rapid on-board preprocessing of a large number of parallel data channels. Experimental verification of some of the principles involved resulted in 1) writing of high-diffraction-efficiency holograms in an iron infused spot in an outdiffused $LiNbO_3$ waveguide, 2) the first demonstration of holographic subtraction in a waveguide hologram, and 3) the first demonstration of holographic writing by guided waves using two-photon absorption. The results thus obtained indicate that there should be no major obstacles toward building the holographic subtraction system.

17. Key Words (Suggested by Author(s)) integrated optics data processing Fourier-transform devices geodesic waveguide lenses holographic subtraction photorefractivity waveguide holograms $LiNbO_3$	18. Distribution Statement Unclassified - Unlimited Subject Category 35

19. Security Classif. (of this report) Unclassified	20. Security Classif. (of this page) Unclassified	21. No. of Pages 115	22. Price* $5.50

*For sale by the National Technical Information Service, Springfield, Virginia 22161

TABLE OF CONTENTS

TABLE OF CONTENTS
(Continued)

TABLE OF CONTENTS
(Continued)

APPENDIX

LIST OF FIGURES

LIST OF FIGURES
(Continued)

LIST OF FIGURES
(Continued)

LIST OF TABLES

FEASIBILITY INVESTIGATION OF INTEGRATED OPTICS FOURIER TRANSFORM DEVICES

C. M. Verber, D. W. Vahey, V. E. Wood,
R. P. Kenan, and N. F. Hartman

Battelle-Columbus Laboratories

SUMMARY

This program had the dual goals of investigating the feasibility of an integrated optics Fourier-transform device and investigating the ways in which some of NASA's current and projected data-handling problems might be solved by integrated optics techniques. Since the key to Fourier-transform processing is the availability of high-quality lenses, much effort was devoted to the lens problem. The key accomplishments of this part of the program were

- Production of near-diffraction-limited geodesic lenses in glass waveguides.
- Development of grinding and polishing techniques for the production of geodesic lenses in $LiNbO_3$ waveguides.
- Development of a characterization technique for waveguide lenses.
- Development of a theory for corrected aspheric geodesic lenses.

As a result of this work we conclude that the production of high-quality large-aperture, low f/number geodesic waveguide lenses is possible.

In addressing the problem of applicability of integrated optics techniques to NASA data handling problems, we devised a holographic subtraction system which should be capable of rapid on-board preprocessing of a large number of parallel data channels. Experimental verification of some of the principles involved resulted in

- Writing of high-diffraction-efficiency holograms in an iron infused spot in an outdiffused $LiNbO_3$ waveguide.

- The first demonstration of holographic subtraction in a waveguide hologram.
- The first demonstration of holographic writing by guided waves using two-photon absorption.

The results thus obtained indicate that there should be no major obstacles toward building the holographic subtraction system.

I. INTRODUCTION

The goals of this program have been to investigate both experimentally and theoretically the possibility of producing an integrated optics data-processing device based upon Fourier-transform or other parallel-processing techniques, and to study the ways in which devices based upon such techniques may be used to upgrade the performance of present and projected NASA systems. Our studies have particularly addressed the problem of reducing the data transmission, storage and reduction requirements which are becoming increasingly onerous in many of NASA's experimental programs.

The Battelle program initially emphasized the construction of a simple one-dimensional Fourier-transform device utilizing integrated optics technology. As a result of discussions with NASA personnel on possible applications of such integrated optics techniques, it became apparent that it would be particularly desirable to develop a device for screening or preprocessing the parallel outputs of a multichannel instrument such as the Multichannel Ocean Color Sensor (MOCS).(1) Accordingly, Battelle devised a concept for a multichannel data preprocessor based upon holographic subtraction in an optical waveguide. Owing to this development, the program has had several areas of emphasis, each of which will be dealt with in this report. These include

- Consideration of the one-dimensional Fourier-transform problem
- Fabrication and characterization of waveguide lenses
- Consideration of NASA applications for integrated optics data processing devices
- Preliminary experimental and design work on the holographic subtraction device.

As a result of the work performed under this contract several classes of potentially useful integrated optics systems have been identified. In addition, preliminary experimental work has been performed to demonstrate some of the concepts involved in these systems and to explore the necessary fabrication techniques. Particular attention was given to the choice of materials which would be most suitable for NASA's purposes. The requirements imposed by the holographic subtraction process, the data input mechanisms, ease of fabrication and high optical quality resulted in the selection of crystalline lithium niobate ($LiNbO_3$) as the primary candidate for the substrate material.

In Sec. II of this report, we first discuss some of the optical data-processing techniques amenable to the planar integrated optics configuration. We then show how the need for producing a variety of device components compatibly upon a single substrate suggests specific combinations of components and specific choices of materials. Section III contains a discussion of the Fourier-transformation properties of waveguide lenses by way of introducing, in Sec. IV, experimental data on a variety of waveguides and lenses tested in this program. Theoretical results, including a new approach for correcting aberrations in geodesic waveguide lenses, are outlined in Sec. IV and discussed fully in References 33 and 40.

A major portion of this program was directed toward designing systems which would be capable of providing solutions to some of NASA's data handling problems. In Sec. V we present a brief discussion of a Fourier-transform approach to preprocessing spectroscopic data such as that originating from the Carbon Monoxide Pollution Experiment (COPE)(2) in addition to the more extended treatment of a holographic subtraction approach to preprocessing multichannel MOCS - type data. This discussion of the multichannel preprocessor is supplemented in Sec. VI by supporting experimental data on holographic subtraction and calculations on the limitations imposed by superimposing metal electrodes on the waveguide structures. Among the specific accomplishments discussed in this report are

- Fabrication of high quality spherical depressions for geodesic lenses in glass and $LiNbO_3$ waveguides
- Development of techniques for the characterization of waveguide lenses
- Theory of aspheric geodesic lenses

- Preliminary design of integrated optics systems compatible with the MOCS and COPE missions
- First demonstration of holographic subtraction in an optical waveguide.

Certain commercial products are identified in this paper in order to specify adequately which products were investigated in the research effort. In no case does such identification imply recommendation or endorsement of the products by NASA, nor does it imply that the products are necessarily the only ones or the best ones available for the purpose. In many cases equivalent products are available and would probably produce equivalent results.

II. INTEGRATED OPTICAL DATA PROCESSING TECHNIQUES

The majority of coherent optical data-processing systems are described by the diagram of Figure II-1. Amplitude and phase information are imposed on a Gaussian beam of laser light as it passes through the input plane of a typical processor. Lenses, spatial filters, and other optical devices further modulate the beam in such a way that the light distribution in the output plane of the processor indicates the answers to specific questions about the input information. These questions, for example, may have to do with the presence or absence of a certain two-dimensional pattern among a group of patterns located at the input plane, or with small differences between two similar scenes. These two examples are typical but by no means exhaustive of the uses to which researchers in the field have applied coherent optical processing.(3)

In this section, our task is to discuss a modified version of optical processing in which the spatially modulated light wave is no longer a three-dimensional beam but is rather a sheet of light propagating within a few microns of the surface of an optical dielectric waveguide.(4) Because the greater part of the optical energy is confined to the volume of a dielectric, the physical means for introducing and processing information on the sheet of light must necessarily be different than for the conventional case of a light beam propagating in free space. The ultimate success of integrated optical data processing rests upon the successful establishment of these means.

EXAMPLES OF INTEGRATED OPTICAL DATA PROCESSORS

Fourier Transform Processors

To illustrate the kinds of systems under consideration, we show in Figure II-2a an integrated optical Fourier-transform processor to be used in one-dimensional spectrum analysis. The device consists of the following elements:

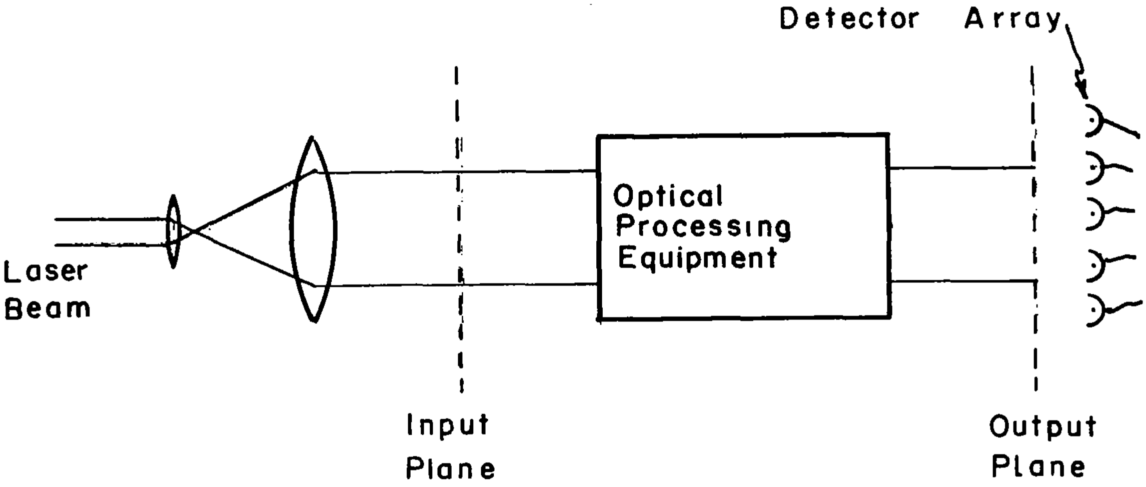

FIGURE II-1. SCHEMATIC DIAGRAM OF A GENERALIZED OPTICAL DATA PROCESSING SYSTEM. OPTICAL PROCESSING EQUIPMENT INCLUDES LENSES, MIRRORS, BEAM SPLITTERS, APERTURES, STOPS, HOLOGRAMS, AND PHOTOGRAPHIC TRANSPARENCIES.

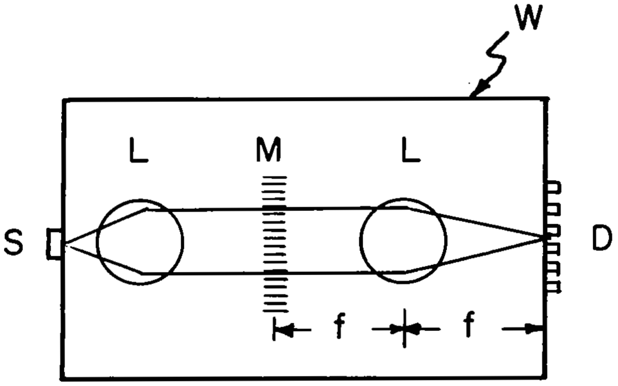

(a) A FOURIER-TRANSFORM PROCESSOR

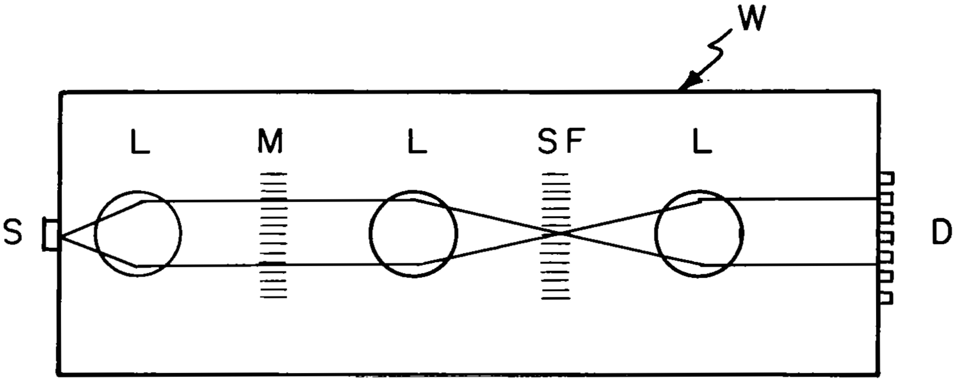

(b) AN OPTICAL CORRELATOR. S = DIODE LASER SOURCE;
L = LENS; M = MODULATOR; D = DETECTOR ARRAY;
SF = SPATIAL FILTER; W = WAVEGUIDE

FIGURE II-2. INTEGRATED OPTICAL PROCESSORS.

(1) An optical dielectric waveguide,

(2) An integrated diode laser source,

(3) A collimating lens,

(4) A modulator for introducing spatial information in a region normal to the propagation direction,

(5) A diffraction limited waveguide lens located one focal length away from the modulator,

(6) A detector array in the back focal plane of the lens for processing information.

A more versatile system, capable of performing optical correlations, is shown in Figure II-2b. The detector array is moved to the image plane of a pair of diffraction-limited waveguide lenses, while a modulator used for spatial filtering is placed in the transform plane. This type of processor is the integrated optical analogue to the three-dimensional processor conventionally used for pattern recognition.(5)

Holographic Subtraction Processors

Another type of processing operation that is useful is the detection of differences between an information input pattern and a prescribed reference pattern. If the differences are small, methods involving spatial filtering in the transform plane of a processor are likely to be insensitive or subject to error. In contrast, the holographic subtraction of input images from a reference image is a difference detection technique that has proven useful in three dimensions.(6) In this technique, spatial filtering is effectively performed in the image plane rather than in the transform plane of a processor.

An integrated optical system designed to perform holographic subtraction of one-dimensional spatial information patterns will be considered at length in Sec. V of this report, in connection with its potential for preprocessing images obtained with NASA's Multichannel Ocean Color Sensor (MOCS)(1). For purposes of the present discussion, we note that the system utilizes the same components as the Fourier-transform processors of Fig. II-2, with the addition of mirrors and beam splitters necessary for the fabrication of an integrated-optical Mach-Zehnder interferometer. Also, the spatial filtering element in this system is required to be a waveguide hologram.

KEY ELEMENTS FOR THE DEVELOPMENT OF INTEGRATED OPTICAL PROCESSORS

The Waveguide

In order for any optical processor to perform at its best, there should be no spurious amplitude or phase distortion of the information-carrying light beam. In three-dimensional processor, the beam usually propagates in still air, a material of such high optical quality that this requirement is often overlooked. In an integrated optical processor, the beam must propagate in a dielectric waveguide. Scattering centers, absorption and refractive-index inhomogeneities distort the amplitude and phase of a guided wave and impair its utility as a carrier of information. The fact that all the components of a processing system can be fabricated on a waveguide chip is no guarantee that the device will function as designed unless the waveguide has a high degree of transparency and spatial uniformity.

The two major classes of planar optical waveguides for integrated optical processors are graded-index guides and thin-film guides. The latter consist of uniform dielectric films about 1 μm thick that are established on substrates of lower refractive index by means such as rf sputtering,(7) epitaxial growth,(8) and solution deposition.(9) Graded-index guides are formed by doping or by perturbing the stoichiometry of a material in the vicinity of its surface. This is usually accomplished by diffusion, effusion, or ion exchange.(10,11) Since the dopant concentration or the stoichiometry varies continuously with depth, the refractive index profile is "graded". This is in contrast to the "step" index profile of thin-film light guides.

Step-index guides have the disadvantage that waveguided light may be scattered by imperfections at both the air-film boundary and the film-substrate interface. Since the latter interface does not exist for a graded-index guide, this type is somewhat easier to fabricate with high optical quality. Waveguides formed in $LiNbO_3$ by Li out-diffusion and by the in-diffusion of various metallic ions are the most often studied graded-index guides.(10,12) Losses in this material are so slight that it is difficult to measure them, but the most common estimate is that they are ≤ 1 dB/cm. Waveguides of only 0.1 dB/cm attenuation may be fabricated in glass by the Ag-ion exchange technique,(11) but some of these waveguides have been observed to deteriorate in time, probably because of chemical reactions involving loosely bound Ag atoms at the surface.

In waveguides formed using thin-film techniques, optical quality depends strongly on the materials and fabrication methods. Losses as low as 0.04 dB/cm have been reported for organo-silicon films,(13) but these guides are suspect for applications because of the prospect of thermal and chemical degradation. Sputtered barium silicate films on microscope slides have shown losses as low as 0.6 dB/cm when care was exercised in substrate preparation.(7) These are clearly candidate waveguides for integrated optical processors, as are epitaxially grown films of ZnO on Al_2O_3(14) and films of $LiNbO_3$ on $LiTaO_3$,(15) which exhibit losses as low as 1 dB/cm.

On the other hand, the epitaxial formation of GaAs and GaAlAs layers has not led to waveguides with attenuations much lower than 4 dB/cm.(15) The reason is that the severe physical conditions under which epitaxy is presently carried out lead to the formation of film-substrate interfaces of poor optical quality. While GaAs is in the forefront of integrated optical materials for communications, owing to the development of miniature electrically pumped lasers in that material,(16) it is not yet suitable for the integrated optical data-processing applications envisioned in this report.

Active Elements for Information Input and Spatial Filtering

Acoustooptic Input Devices

In three-dimensional processors, photographic transparencies and bulk acoustic waves are the devices most often used for imposing phase and amplitude information on a coherent beam of light. Surface acoustic waves are natural candidates for use in modulating waveguided light in integrated optical processors, and considerable work is already underway in this area. Most of it has been done in high quality waveguides of out-diffused $LiNbO_3$, owing to the excellent piezoelectric properties of this material.(17) ZnO thin-film waveguides are also piezoelectric and may be used for integrated acoustooptic processing.(18) The other candidate waveguide for integrated optical processing, sputtered glass film, can be used if the substrate is a piezoelectric material like quartz, or if an acoustic wave is generated in ZnO film and subsequently coupled into the glass guide. The acoustooptic interaction has been studied in several other types of waveguides that are less well known than those we have described.(19,20) It is possible that one or more of these will eventually prove useful for integrated optical processing.

Electrooptic Input Devices

A second means for spatially modulating the phase of a guided wave may be based on the electrooptic effect. To utilize this effect, a series of electrodes is established on the surface of a waveguide directly above and parallel to the path of a guided beam. After the beam passes beneath the electrodes, the curvature of its phase wavefront is linearly related to the electric field pattern induced in the guide by voltages applied to the electrodes. The effect is analogous to that which occurs in a three-dimensional processor when the beam passes through a phase object. The difference is that the phase object in the integrated optical case may be changed in times expected to as short as several nanoseconds by varying the voltages applied to the electrodes. This rapid response capability cannot be achieved in three-dimensional optical processors. Even the speed of acoustooptic devices is limited to the microsecond range by the time it takes sound to traverse a 5 mm wide processing beam.

Both $LiNbO_3$ and ZnO waveguides are electrooptic and information-input devices based on this effect may be fabricated in either material. However, it is difficult to see how a practical electrooptic input device could be designed for use with sputtered-glass thin-film waveguides. Though these have the prerequisite high quality for optical processing, it appears that their utility will be limited to acoustooptic systems.

The choice between electrooptic and acoustooptic input techniques depends on the nature of the processing to be done. Our experience suggests that acoustooptic input devices will be appropriate for one-dimensional spectral analysis, while electrooptic input devices will be appropriate for image-comparison processing.

Spatial Filters and Holograms

The simplest spatial filters are amplitude masks with a spatially varying transmittance of either 0 or 1.(3) In integrated optics these can be fabricated by terminating a waveguide or building an output coupler in regions where 0 transmittance is desired. More complicated spatial filters for use in optical correlation and image comparison require the fabrication of waveguide holograms.(3) One possible way to accomplish this would be to establish a photosensitive film on the surface of a waveguide, and then expose it to the evanescent waves of two interfering guided beams. The difficulty with this technique is that most of the optical energy propagates inside the waveguide and away from the photosensitive material. This results in low writing sensitivities and low diffraction efficiencies.

While this approach is unattractive, it appears to be the best way to perform holography in waveguides such as ZnO and sputtered glass. By good fortune, $LiNbO_3$ differs from these materials in that it is useful for holography as well as integrated optics.(21) We have recorded holograms directly in waveguides of this material without the use of photosensitive overlays.(22) The holograms can be thermally fixed and subsequently thermally erased at a higher temperature.(23) This makes it possible to use the same $LiNbO_3$ processor with a variety of spatial filters and holograms.

One other integrated optical material that has the capability for holography is Ag-ion exchanged or F-outdiffused photochromic glass.(24) Photochromic glass is complimentary to $LiNbO_3$ in that it is used to form amplitude holograms, while $LiNbO_3$ is used to form phase holograms. Traditionally amplitude holograms have been used as spatial filters in the transform plane of optical correlators; however, phase holograms do not absorb light and have the capacity for higher diffraction efficiency.

They appear more useful for integrated optical-processing applications. Apart from this, waveguides of photochromic glass are less versatile than $LiNbO_3$ waveguides because they lack the electrooptic and acoustooptic capabilities, and they can exhibit a loss of optical quality with time.(11)

Passive Elements for Integrated Optical Processing

Waveguide Lenses

The principal component of optical spectrum analyzers and correlators, such as those shown in Figure II-2, is a diffraction-limited lens. The establishment of such lenses in optical waveguides was the principal experimental goal of this program, and our results are discussed extensively in Sec. IV.

Figure II-3 shows three types of waveguide lenses that are candidates for use in integrated optical processor: mode-index lenses,(25,26) Luneburg lenses,(27,28) and geodesic lenses.(29-31) The mode-index variety is most similar to conventional three-dimensional lenses in that focusing is accomplished by refraction at a curved interface between two waveguides. A Luneburg lens is a circular type of mode-index lens in which the mode-index decreases concentrically from its maximum value at lens center to the mode index of the waveguide at the circumference. Geodesic lenses consist of a non-planar waveguide region, usually in the form of a dome or depression, in an otherwise planar waveguide. They accomplish focusing by perturbing the physical path of rays rather than the index of the waveguide through which the rays travel.

Both mode-index and Luneburg lenses may be fabricated by sputtering lens material onto a waveguide through an appropriately shaped mask. To obtain lenses of high power, the refractive index of the lens material should be significantly higher than that of the waveguide mode being focused. Typical combinations have been Nb_2O_5 and ZnS lenses ($n \sim 2.3$) on glass waveguides and substrates ($n \sim 1.5$).(25,27) Care must be taken to minimize scattering losses from mode mismatch as waveguided light enters the high-index lens region. Since the Luneburg lens has a

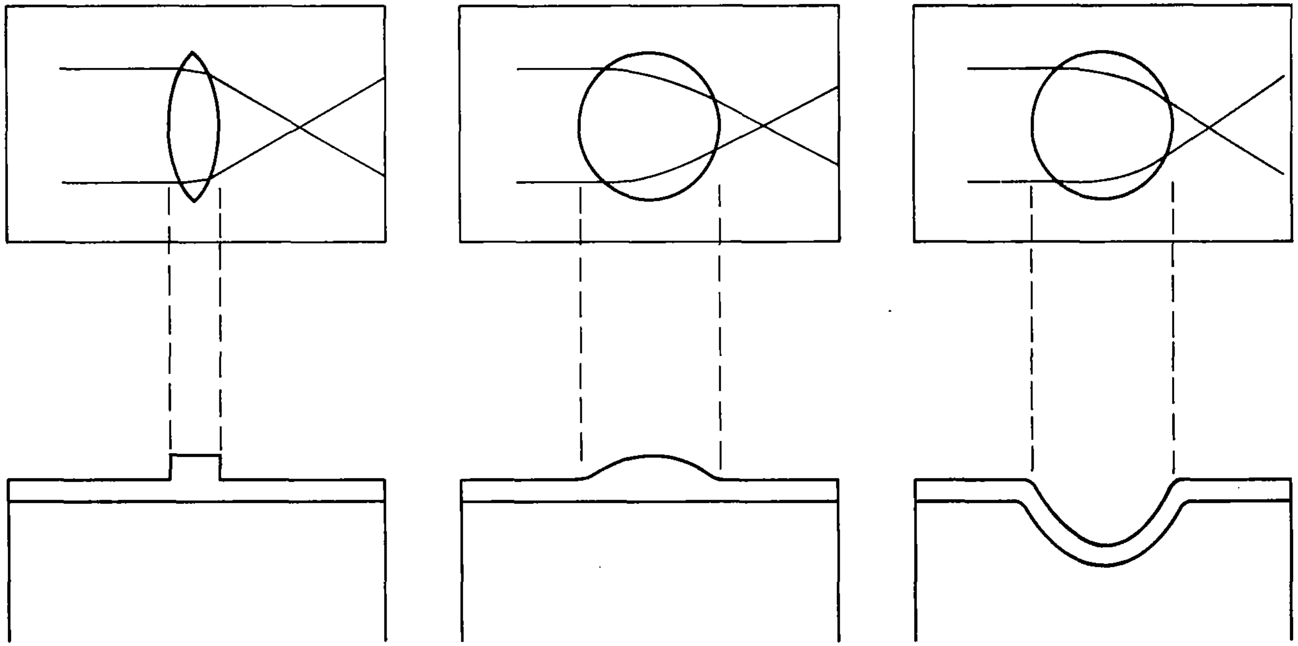

(a) MODE-INDEX LENS (b) LUNEBERG LENS (c) GEODESIC LENS

FIGURE II-3. THREE TYPES OF WAVEGUIDE LENSES.

tapered transition region, its optical quality will generally be superior to that of a sharp-transition mode-index lens.

An inherent disadvantage of these lens types for integrated optical processors is that they require a low-index waveguide, while high quality $LiNbO_3$ and ZnO waveguides have indices of 2.2 and 2.0 respectively. Consequently, lenses of the mode-index or Luneburg variety should be isolated from these waveguides by means such as have been devised by Tien et al,(32) which involve the fabrication of tapered multilayer films. Another complexity is introduced by the requirement that the lens be corrected for spherical aberrations. Any correction scheme would require accurate control of the shape of the mask through which the lens is sputtered, the sputtering rate, and the composition of the sputtered material. Although good quality lenses of the Luneburg and mode index variety have been fabricated,(26,27) no quantitative procedures have yet been presented for elimination of spherical aberrations in these lenses.

In contrast, means have been developed for the correction of paraxial spherical aberrations in geodesic depression lenses,(30) and these lenses are compatible with waveguides of either low or high refractive index. As part of this program,(33) we have considered how corrected geodesic lenses can be fabricated without the need for multiple waveguiding layers in the lens region. With a single waveguide layer, comparable optical quality of the waveguide and the lens regions is virtually assured.

Geodesic lenses appear superior to the Luneburg and mode-index lens for use with integrated optical processors established on sputtered glass and $LiNbO_3$ waveguides. The suitability of geodesic lenses for a processor utilizing a high quality $ZnO\text{-}Al_2O_3$ waveguide(14) has yet to be determined. These waveguides are grown by the method of close-spaced vapor transport, and this method may not be adaptable to the curved surface of a geodesic lens. In this case, transitions from ZnO to sputtered-glass waveguides will probably be required in order to fabricate lenses, and the versatility of this material for integrated optical processing will be limited.

Mirrors and Beam Splitters

In view of the fact that at least one class of integrated optical processors will make use of holograms and holographically formed spatial filters, it will be necessary to develop waveguide mirrors and beamsplitters to generate and interfere the coherent beams required for their fabrication.

The first waveguide mirror that was developed was based on the principle of total internal reflection of guided light.(25) It consisted of a sputtered ZnS film that was abruptly terminated by masking the substrate. The edge that marked the boundary of the waveguide was sufficiently abrupt to reflect waveguided light in accord with the laws of physical optics for three-dimensional beams. The technique for forming mirrors lends itself naturally to sputtered film waveguides, and may be possible for some epitaxially grown film waveguides like $ZnO-Al_2O_3$.

Another alternative is to form a glass waveguide on a crystalline substrate which has been cleaved along the edge which is to reflect light. For example, a wafer of Si may be cleaved and then heat treated to form an SiO_2 layer on its surface. A film may be sputtered onto the SiO_2 to form a waveguide. If the sharp edge of the cleaved Si substrate is preserved in the waveguide, total internal reflection of guided light should be possible.

Another means for fabricating either a mirror or beam splitter is based on the establishment of grooves or ridges in an otherwise planar waveguide. Since these locally perturb the refractive index of the waveguide, they serve to reflect an incident beam of guided light. Beam splitters of this type have been demonstrated in waveguides with a SiO_2-Si substrate.(34) Grooves were established by the method of preferentially etching the Si substrate prior to the fabrication of the waveguiding layers. By making the grooves sufficiently wide, a totally reflecting mirror could be obtained. The researchers suggest that this technique is applicable to other crystalline waveguiding materials, such as $LiNbO_3$, but this has not yet been demonstrated.

An optional procedure for the fabrication of mirrors and beam splitters in $LiNbO_3$ makes use of its holographic properties. Reflection and transmission gratings fabricated by interfering guided waves in this material accomplish the desired functions.(22) While a totally reflecting mirror cannot be obtained in this way, the method is particularly attractive for the fabrication of beam splitters. The reflectivity of grating beam splitters can be adjusted by varying the conditions under which the grating is formed and thermally fixed.

The option of fabricating beam splitters by waveguide holography is not open to other candidate waveguides for integrated optical processing. However, gratings to serve as beam splitters may be fabricated photolithographically in any type of planar waveguide.(35) This technology is well developed since photolithographic gratings are commonly used as beam-to-waveguide couplers.(36)

Conclusions

Table II-1 summarizes the properties and capabilities of the materials that presently appear to have the most potential for use in integrated optical processing. $LiNbO_3$ is the most versatile of the candidate materials and presently offers the greatest prospect for fabricating a complete processing system without resorting to waveguide hybridization. The ZnO and glass materials are complementary in that the former is more useful for fabricating active elements, while the latter is more useful for fabricating passive elements. A hybrid approach involving ZnO and glass waveguides could be employed to fabricate an integrated optical processor; however the holographic capabilities of this system would be questionable. If these capabilities are not required for a particular application, a sputtered-glass film acoustooptic processor is presently feasible.

TABLE II-1. THE CAPABILITIES OF CANDIDATE MATERIALS FOR INTEGRATED OPTICAL PROCESSORS

Material	Waveguide Capabilities	Attenuation	Information Input Capabilities	Holographic Capabilities	Lens Capabilities	Mirror-Beam Splitter Capabilities
$LiNbO_3$	Out-diffused Metal in-diffused Epitaxial thin film	$\leqslant$ 1 dB/cm	Electrooptic Acoustooptic	Photorefractive	Geodesic	Holographic Preferential Etch(?) Photolithographic
ZnO	Epitaxial thin film on Al_2O_3	$\sim$ 1 dB/cm at $\sim$ 1.0 μm	Electrooptic Acoustooptic	None	Geodesic(?) Luneburg(?) Mode-index(?)	Preferential Etch(?) Photolithographic Waveguide Edge
Glass	Sputtered thin film Ag-ion exchange	$\leqslant$ 1 dB/cm $\leqslant$ 1/2 dB/cm initially	Acoustooptic(?)	Photochromic(?)	Geodesic Luneburg Mode index	Preferential Etch Photolithographic Waveguide Edge Cleaving

III. COMMENTS ON ONE-DIMENSIONAL FOURIER TRANSFORM DEVICES

In this section we review the Fourier-transformation properties of conventional lenses and we consider their extension to lenses that are established in an optical waveguide. As an aid to interpreting some of the experimental results of Sec. IV, we present formulas describing the resolving power of waveguide lenses that are both diffraction-limited and spherical-aberration-limited. We also show that light scattering by waveguide inhomogeneities affects resolution and makes it meaningful to define a signal-to-noise ratio for a waveguide-lens processing operation.

THE FOURIER TRANSFORM RELATIONSHIP

The Fourier-transformation properties of lenses have been discussed in many books and articles,(37,38) and we present them here without derivation. Consider a monochromatic plane wave of light incident on a transparency placed in the front focal plane of a diffraction-limited lens, as shown in Fig. III-1. After passing through the transparency the complex amplitude of the plane wave is $\hat{U}_o(x_o,y_o) = A\hat{t}_o(x_o,y_o)$ where A describes the initial amplitude and $\hat{t}_o(x_o,y_o)$ describes amplitude and phase variations imposed on the wave by the transparency. Apart from an unimportant phase factor, the complex amplitude of the wave in the back focal plane of the lens will be(37)

$$\hat{U}_f(x_f,y_f) = (A/if\lambda)\iint_{-\infty}^{\infty} \hat{t}_o(x_o,y_o)e^{-i(2\pi/\lambda f)(x_o x_f + y_o y_f)}\, dx_o dy_o \quad , \tag{III-1}$$

which is just a Fourier transform of the mask function $\hat{t}_o(x_o,y_o)$.

An ideal waveguide lens has no focusing power in the direction normal to the plane of the waveguide; consequently, its focal properties are comparable to those of a cylindrical lens. If the spherical lens of Fig. III-1 is replaced with a cylindrical lens having focusing power in the x direction, and if the input transparency is of the form $\hat{t}_o(x_o)$, the Fourier transform relationship becomes(38)

$$\hat{U}_f(x_f) = (A/\sqrt{if\lambda}) \int_{-\infty}^{\infty} \hat{t}_o(x_o)e^{-i(2\pi/\lambda f)x_o x_f}\, dx_o \quad . \tag{III-2}$$

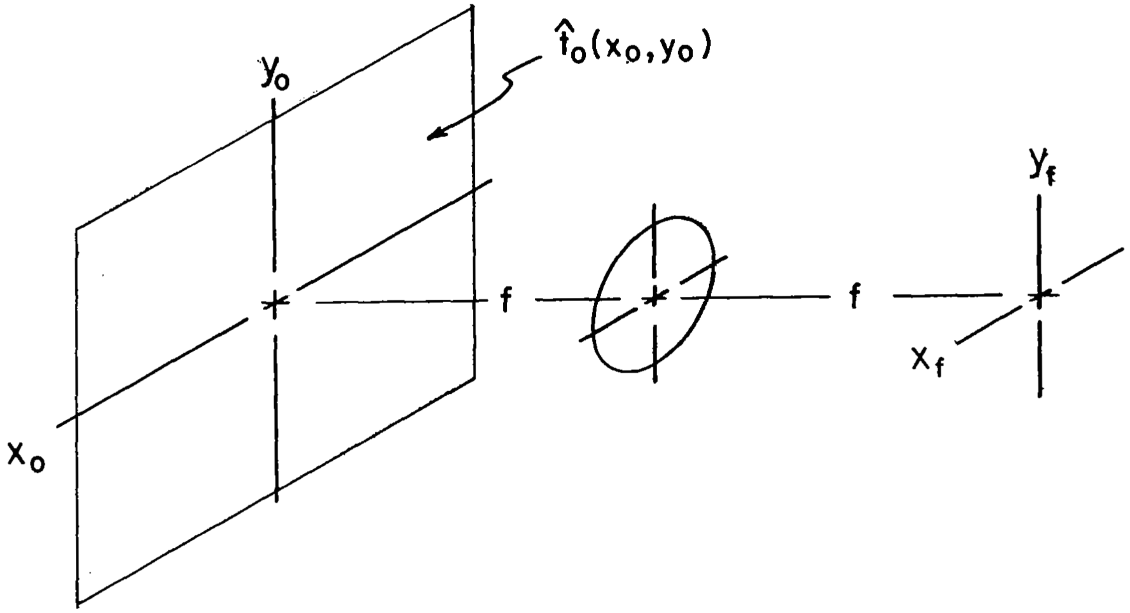

FIGURE III-1. COORDINATE SYSTEM FOR THE DESCRIPTION OF THE FOURIER-TRANSFORM PROPERTIES OF A LENS.

This equation may be applied directly to analyze the performance of an ideal waveguide lens. Figure III-2 shows the geometry of the integrated optical system under consideration and two forms of input "transparencies" that will be of interest.

The Effect of Aperturing

If the beam incident on the waveguide lens is apertured by the function shown in Fig. III-2b,

$$\begin{aligned}\hat{t}_o(x_o) &= \text{rect}\,(x_o/d) = 1 \quad , \quad 0 \le |x_o| \le \tfrac{1}{2}\,d \quad , \\ &= 0 \quad , \text{ otherwise} \quad , \end{aligned} \tag{III-3}$$

the amplitude in the Fourier transform plane will be

$$\hat{U}_f(x_f) = A(d/\sqrt{i\lambda f})\,\text{sinc}\,(\pi x_f d/\lambda f), \tag{III-4}$$

where $\text{sinc}(z) \equiv \sin(z)/z$. The corresponding intensity, $\hat{U}_f\hat{U}_f^*$, is plotted in Fig. III-3a. The characteristic focal spot size s is usually taken as the distance between the first zeros of $\hat{U}_f$:

$$s = 2f\lambda/d \quad . \tag{III-5}$$

The Effect of Amplitude Modulation

If the input transparency is of the form shown in Fig. III-2c,

$$\hat{t}_o(x_o) = \text{rect}(x_o/d)\ (1 + 2a\cos Kx_o) \quad , \tag{III-6}$$

the resultant amplitude in the Fourier transform plane is

$$\begin{aligned}\hat{U}_f(x_f) = A(d/\sqrt{i\lambda f})\ &\{\text{sinc}\,(\pi x_f d/\lambda f) \\ &+ a\ \text{sinc}\ [(K-2\pi x_f/\lambda f)d/2] \\ &+ a\ \text{sinc}\ [(K + 2\pi x_f/\lambda f)d/2]\} \quad . \end{aligned} \tag{III-7}$$

The intensity distribution in the Fourier—transform plane consists of three dominant peaks (see Fig. III-3b). The width of each peak is

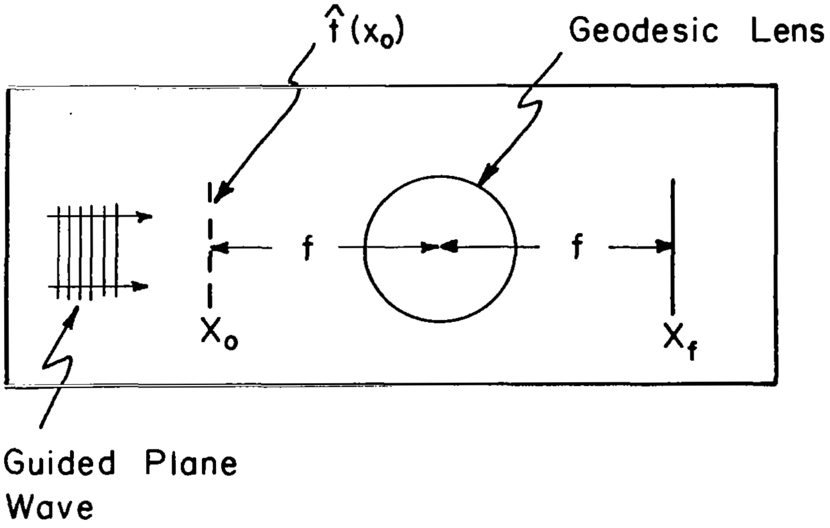

(a) A PLANAR FOURIER TRANSFORM SYSTEM

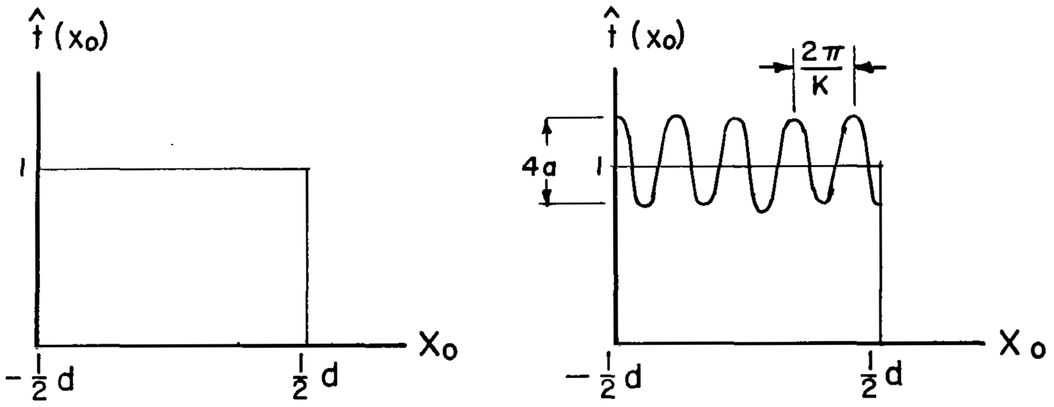

(b) TWO INPUT FUNCTIONS OF INTEREST

FIGURE III-2. INTEGRATED OPTICAL FOURIER TRANSFORMATION OF SIMPLE INPUT FUNCTIONS.

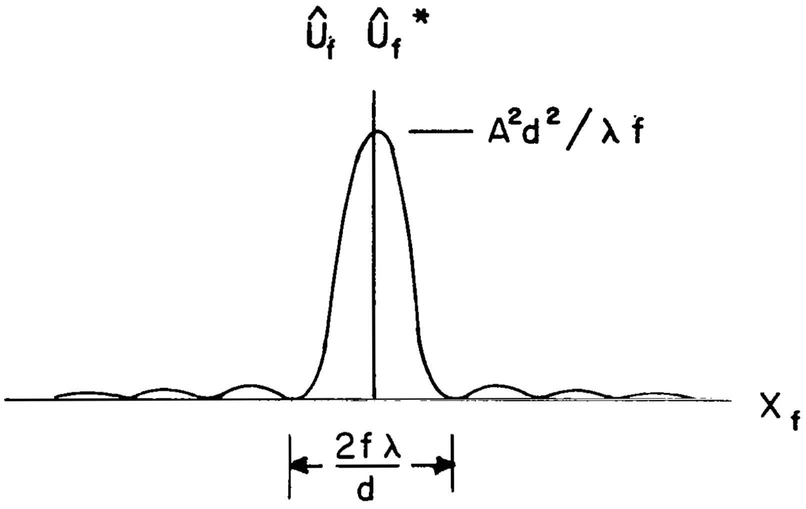

(a) INTENSITY DISTRIBUTION AT THE FOCUS OF A DIFFRACTION-LIMITED WAVEGUIDE LENS STOPPED TO AN APERTURE d

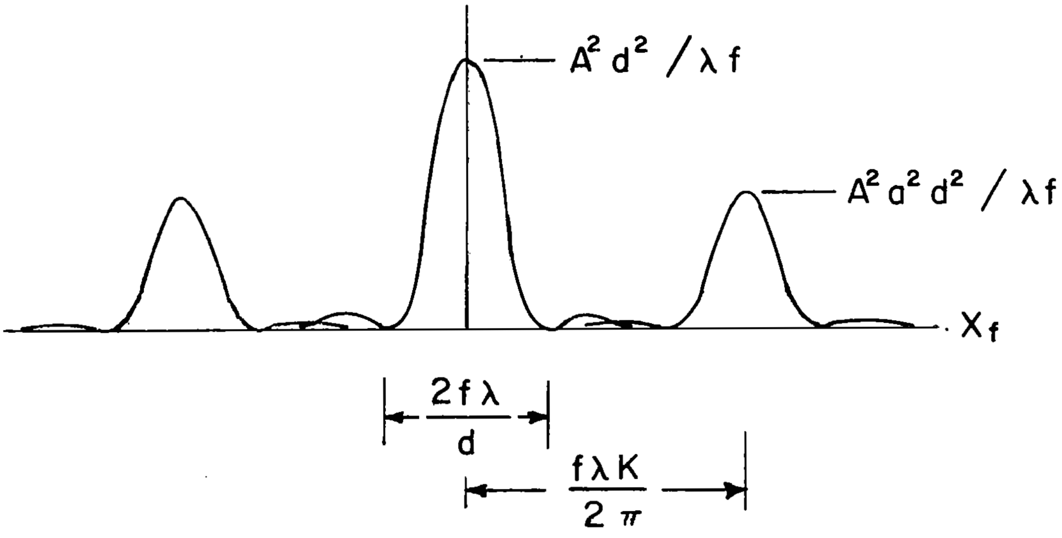

(b) INTENSITY DISTRIBUTION FOR THE CASE OF A SINUSOIDALLY MODULATED AMPLITUDE TRANSPARENCY PLACED OVER THE INPUT APERTURE

FIGURE III-3. RESULTS OF INTEGRATED OPTICAL FOURIER TRANSFORMATION OF SIMPLE INPUT FUNCTIONS.

$s = 2f\lambda/d$, determined by the width of the aperture. The separation between peaks is

$$\Delta x_f = K\lambda f/2\pi \quad , \tag{III-8}$$

determined by the modulation frequency K. When $K = 2\pi/d$, the maximum of each satellite peak falls upon the first zero of the central peak. If the peaks are of comparable magnitude they will be barely resolved. Spatial frequencies smaller than $2\pi/d$ cannot be detected in the back focal plane of the lens. Making d larger is an obvious way to increase resolution, but it will fail unless the lens remains diffraction-limited over the new, larger aperture. If d_{max} is the largest diffraction-limited aperture, $K_{min} = 2\pi/d_{max}$ is the smallest spatial frequency whose Fourier transform may be resolved by the lens.

PRACTICAL LIMITATIONS OF INTEGRATED OPTICAL FOURIER TRANSFORM PROCESSORS

Spherical Aberrations

While means have been presented for the correction of spherical aberrations in waveguide lenses, both as part of this program and elsewhere,(30, 33) the experimental procedures are not yet well enough established to obviate the need for considering the deleterious effects of these aberrations on integrated optical processing. To define what is meant by the term spherical aberration, consider the path of a ray incident on a lens at a distance x from the axis, propagating parallel to it. After being refracted at the lens, the ray crosses the axis at a distance

$$f(x) = f_o + f_1x^2 + f_2x^4 \ldots \tag{III-9}$$

from the lens, where f_o is the paraxial focal length, and f_n is the coefficient of the (2n+1)th-order spherical aberration.(39)

Figure III-4 shows the paths of equispaced, parallel rays incident on a geodesic lens. The trajectories of the output rays are calculated for a lens having third-order spherical aberrations alone, so that only f_o and $f_1 \neq 0$. The envelope of rays determines a minimum focal spot size

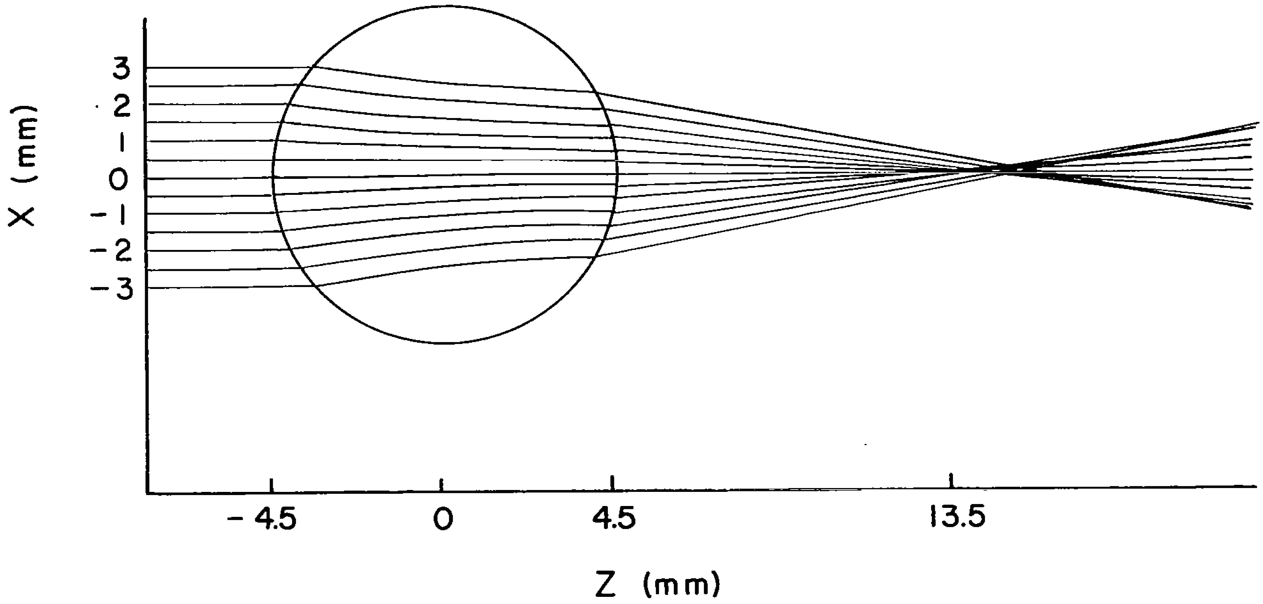

(a) RAY DIAGRAM FOR A GEODESIC LENS WITH THIRD-ORDER SPHERICAL ABERRATIONS

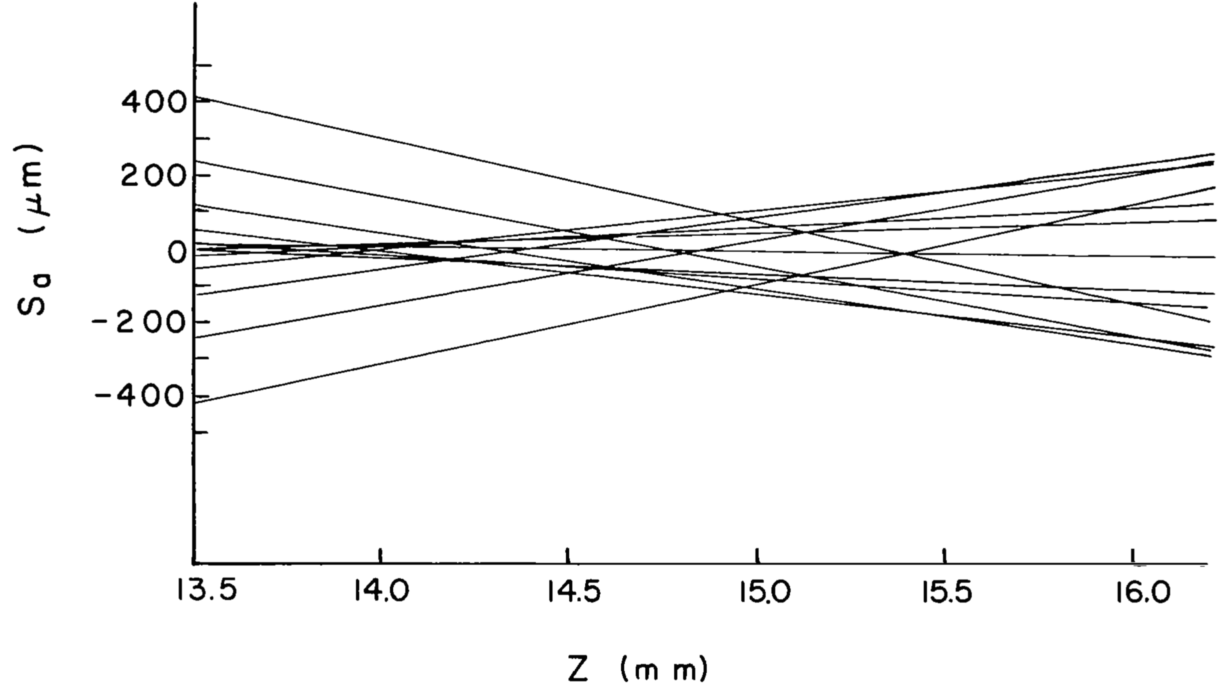

(b) DETAILS OF THE FOCAL REGION

FIGURE III-4. LENS FOCAL CHARACTERISTICS IN THE PRESENCE OF SPHERICAL ABERRATIONS.

given by

$$s_a \simeq f_1 d^3/16f_o \quad , \qquad \text{(III-10)}$$

where d is the full aperture of rays incident on the lens, chosen to be 6 mm in the example plotted in Fig. III-4. Equation (10) is to be compared to Eq. (5) for the spot size s of a diffraction-limited lens. As long as $s_a \leqslant s$, the aberrated lens should exhibit near diffraction-limited performance. This is the case as long as

$$d \leqslant d_{max} = 2(2f_o^2 \lambda/f_1)^{1/4} \quad . \qquad \text{(III-11)}$$

For apertures larger than d_{max} the lens is aberration-limited. Spatial frequencies K introduced on a guided wave in the front focal plane of the lens can only be resolved if

$$K > \pi s_a/f_o\lambda = \pi f_1 d^3/16f_o^2\lambda \quad . \qquad \text{(III-12)}$$

In the numerical example plotted in Fig. III-4, $f_o = 13.7$ mm, $f_1 = 0.2\ \text{mm}^{-1}$, and d = 6 mm. The aberrated spot size is $s_a = 0.2$ mm, compared to $s = 2f_o\lambda/d = 0.002$ mm for a diffraction-limited lens of the same aperture. The wavelength used in the calculation is $\lambda = 0.422$ µm corresponding to the wavelength of red He-Ne laser light propagating in a glass waveguide of refractive index n = 1.5. The ratio $s_a/s = 100$ is characteristic of the relative performance of the two lenses. The diffraction-limited lens can be used to detect spatial frequencies as low as $\sim 1\ \text{mm}^{-1}$, while the aberrated lens is sensitive only to spatial frequencies $\gtrsim 100\ \text{mm}^{-1}$.

The optimum aperture for the aberrated lens of Fig. III-4 is $d_{max} = 1.0$ mm, calculated using Eq. (11). When the lens is stopped to this aperture, its performance is essentially diffraction-limited, and it can detect spatial frequencies as low as $6\ \text{mm}^{-1}$.

Waveguide Inhomogeneities

The presence of scattering centers in a waveguide modulates the amplitude and phase of a guided beam. This modulation is random and is distinct from spatial information that may be purposely introduced on a wave as part of an optical processing operation. To model the limitations that waveguide inhomogeneities impose on the performance of a Fourier transform processor, suppose that their effect on a guided beam is equivalent to that of an input mask of the form

$$\hat{t}_o(x_o) = \{\sum_{i=1}^{N} \mathrm{rect}[(x_o - x_i)/\delta]\}\ \mathrm{rect}(x_o/d). \qquad \text{(III-13)}$$

This function, plotted in Fig. III-5a, is a set of N windows of width δ, randomly spaced at positions x_i in the front focal plane of the waveguide lens. If the lens has no spherical aberrations, the intensity distribution in the Fourier-transform plane is calculated from Eq. (2):

$$\hat{U}_f(x_f)\hat{U}_f^*(x_f) = (A^2\delta^2/\lambda\ f)\quad \mathrm{sinc}^2(\pi x_f\delta/\lambda f)\ \left|\sum_{i=1}^{N} \exp(-2\pi i x_f x_i/\lambda f)\right|^2 \qquad \text{(III-14)}$$

The first factors on the right are simply the Fourier transform of a single window function, centered at $x_f = 0$ and possessing a width $s = 2f\lambda/\delta$. The absolute value factor has the value N^2 for $x_f = 0$, but drops to a value on the order of N for $2\pi x_f \geqslant f\lambda/d$. Consequently, the intensity distribution in the back focal plane is approximately given by the superposition of two sinc-squared functions: one of relative height N^2 and relative width $1/d$; the other of relative height N and relative width $1/\delta$. This is illustrated in Fig. III-5b. The sharp peak corresponds to the focal plane distribution that would result in the absence of waveguide scattering. The broad peak represents, in effect, scattering-induced noise.

The presence of this noise background reduces the ability of the lens to resolve spatial frequencies in the range $2\pi/d \leq K \leq 2\ \pi/\delta$. If the amplitude of a guided wave is modulated according to

$$\hat{t}_o(x_o) = \mathrm{rect}(x_o/d)\ (1 + 2a\cos K\ x), \qquad \text{(III-6)}$$

the peaks produced in the Fourier–transform plane at $x_f = \pm K\lambda f/2\pi$ have an intensity $A^2a^2d^2/\lambda f$. If K is between $2\pi/d$ and $2\pi/\delta$, the intensity of the noise signal at these values of x_f is $\sim A^2N\delta^2/\lambda f$. The condition for a signal-to-noise ratio of unity is $a^2d^2 = N\delta^2$. If the

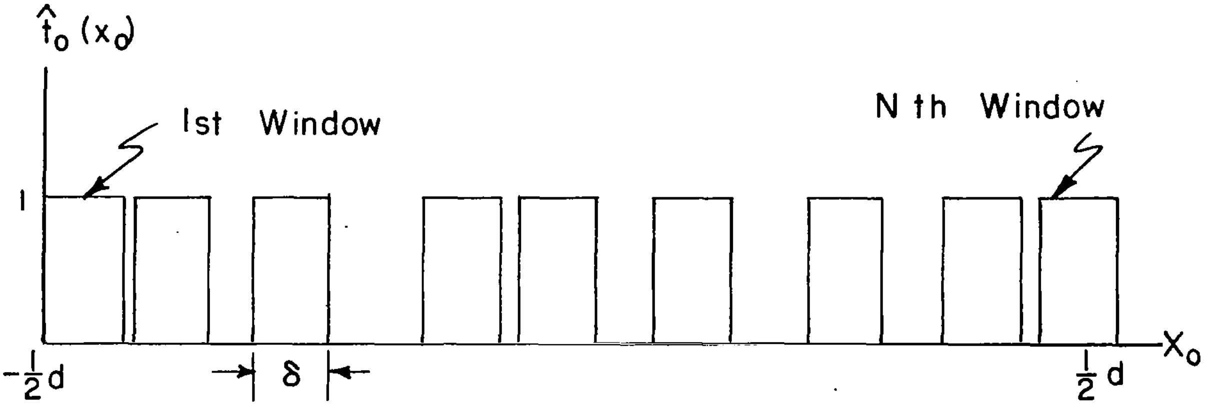

(a) FRONT FOCAL-PLANE TRANSMISSION $\hat{t}(x_o)$ USED TO MODEL WAVEGUIDE SCATTERING

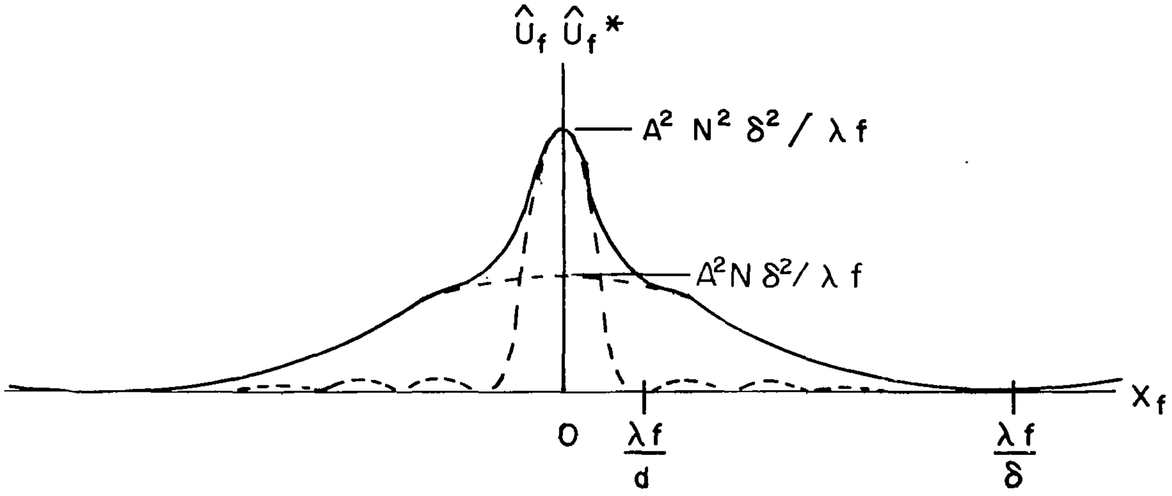

(b) CORRESPONDING BACK-FOCAL-PLANE INTENSITY DISTRIBUTION

FIGURE III-5. THE EFFECT OF SCATTERING ON THE FOCAL CHARACTERISTICS OF A DIFFRACTION-LIMITED WAVEGUIDE LENS.

losses due to scattering are not too severe, we may take $N\delta \simeq d$. In that case

$$a \geqslant 1/\sqrt{N} = \sqrt{\delta/d} \qquad \text{(III-15)}$$

is the condition for resolving sidebands in the range $2\pi/d \le 2\pi/\delta$.

Conclusions

Table III-1 presents formulas that summarize the main results of the present section. The deleterious effects of spherical aberrations are much the same for a waveguide lens as for a conventional three dimensional lens, and our discussion of these has been largely a review. In contrast, the harmful effects of scattering in the waveguide medium are largely unique to integrated optical processors. Calculations presented in this section show the interesting result that a diffraction-limited lens fabricated on a waveguide of poor optical quality may be inferior to a spherically aberrated lens fabricated on a high quality waveguide. This emphasizes the need for care in selecting materials for use in integrated optical processors, as well as care in selecting fabrication techniques that minimize the introduction of scattering inhomogeneities.

TABLE III-1. PERFORMANCE CAPABILITIES OF WAVEGUIDE LENSES

Lens Characteristics	Diffraction Limited	Aberration Limited	Scattering Limited
Focal spot size s	$2f\lambda/d$	$f_1d^3/16f_o$	$2f\lambda/\delta$
Minimum spatial frequency K	$2\pi/d$	$\pi f_1d^3/16f_o{}^2\lambda$	$2\pi/d$ or $2\pi/\delta$
Minimum amplitude modulation a	~ 0	~ 0	$\sqrt{\delta/d}$

IV. EXPERIMENTAL AND THEORETICAL INVESTIGATIONS OF THE FEASIBILITY OF AN INTEGRATED OPTICAL FOURIER-TRANSFORM DEVICE

This section describes the development of fabrication techniques for a prototype integrated optical Fourier-transform processor, consisting of a waveguide, an integrated lens, and an information input device. Because the development of waveguides and modulating devices for information input has been the subject of hundreds of papers in the nine years since integrated optics began in earnest, we concentrated our efforts on the fabrication of high quality waveguide lenses. Only six important papers describe work in this area between 1971 and 1975.(25-30) The present program has led to three additional papers.(31,33,40)

The major results to be described in this section are as follows:

(1) Development of the first experimental technique for quantitatively evaluating the performance of waveguide lenses.

(2) The observation of near diffraction-limited performance by a geodesic depression lens formed in an ion-exchanged Pyrex glass waveguide.

(3) The resolution of spatial frequencies as small as 50 mm^{-1} by a geodesic depression lens formed in an ion-exchanged Photobrown^{TM} waveguide.

(4) Development of techniques for the fabrication of depressions in $LiNbO_3$ waveguides.

(5) Theoretical evaluation of the effect of rim rounding on the performance of a spherical geodesic depression lens.

(6) Theoretical development of procedures for correction of spherical aberrations in geodesic lenses by means of aspheric shaping.

In addition to discussing the above accomplishments, we present in this section a discussion of several types of waveguide and, more importantly, a description of techniques used in the construction of high-quality $LiNbO_3$ waveguides. Some of the material on $LiNbO_3$ waveguides was obtained in connection with other integrated optics programs at the Battelle Columbus Laboratories(41,42) and is presented here for the sake of completeness.

WAVEGUIDE AND GEODESIC LENS FABRICATION PROCEDURES

Waveguides for Geodesic Lenses

The decision to fabricate waveguide lenses of the geodesic variety was arrived at early in the program on the basis of considerations enumerated in Sec. II. In contrast, as many as four different types of waveguides were examined during the course of the program. These were (a) polystyrene thin films solution-deposited on PMMA substrates,(43) (b) Corning 7059 glass sputtered on fused quartz substrates,(44) (c) Ag-ion exchanged graded-index guides in various kinds of glass,(11,24) and (d) out-diffused graded-index guides in $LiNbO_3$.(10,12) While only sputtered glass and $LiNbO_3$ waveguides are definite candidates for integrated optical processor applications, the other waveguides examined offered potential advantages in economy and ease of fabrication. These were important considerations for a program designed to establish feasibility, since it was desirable to be able to test and compare a large number of samples.

Polystyrene and Sputtered-Glass Thin-Film Waveguides(43,44)

Initial attempts to fabricate geodesic lenses were performed using Polystyrene-on-PMMA waveguides and sputtered-glass-on-fused-quartz waveguides. The former was chosen because of the softness of the substrate material. It was hoped that a spherical depression could be easily fabricated in PMMA by heating the polymer to its softening point (~ 100°C) and depressing a steel ball bearing into the surface to deform it into the required shape. Sputtered-glass films were selected for experimentation because they are candidate waveguides for integrated acoustooptic processors, and because a geodesic lens had previously been fabricated and corrected in this type of waveguide.(30)

Our attempts to press depressions into softened PMMA were unsuccessful for two reasons. First, the material tended to bunch at the rim of the depression; second, the forces applied to deform the material generated fracture lines at the base of the depression. Although we were able to obtain good quality films of polystyrene on flat substrates of PMMA by solution deposition, the development of a vapor deposition technique was seen to be necessary in order to form a uniform film in the vicinity of a depression lens. The actual and potential problems with the polystyrene-PMMA system led us to abandon further consideration of it.

In the case of sputtered-glass waveguide lenses, depressions could be fabricated by the abrasive grinding and polishing techniques described below. Moreover, the sputtering operation was known to lead to uniform films as long as certain elementary precautions were taken. The problem that we encountered with this material was that of fabricating waveguides of good optical quality. In a sampling of seven different waveguides formed by sputtering Corning 7059 glass on fused quartz substrates, the typical result was that shown in Fig. IV-1. A beam of light coupled into the film was attenuated in about a centimeter. Only one waveguide showed losses sufficiently low that the beam was visible across the entire surface. Yet this is a requirement for testing and evaluating a geodesic lens having a focal length comparable to the surface dimensions.

Since a sputtered film cannot readily be removed from a substrate, the work done to fabricate a highly polished lens depression is wasted if a poor quality film is subsequently sputtered onto it. Our initial success ratio of 1/7 showed the need for considerable effort in the development of sputtering techniques before a lens evaluation program could be based upon this method. Since other waveguide fabrication techniques were available and readily implemented, we terminated our work in this direction.

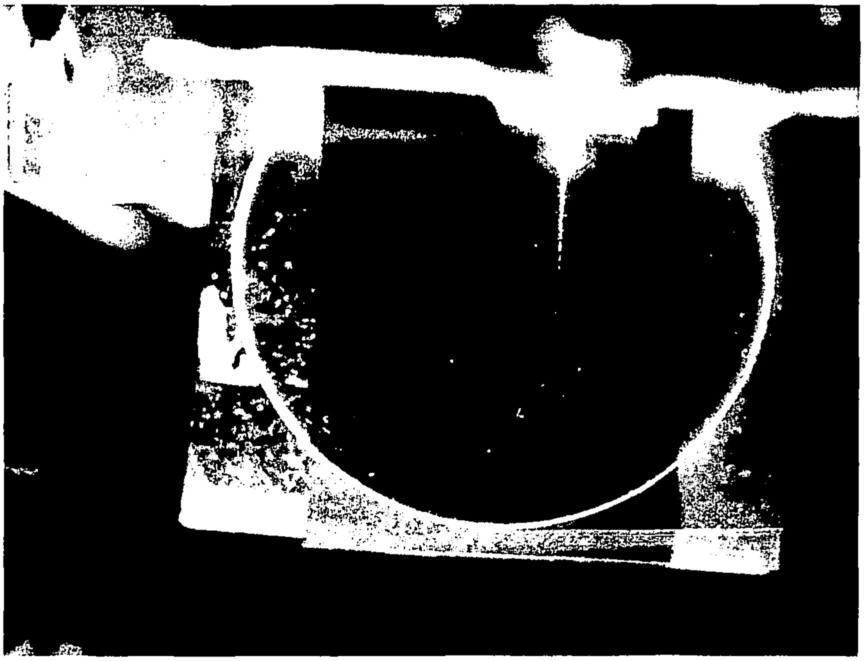

FIGURE IV-1. A SPUTTERED CORNING 7059 GLASS WAVEGUIDE ON A 5.08 cm (2 inch) DIAMETER FUSED-QUARTZ SUBSTRATE SHOWING A HIGHLY ATTENUATED GUIDED WAVE.

Glass Waveguides Formed by Silver-Ion Exchange (11,24)

Graded-index waveguides are formed by immersing a polished glass slab in molten $AgNO_3$ for times ranging from several minutes to one day at temperatures in the vicinity of 225°C - 275°C. Under these conditions, silver ions diffuse into the glass surface to replace sodium ions that diffuse into the molten salt. Only glasses that lack sodium, potassium, or some other relatively mobile ion cannot be employed with this technique.

Waveguides formed by silver-sodium ion exchange were found to be ideal for a geodesic lens testing program for the following reasons:

(1) The waveguides exhibit low losses ($\leq$ 0.5 dB/cm). At the same time, there can be sufficient surface scattering to permit visual observation and photography of the guided light.

(2) The success ratio in the fabrication of high quality waveguides is essentially unity, even in the absence of previous training.

(3) The method is rapid and economical. The minimum requirements are a microscope slide, hot plate, and enough $AgNO_3$ crystals to cover the bottom of a petri dish.

(4) The method is reversible. A waveguide may be effectively removed by heating the specimen in air. Thus, a given geodesic lens depression can be tested in conjunction with more than one waveguide.

(5) Geodesic lens depressions fabricated in glass make use of grinding and polishing techniques that have been established and refined over a period of many years.

(6) Glass can be made photochromic, allowing for the introduction of amplitude information in the front focal plane of a waveguide lens.

(7) Masking techniques can be employed in waveguide fabrication. A silver film evaporated through a mask may be employed in place of molten $AgNO_3$. This makes it possible to vary the parameters of a waveguide in the vicinity of a geodesic lens, a technique that has been employed for lens correction.(30)

The chief disadvantage of glass waveguides formed by silver-sodium ion-exchange is that their optical quality has been observed to deteriorate in time. This has been attributed to chemical reactions involving loosely bound silver atoms.(11) We have found that the quality of of our waveguides could always be restored by immersing them in diluted nitric acid for a moment. Consequently, the effect was not deleterious to our experiments.

Figure IV-2 shows the quality attained with only the second waveguide we fabricated by the ion-exchange technique. The beam is confined to a microslide that was treated in molten $AgNO_3$ for 10 h at ~ 250°C. The guide supported 18 modes, each of which probably consisted of nearly degenerate TE and TM modes. The photograph shows some attenuation of the guided light over its 4.2 cm path. If the total attenuation is estimated at 3 dB, the loss coefficient is 0.7 dB/cm. In our first experiment, a microslide was treated for 8 hours at 300°C, and a waveguide with 37 modes resulted. Guiding was of comparable quality to that shown in Fig. 2.

Since laboratory microslides are too thin to permit the fabrication of depressions for geodesic lenses, we investigated waveguiding in commercially available glasses that could be obtained in thicknesses of 3 mm or more. A problem we encountered was that commercial sheet glass is manufactured using the float technique, in which the glass surface comes into contact with liquid tin. This apparently contaminates the surface and make it unsuitable for the formation of a waveguiding layer. When this contaminant is removed by abrasive grinding, the repolished surface is useful for waveguiding.

We fabricated good waveguides in Pyrex slabs that were first ground and polished. A lens (L2) that was treated at 250°C for 15-1/2 h

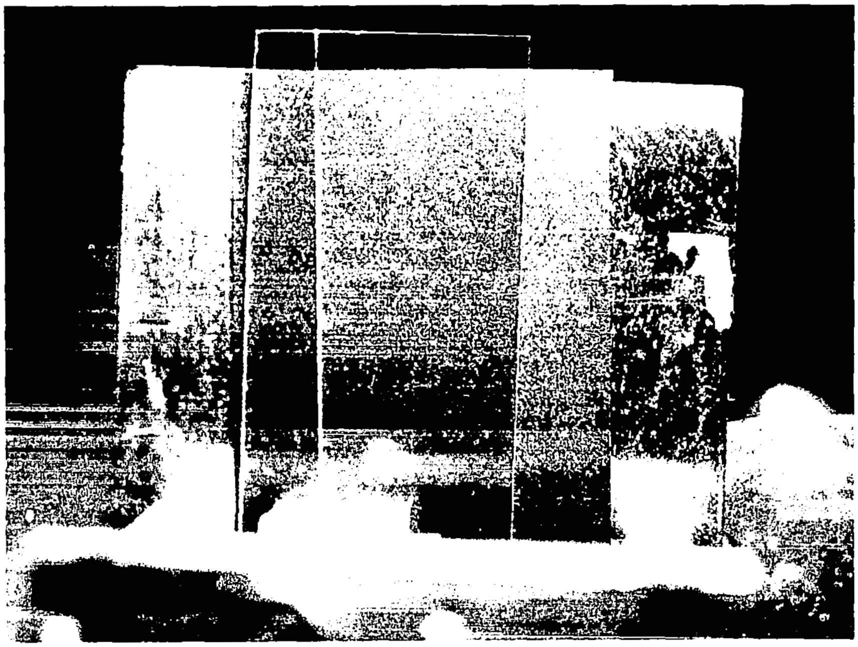

FIGURE IV-2. WAVEGUIDE ON A MICROSCOPE SLIDE FORMED BY ION-EXCHANGE IN MOLTEN SILVER NITRATE FOR 10 HOURS AT 250°C. THE GUIDED WAVE ATTENUATION IS ABOUT 0.7 dB/cm.

showed 3 composite TE-TM modes. This number is markedly lower than would be obtained for a microslide under the same condition because Pyrex has a lower sodium content (~ 4% vs ~ 12%). However, any differences in waveguide quality that resulted from the difference in glass composition were not apparent to the eye.

Other ion-exchange waveguides studied during this program were fabricated in samples of Corning photochromic glass. Two lens blanks of Photogrey™ were obtained commercially, while Nicholas Borrelli and Thomas P. Seward III of the Corning Research Laboratories graciously provided us with other samples. These consisted of Photobrown™ lens blanks and samples from a special melt of highly darkenable glass like that described in Ref. 24.

We found that good quality ion-exchange waveguides were obtained in all varieties of photochromic glass tested. However, there was a somewhat greater concentration of scattering centers in this material than in either Pyrex or microslide glass. The scattering of red light from a He-Ne laser was visible as it propagated through the bulk of the photochromic samples. This effect was not observed for other glasses studied. However, the additional scattering was not sufficient to impair the usefulness of the samples to the program of geodesic lens evaluation.

$LiNbO_3$ Waveguides

The lens testing and evaluation done in this program was performed with glass, rather than $LiNbO_3$, for reasons of convenience and economy. However, the discussion of Sec. II showed $LiNbO_3$ to be the leading candidate waveguide material for integrated optical processors. In accord with its importance, we herein describe the state of the art of waveguide fabrication in this material.

Waveguides may be fabricated in $LiNbO_3$ by a number of techniques,(10) two of which are particularly suitable for the needs of the present program. These two techniques are out-diffusion (or "effusion") of lithium, and in-diffusion ("infusion") of a transition metal.

We have developed a simple procedure for producing out-diffused guides. A Y-(or X-) cut single-crystal plate of $LiNbO_3$ is heated in slowly flowing oxygen (or air) at temperatures generally from 900-1100°C for times varying from a few minutes to several hours, depending on the number of modes and depth of guide desired. This heating drives off lithium, changing the crystal stoichiometry at the surface, and resulting in a region of increased refractive index. $LiNbO_3$ is optically uniaxial, and it happens that it is primarily the extraordinary index n_e that is increased. Waves responding to the ordinary index n_o (TM waves for propagation along the z-axis) are generally not guided. The refractive-index-change profile in effused waveguides has the shape of an integral co-error function,(12) rather than the Gaussian or co-error function shapes ordinarily found in infused guides. Also, the overall index change obtainable is not as large—about 0.004 is a practical maximum. In consequence, an effused guide supporting a given number of modes tends to run somewhat deeper than a corresponding infused guide, a disadvantage when electrooptical modulation is contemplated. On the other hand, guides produced by this method are of excellent optical quality, observable attenuation scarcely ever occurring. This, and the ease of fabrication, are strong arguments for using effused guides when possible.

Infusion of any of a wide variety of transition-metal ions(10) from a metal film deposited on the crystal surface produces regions of increased index capable of supporting both TE and TM modes. Titanium is widely used as a diffusing element because it yields a large index increase (up to .04 for TE modes) and because it is known to yield waveguides of good optical quality. Channel waveguides are frequently made by Ti-infusion from a thin ribbon source. Titanium is a very slow diffuser in $LiNbO_3$, but this allows easy control of the diffusion length, so that single-mode guides, for instance, may be readily produced. We have produced a number of planar waveguides by electron-beam-evaporating 10-50 nm thick films of high-purity Ti onto $LiNbO_3$, heating from 3-6 hr in argon at 900-950 C, and cooling in flowing oxygen. The optimum experimental conditions for producing Ti waveguides have not yet been worked out; however, a procedure as above generally gave good quality guides supporting 1-4 modes. The diffusion temperature must be maintained at 900°C or higher to avoid attenuation resulting from formation(45) of small amounts of $LiNb_3O_8$. If the initial Ti layer is too thick, a hazy residual surface layer, presumably of TiO_2, causes some attenuation and inhibits effective coupling; sometimes this layer can be successfully polished off, though.

Two characteristics of these waveguides not noted in the published literature are the following:

(1) The guides in some instances show photorefractive behavior (see Sec. VI), as evidenced by the ready formation of a grating by intersecting guided beams. It is not yet known whether this effect is due to the titanium itself or to the accidental introduction of some impurity.

(2) During the infusion process, some lithium does tend to evaporate from the crystal, tending to form an effused guide superimposed on the infused guide. This complicates the TE modes, and makes use of TM modes generally preferable. Of course, in devices where it is possible to propagate the light substantially parallel to the optic axis, the effused-guide effect will not occur.

Fabrication of Depressions for Geodesic Waveguide Lenses in Glass and in $LiNbO_3$

Depressions for geodesic waveguide lenses were fabricated using abrasive grinding and polishing techniques. The steps that were employed varied somewhat according to the nature of the material being worked. $LiNbO_3$ was the most difficult material to polish, Pyrex glass was the easiest, and the photochromics were intermediate to these extremes.

Grinding

The basic procedures for grinding lens depressions were established with Pyrex and used with appropriate modifications throughout the program. A rectangular slab of the material to be ground is centered and positioned normal to the rotation axis of a drill press. The chuck contains a brass rod, the working end of which is hollowed out to accept a steel ball bearing of typical diameter 1.0 - 2.5 cm. To grind a depression, the ball, slab, and rod are brough into contact, a slurry of abrasive grit is applied to the ball-glass interface, and the ball is rotated. Pressure is applied carefully in repeated short intervals until the desired amount of material is removed. The steel ball is held to the brass rod only by friction. Occasionally, the ball is reoriented to limit any asphericity that might be induced in it by the action of the abrasive.

A problem with this system for depression grinding is that the velocity of the abrasive decreases to zero along the rotation axis of the ball. Grit and metal particles from the ball tend to accumulate in the base of the depression, so that the finished surface does not have the uniformly frosted appearance that is desired. This effect can be minimized by repeated flushing of the depression during the grinding process. Some of the nonuniformity can also be removed during subsequent polishing. However, this effect is likely the source of the asphericity that we observed in our lens surfaces.

A modified technique was employed successfully in fabricating a depression in $LiNbO_3$. To implement this technique, a small depression is first machined into the $LiNbO_3$ slab using a lathe and a rounded cutting tool. The depth of the depression is close to that desired for the lens, but the diameter of the rim is much less. The machined slab is placed on the drill press and a steel ball is used with abrasive to enlarge the depression to the required dimensions. Although abrasive accumulates in the base of the depression, this area is not in contact with the ball until the grinding process is virtually completed. The result is an improvement in the uniformity of the ground surface.

The choice of grit to use in grinding a depression does not appear to be critical. 400 grit silicon-carbide-water slurries were used in the fabrication of depressions in Pyrex, while 15 μm - size diamond particles in a paste were used for $LiNbO_3$.

Polishing

The ground depressions have a frosted appearance which is removed by working the surface with successively finer abrasives. For this operation a slab is mounted on a turntable so that the depression can be worked by hand from above. The base of the depression is centered over the axis of the turntable, which is rotated at about 550 rpm. A steel ball of the same size used to grind the depression is placed in the hollowed tip of a truncated cone made by casting epoxy in a small laboratory funnel. The larger end of the truncated cone provides a convenient surface for the craftsman to grip and control the ball. For fine polishing, one or more layers of ~ 150 μm nylon cloth are draped over the ball and secured tightly. The purpose of this cloth is twofold: first, it prevents the steel ball from marring the finish of the surface; second, it rounds the rim of the depression so that waveguided light will encounter no sharp edges as it passes into and out of the finished lens.

As the craftsman polishes the depression surface, he imparts a rocking motion to the cloth-covered ball. This helps to keep abrasive from building up in the base of the depression, and provides a more uniform polish than would otherwise be obtained. After the depression has been taken to a fairly good polish using, for example, 1.5 μm diamond particles, the specimen is removed from the turntable and the flat part of the surface is polished using a soft cloth and the same series of abrasives. Final polishing of the depression region and the flat then conclude the fabrication process.

The optimum choice of abrasive compounds for polishing depends on the material being worked, especially as the final polishing stages are approached. A procedure that worked well for Pyrex made successive use of 600 grit silicon carbide, 305 emery, 1.5-μm diamond, and cerium oxide. In the case of $LiNbO_3$, it was possible to go from 15-μm diamond to 1.5 μm diamond without difficulty. However, various attempts to attain a good quality final polish were only partially successful. Cerium oxide and Glennel gamma alumina galled the surface. The highest quality was obtained with 0.25 μm-diamond particles, but results were variable. A polishing compound called Syton™ HT-30, known to be useful for polishing $LiNbO_3$, was not purchased sufficiently early in the program to be tested.

Owing to the difficulty of attaining a good final polish on $LiNbO_3$, the surface of the depression fabricated in this material had to be worked excessively. As a result, a dimple of about 1 mm diameter developed at the base of the depression. The same effect occurred to a degree in Pyrex glass lenses. Since the polishing operation took less time in glass, the dimples were not as pronounced; however, their dimensions of 1/2-1 mm diameter were comparable to the diameter of the dimple in $LiNbO_3$. The glass dimples contained circular fracture lines which served to scatter a small amount of waveguided light.

These artifacts are believed to result from our particular method of depression fabrication, in which rapid circular motion is imparted to either the steel ball used for grinding or the sample being polished, but not to both. This causes material at the base of the depression to be removed more slowly than material at the rim, in accord with the low velocity of abrasive particles in that region. The same effect probably causes the overall shape of the depression to be aspherical: spherical depressions are not produced by the methods employed here. However, this will be seen to be a potential advantage for the fabrication of lenses with low spherical aberrations.(33)

A final consideration has to do with the necessity for cleaning and inspecting the depression surface at intervals throughout its fabrication. If the sample is not accurately repositioned in its mount, or if the steel ball is not accurately centered in the depression before force is applied to it, an asymmetric surface will result. Asymmetries are more likely to be introduced in fabrication schemes that rely heavily on human judgment, as ours did. Fortunately, completely automated techniques have been developed by the optics industry for fabricating high quality precision depressions in optical materials. These should be used in the future to obtain the best performance from geodesic waveguide lenses. The potential of this type of lens for integrated optical processing, suggested in Sec. II, is further corroborated by our experience. In view of the problems we encountered with manual fabrication, including dimples and surface asymmetries, the performance we attained from our lenses was outstanding.

EXPERIMENTAL STUDIES OF GEODESIC WAVEGUIDE LENSES

Dependence of Focal Length on Lens Geometry

Figure IV-3 is a photograph of waveguide lenses that were fabricated in glass during the course of this program. The lens at the left was broken before any tests could be performed with it. The smaller lenses at the center of the photograph were fabricated in Pyrex with the aid of a 14.3 mm steel ball like that shown between them. The other two lenses were made in the photochromic glass supplied to us by Corning Research Laboratories. They were ground using a 23.8 mm diameter ball like that shown at the right in the figure.

Table IV-1 shows relevant numerical data for each glass lens tested. These include R_B, the radius of the ball; R_c, the radius of the rim; h, the depth of the depression, and f_o, the focal length for paraxial rays. If the lens depression is known to be spherical, R_c and h determine its radius of curvature,

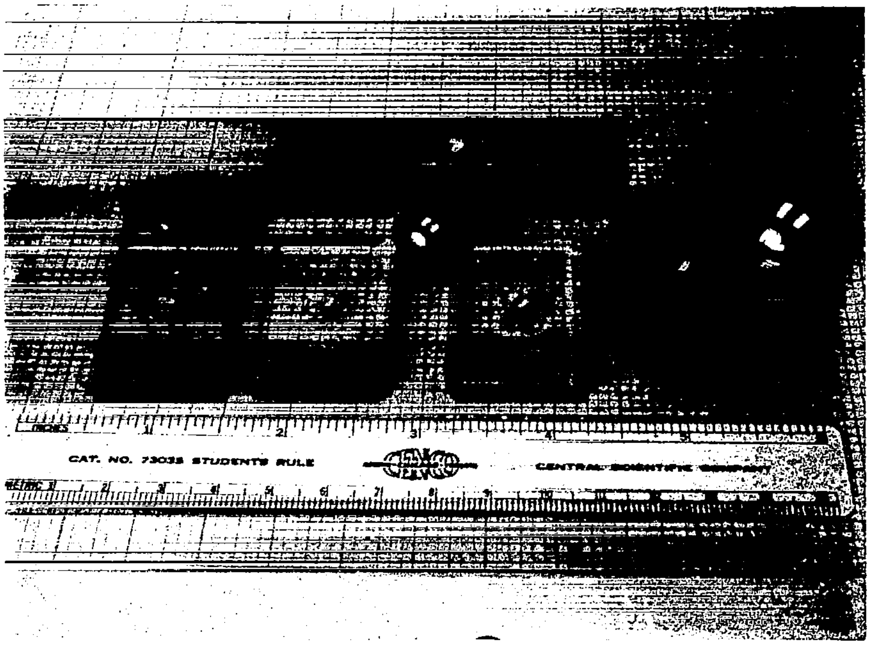

FIGURE IV-3. GEODESIC LENSES FABRICATED IN SILVER-ION-EXCHANGED GLASS WAVEGUIDES.

TABLE IV-1. GEOMETRIC AND FOCAL CHARACTERISTICS OF GEODESIC LENSES IN GLASS WAVEGUIDES. PARAMETERS ARE DEFINED IN THE TEXT AND EVALUATED IN MILLIMETERS

Lens	Material	R_c	h	R_S	R_B	f_o	f_t
L2	Pyrex	4.5	1.41	7.9	7.1	13.6	12.7
L3	Pyrex	4.6	1.35	8.5	7.1	11.3	14.5
L4	Photobrown^{TM}	5.8	1.24	13.9	11.9	28	32.2
L5	Corning melt GGXXI	6.2	1.50	13.4	11.9	~ 27	27.5

$$R_s = (1/2)\ (h + R_c^2/h) \qquad \text{(IV-1)}$$

The theoretically expected paraxial focal length is(30)

$$f_t = (R_c/4)(1 + R_c^2/h^2) \quad . \qquad \text{(IV-2)}$$

Both R_s and f_t are presented in Table IV-1 for comparison with the experimental values R_B and f_o. Measured focal lengths tend to be somewhat different than expected from Eq. (2). Theoretical considerations presented in Ref. (33) suggest that precise fabrication tolerances must be met to obtain lenses having a focal length close to a given value. This is indicated by the results of Fig. IV-4, which shows a profile of the Pyrex lens L2. The experimental points were measured using a microscope in which the horizontal (vertical) displacements of the stage (objective) were calibrated. The curve through the data is a circular arc of radius R_s = 7.932 mm, calculated using Eq. (1) with h = 1.4 mm and R_c = 4.5 mm. The deviation of the data points from the circle is typically 0.05 mm, or about $0.006R_s$. Yet the 13.6 mm focal length measured for the lens is about 1 mm longer than the value calculated from Eq. (2). Automatic fabrication of geodesic lens depressions will be necessary in order to meet the tolerance requirements suggested by these results.

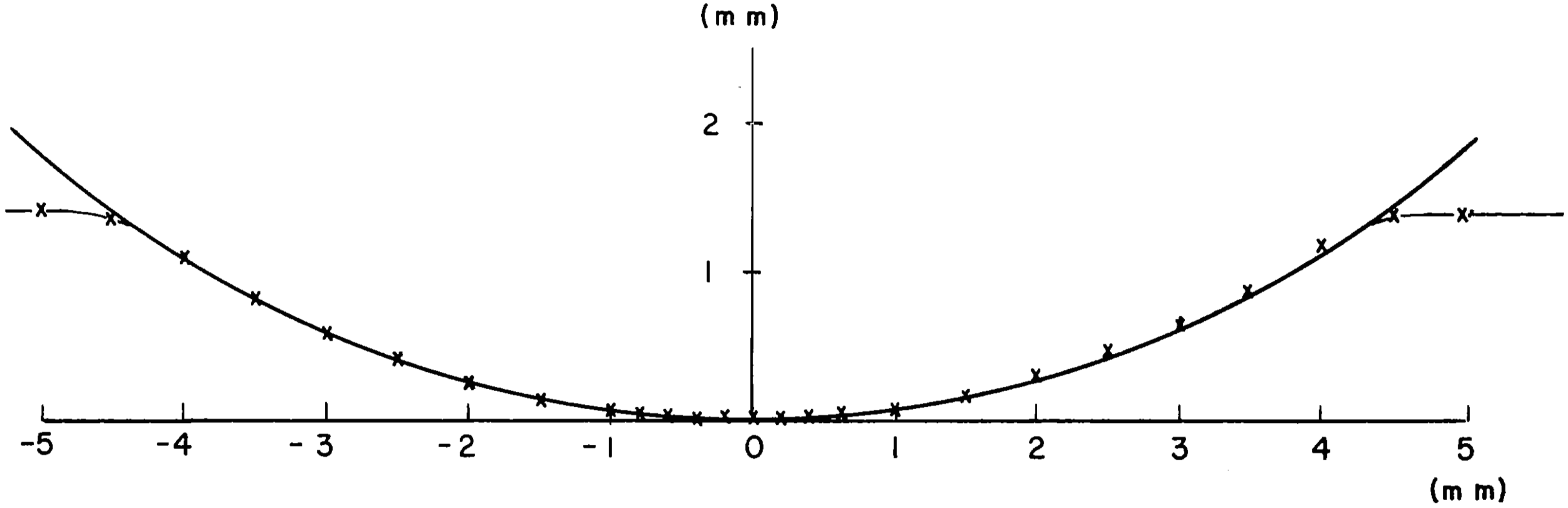

FIGURE IV-4. PROFILE OF THE DEPRESSION OF PYREX LENS L2. CROSSES DESIGNATE EXPERIMENTAL POINTS. THEORETICAL FIT IS AN ARC OF THE CIRCLE HAVING RADIUS R_s = 7.93 mm.

Effects of Spherical Aberrations on Lens Performance

Figure IV-5a shows the performance of the Pyrex lens L2 when five parallel rays are incident on it. The three interior rays apparently intersect at the same point, which is approximately one paraxial focal length from the center of the 9 mm diameter lens. The outer rays, separated by 6 mm, cross the lens axis considerably beyond this point, thus indicating the presence of spherical lens aberrations. The spot size suggested by the confusion of rays is $s_a \simeq 1$ mm.

Figure IV-5b shows the same lens in operation from a somewhat different point of view. A 4.5-mm-wide beam is coupled into the guide and focused, rather than a set of discrete rays. Use of a smaller aperture in this experiment results in a smaller focal spot size, estimated from the photograph to be $s_a \simeq 0.2$ mm.

Photographs such as those shown in Fig. IV-5 are useful for qualitative evaluation of lens performance, but measurements made from them are imprecise for two reasons: (1) photographic film is a nonlinear recording medium, and (2) observed light is that which has been scattered by randomly located inhomogeneities on and within the waveguide, and is not necessarily a true reflection of the intensity of light confined to the waveguide. In fact, to obtain pictures like that of Fig. IV-5b, it was helpful to introduce scattering centers on the waveguide surface in the form of a smeared thumbprint or condensed moisture from a breath of warm air. This viewing technique is less than optimum because the scattering centers degrade the performance of the lens at the same time that they help one to observe it.

For these reasons we devised an experimental technique that made it possible to look at an image of the actual waveguided beam rather than an image of scattered light from the waveguide surface. By detecting this image electronically, rather than photographically, we avoided the problems of film nonlinearity. Figure IV-6 shows a schematic diagram of the experiment. Collimated light from a He-Ne laser is prism-coupled into the waveguide, focused by the geodesic lens, prism-coupled out of the waveguide,

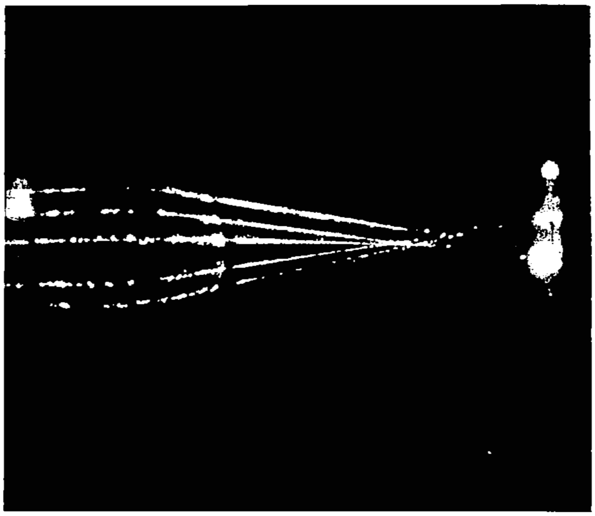

(a) FOCUSING OF FIVE PARALLEL RAYS

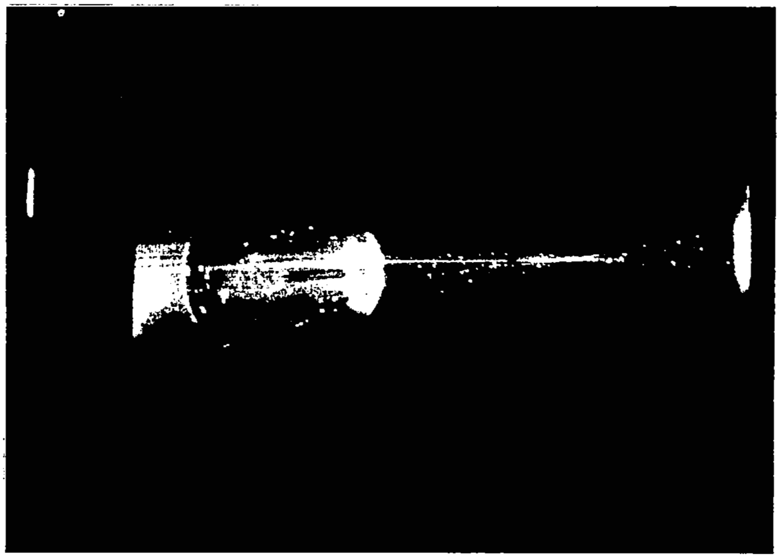

(b) FOCUSING OF A WIDE-APERTURE BEAM

FIGURE IV-5. FOCAL PROPERTIES OF PYREX LENS L2
FROM TWO POINTS OF VIEW.

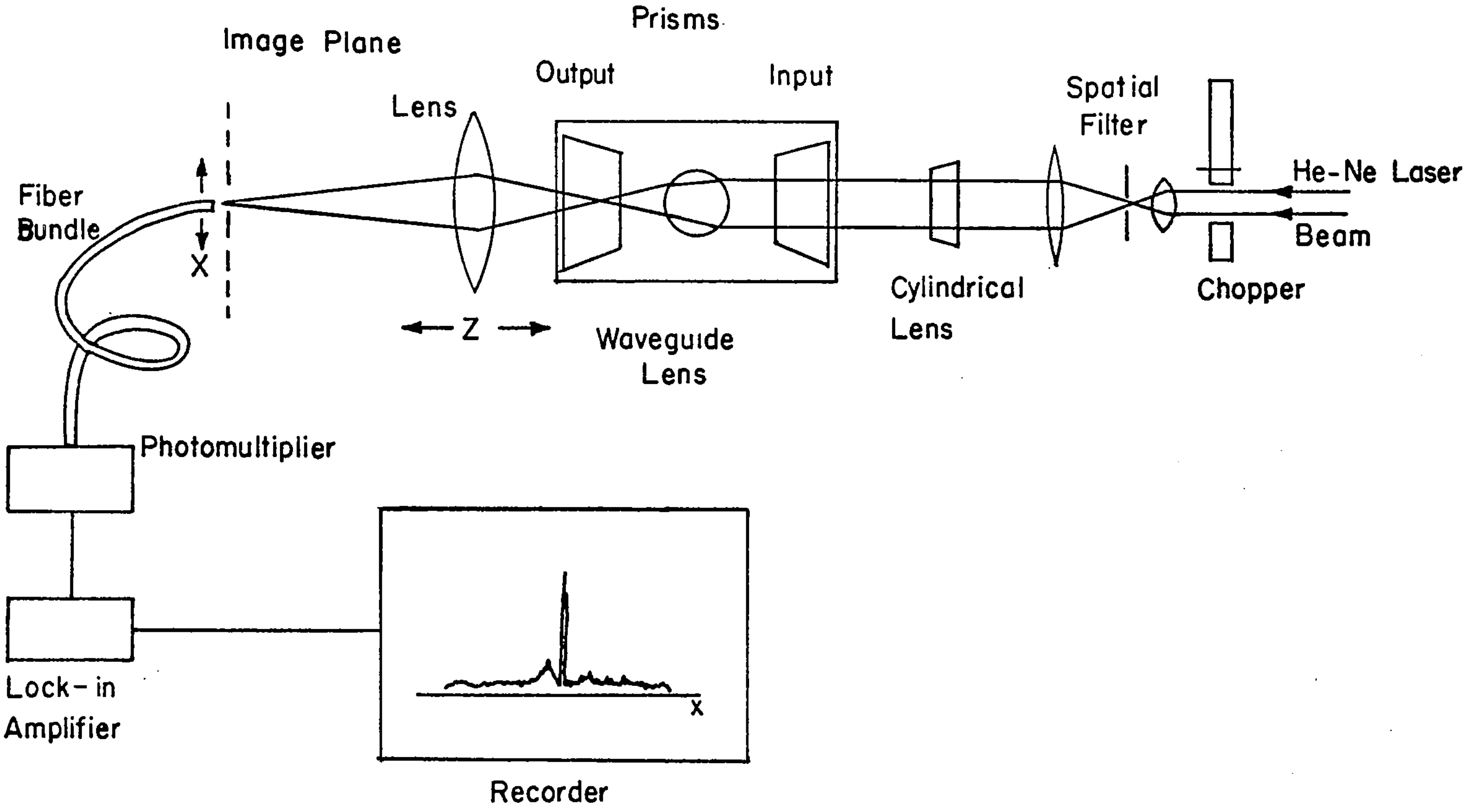

FIGURE IV-6. EXPERIMENTAL CONFIGURATION FOR MEASURING LIGHT INTENSITY IN THE FOCAL REGION OF A WAVEGUIDE LENS.

and passed through a 50 mm, f/3.75 Argus C3 lens. The lens projects a magnified (~ 15X) image of the focal spot at a plane which is scanned by a fiber bundle stopped to an aperture of 25 μm. Light intensity transmitted by the fiber bundle to a photomultiplier is converted to voltage and displayed on a recorder as a function of the fiber-bundle position. Owing to the small size of the aperture over the fiber bundle, the photomultiplier is subjected to low light levels. Consequently, lock-in detection is employed to improve the signal-to-noise ratio.

The recorder output is indicative of the distribution of intensity of waveguided light in a direction x normal to the axis of the geodesic lens. This distance may be calculated from Z, the known position of the camera lens. Figure IV-7 defines the parameters used in the calculation. Refraction at the air-prism and prism-waveguide interfaces is ignored to simplify the figure, but it may be taken into account approximately by converting distances to their optical values after the calculations. In accord with the laws of geometrical optics,

$$z = D_2 + Z - F(D_1 - Z)/(D_1 - Z - F) \qquad \text{(IV-3)}$$

where $F = 5.0$ cm is the focal length of the camera lens. D_1 and D_2 may be adjusted so that the optical distance nz is near the geodesic lens focal length f_o when $Z = 0$. By recording intensity profiles over a range of values of Z, a detailed mapping of light intensity in the focal region of the geodesic lens is obtained. For our system, $D_1 \simeq 80$ cm $\gg D_2$, Z, and F, so that

$$nz \simeq f_o + nZD_1/(D_1 - F) \qquad \text{(IV-4)}$$

Figure IV-8a shows measured intensity profiles obtained for the case of a 5-mm plane wave incident on the Pyrex lens L2. Profiles were taken for five different values of Z that corresponded to distances nz in the range 13.3-15.5 mm from the geodesic lens center. Figure IV-8b presents a ray diagram showing the output set of rays transmitted by the lens for a uniformly spaced input set within the 5-mm entrance aperture, as calculated from the equation

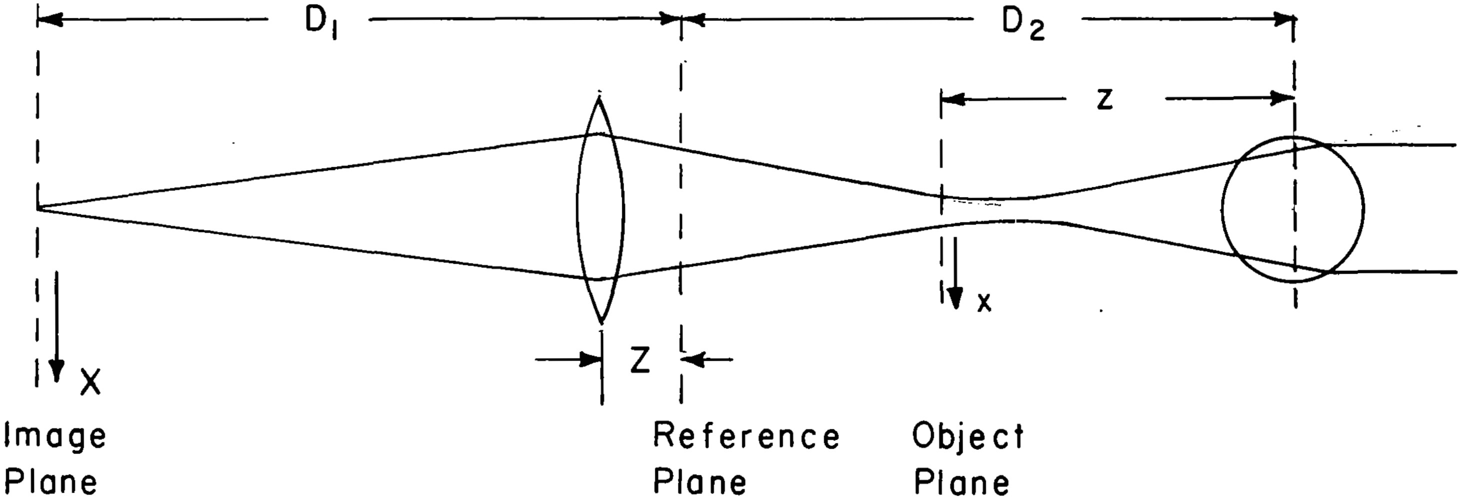

FIGURE IV-7. DETAILS OF THE OPTICAL SYSTEM USED TO IMAGE THE FOCAL REGION OF A WAVEGUIDE LENS.

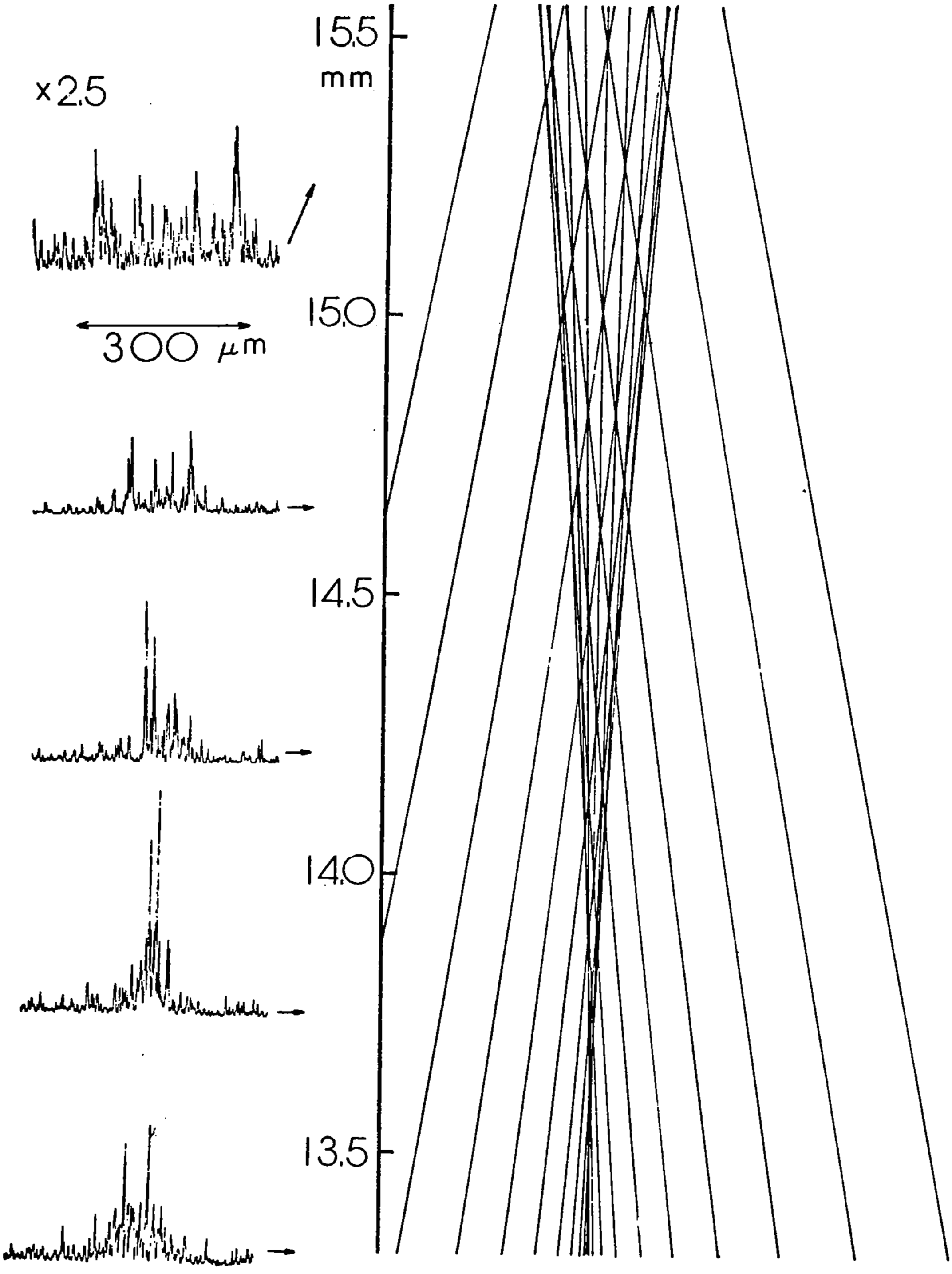

(a) INTENSITY PROFILES (b) RAY DIAGRAM

FIGURE IV-8. EXPERIMENTAL INTENSITY PROFILES AND THEORETICAL RAY DIAGRAM OF THE FOCAL REGION OF PYREX LENS L2.

$$f(x) = f_o + f_1x^2 \quad , \qquad \text{(IV-5)}$$

valid for a lens with third-order spherical aberrations. In these calculations, $f_o = 13.6$ mm and $f_1 = 0.47$ mm^{-1} have been chosen so that the density of rays at a given position correlates with the intensity distribution at that position. The fact that the correlation appears to hold throughout the 2.2 mm depth of the focal region examined suggests the validity of Eq. IV-5. The profiles are generally symmetric about the lens axis, consistent with this equation, except for the profile taken at 14.2 mm from the lens. This asymmetry apparently results from small structural asymmetries in the geodesic lens depression, but why this should affect only one of the focal scans is not presently known.

Figure IV-8a shows a 40-μm-wide high-intensity spot 13.75 mm from the center of the lens. This spot is about 25 times smaller than the total width of the ray envelope at this distance from the lens, indicating that only paraxial rays are contributing to the observed intensity maximum. Focal cross sections taken at 14.7 and 15.5 mm show two widely separated peaks due to the concentration of light energy along the caustics of these paraxial rays.

The fine structure observed in the intensity profiles appears to be associated with the interference pattern set up by intersecting rays. Figure IV-9 shows the results of an experiment designed to check this. In Fig. IV-9a, an intensity profile is obtained for Pyrex lens L3 when input rays are distributed symmetrically about the lens axis over a full aperture of 5 mm. In Fig. IV-9b, rays are blocked from entering the lens above its axis. In the former case, the ray diagram suggests the existence of wavelets entering the focal region from above and intersecting similar wavelets coming up from below. Since the intersecting wavelets are coherent and in general travel different optical path lengths, they are the source of a complicated interference pattern which is resolved in the focal scan. When rays are blocked from above the lens axis, the ray diagram of Fig. IV-9b shows them to intersect less often and at smaller angles. The expected reduction in interference structure is observed experimentally in the

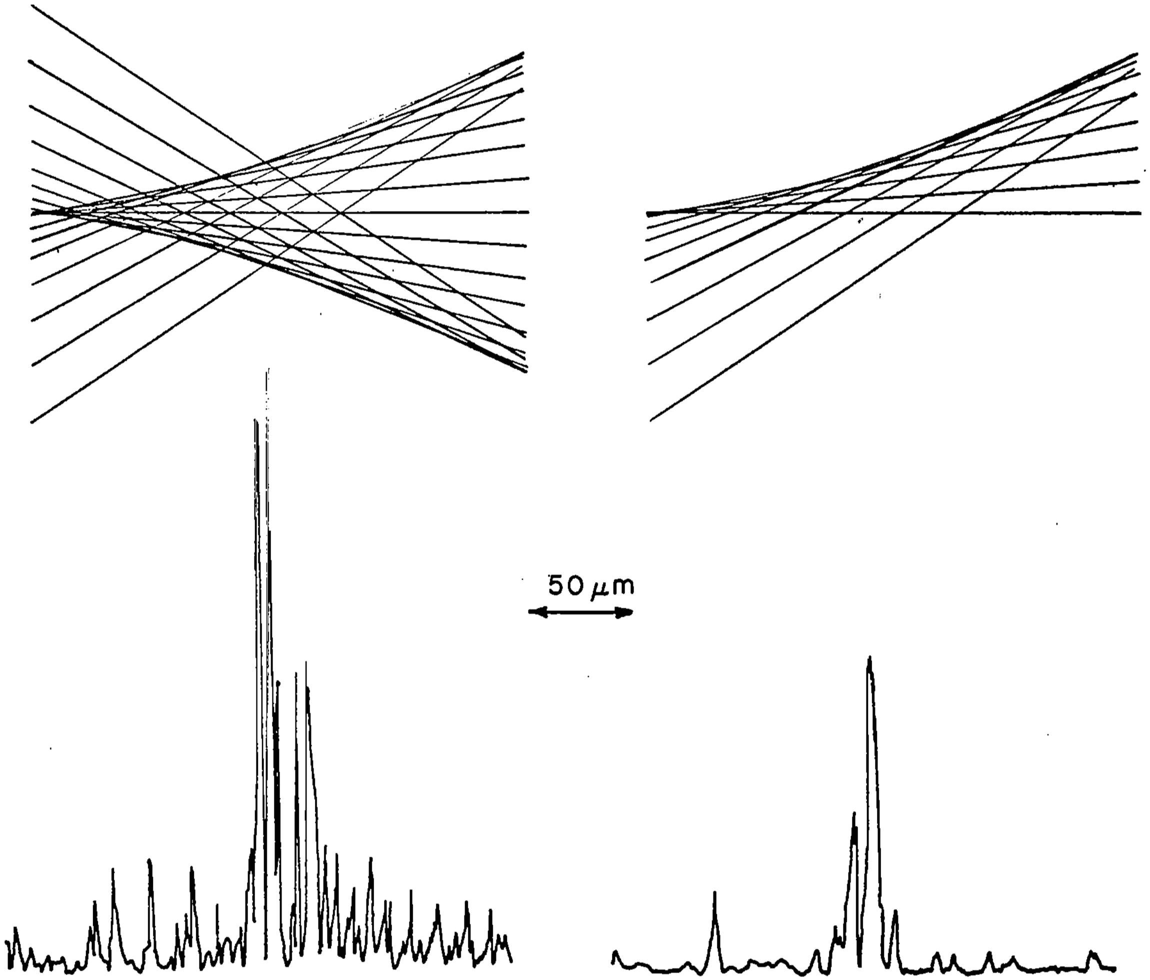

(a) RAYS INCIDENT ON THE LENS SYMMETRICALLY ABOUT ITS AXIS

(b) RAYS INCIDENT ON ONE SIDE OF THE AXIS ONLY

FIGURE IV-9. RAY DIAGRAMS AND INTENSITY PROFILES OF PYREX LENS L3, SHOWING THE CORRELATION BETWEEN RAY CROSSINGS AND FINE STRUCTURE IN THE FOCAL REGION.

corresponding focal scan. However, this effect can not account for the appearance of structure far removed from the lens axis, where rays do not intersect. This structure must be attributed to scattering by waveguide inhomogeneities.

Lens Performance Near the Diffraction Limit

From Sec. III, the focal spot size of a lens with spherical aberrations is $s_a = f_1 d^3/16f_o$, and the maximum aperture over which the lens is diffraction limited is $d_{max} = 2(2f_o{}^2\lambda/f_1)^{1/4}$. As determined from Fig. IV-8 for lens L2, $f_o = 13.6$ mm and $f_1 = 0.47$ mm^{-1}. For light of wavelength $\lambda = 0.633$ µm/1.49, $d_{max} = 1.52$ mm. The corresponding diffraction limited spot size is $s_a = 7.6$ µm.

Figure IV-10 shows the results of a focal scan for Pyrex lens L3, which was fabricated to have properties as close to those of L2 as our techniques could produce. The scan differs from those of Figs. IV-8 and IV-9 in that the input aperture was reduced to the vicinity of a millimeter, as suggested by the above calculations, to determine if lens performance became diffraction-limited. Qualitatively, the reduction in structure in the dominant peak of Fig. IV-10 indicates that rays which arrive at the focal point have traveled equal optical path lengths. This is required for a diffraction-limited lens. Quantitatively, the observed full width at half height of the dominant peak, 8 µm, is slightly larger than the value 4.7 ± 1.0 µm calculated from the diffraction formula $s/2 = f\lambda/d$, where $d = (1.25 \pm 0.25)$ mm in this experiment.

There are a number of physical effects that may account for the observed discrepancy. Even if diffraction is the dominant mechanism affecting focal spot size, spherical aberrations will broaden the focal spot somewhat beyond its minimum diffraction-limited value. Other broadening mechanisms are associated not with the waveguide lens but with the experimental measuring apparatus shown in Fig. IV-6. The 25 µm-diameter pinhole over the fiber bundle, when projected into the object plane of the camera lens, has an effective diameter of 1.6 µm. While this causes

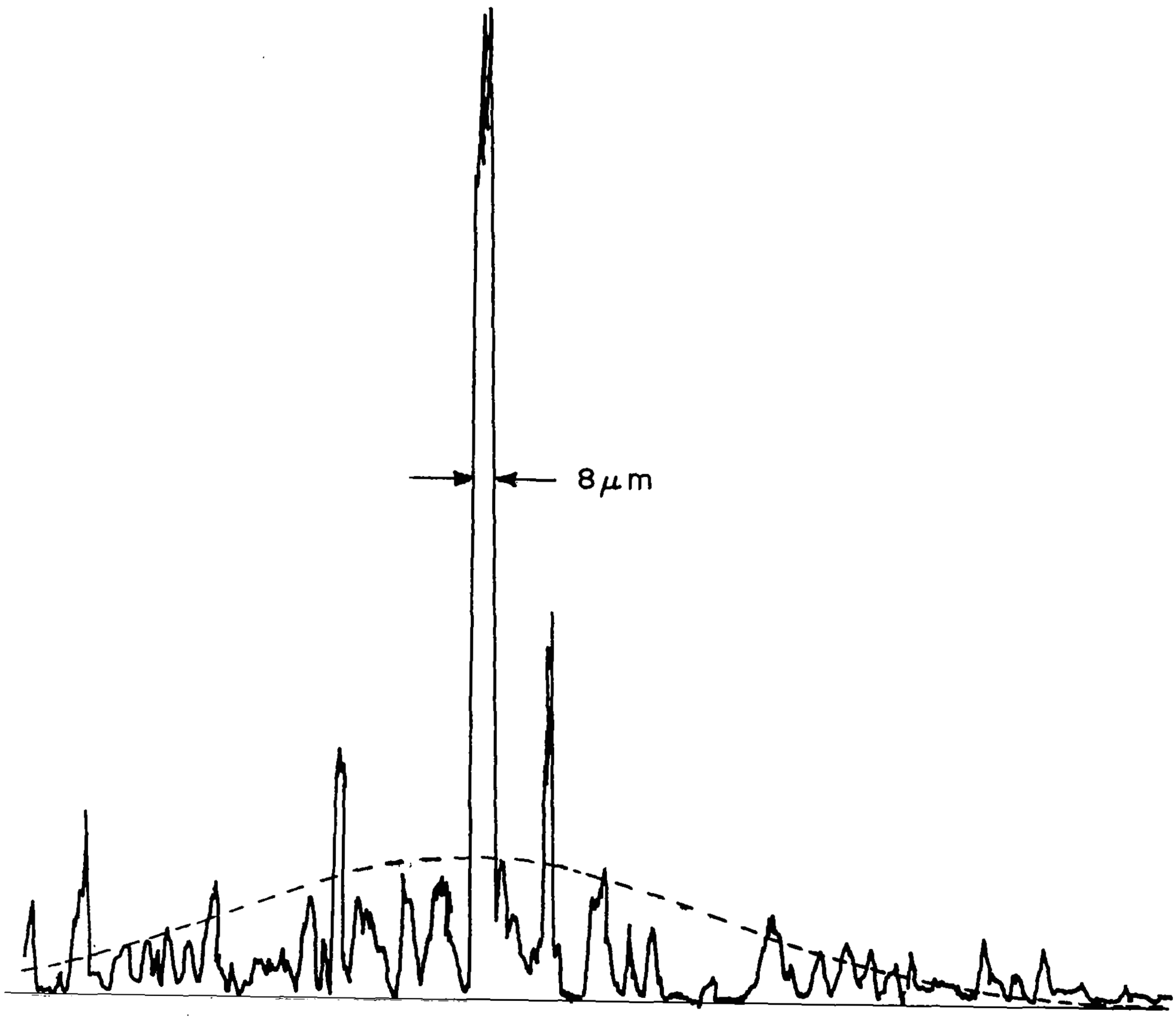

FIGURE IV-10. FOCAL SCAN OF PYREX LENS L2 FOR A 1.25-mm-WIDE INPUT BEAM. DASHED CURVE IS A SINC-SQUARED ENVELOPE FUNCTION DETERMINED BY THE AVERAGE LEVEL OF BACKGROUND SCATTERING.

the observed focal spot to be increased over its actual size, a more significant discrepancy is introduced by diffraction effects in the imaging system. Even if the waveguide lens were able to produce a perfect point focus, the apparent size of the spot as measured in the image plane would be 1.22 $F\lambda/D$, where F/D is the f/number of the camera lens. Taking $F/D = 3.75$ and $\lambda = 0.633\,\mu m$, 1.22 $F\lambda/D = 2.9\,\mu m$. This is very nearly equal to the difference between the measured spot size, 8 μm, and the 4.7 μm value based on diffraction theory. This suggests that the performance of the waveguide lens is virtually diffraction limited.

Effects of Waveguide Scattering on Lens Performance

Figure IV-10 shows, in addition to a dominant central peak, a highly structured background of scattered radiation. The effects of scattering on the focal characteristics of a waveguide lens were considered in Sec. III. The simplified theoretical treatment developed there predicted a narrow diffraction peak superimposed on a broad structureless background. The model used for the calculation was somewhat artificial, since it assumed that all scattering centers were opaque and were located in the front focal plane of the waveguide lens, while the spaces between scattering centers were of equal width. In view of the limitations of this theoretical model, the best use of the experimental data may be made by drawing an approximate envelope function over the background distribution of scattered light in Fig. IV-10, and assuming that the considerations of Sec. III apply to the shape of this envelope. In that case, the height of the envelope shown in Fig. IV-10 relative to the height of the diffraction peak suggests that the effect of waveguide scattering is equivalent to that of $N \simeq 8$ windows in the front focal plane. The width of the envelope relative to the width of the diffraction peak suggests that the size of the windows is $\delta \simeq 0.03\ d$, or about 0.0375 mm. The total transmission of the waveguide from front focal plane to back focal plane (a distance of 27.4 cm) is $N\delta/d = 0.24$, corresponding to an attenuation of 2.26 dB/cm. This is at least twice as large as attenuations typically measured in ion-exchanged glass waveguides, but scattering associated with lens imperfections may account for part of the difference.

Figure IV-11 shows a focal scan obtained using a 28-mm focal length lens fabricated in Photobrown^{TM} glass. This lens appears to be superior to either Pyrex lens with regard to both spherical aberrations and waveguide scattering. The sharpness of the focal peak is especially impressive in view of the fact that the width of the beam being focused was about 6 mm, or slightly more than 50% of the full lens aperture. The 10-μm focal spot size and the 6-mm beam width may be inserted into Eq. 10 to determine the ratio $f_1/f_o = 7.4 \times 10^{-4}$ mm^{-2}. The corresponding ratio for the Pyrex lens L2 was 3.5×10^{-2} mm^{-2}, indicating a 50X reduction in spherical aberrations. Figure 16 also suggests that waveguide scattering is much less in the case of the Photobrown^{TM} lens. The height and width of the background noise is equivalent to that produced by N = 10 windows in the front focal plane, each having an aperture $\delta = 0.4$ mm. The waveguide attenuation calculated from these figures is only 0.3 dB/cm. The dramatic improvement over the results in Pyrex is thought to be due in part to better surface polish and to the fact that the Photobrown lens was precleaned in nitric acid prior to experimentation.

Resolution Capabilities of Geodesic Waveguide Lenses

Figure IV-12 shows the results of a simple resolution test performed using the Pyrex lens L2. In Fig. IV-12a a single 3.5-mm-wide beam is focused by the lens. Experimental conditions are similar for Fig. IV-12b except that a diffraction grating is placed in the laser beam before it is coupled into the waveguide. The grating was fabricated holographically in a slab of $LiNbO_3$(21) and had a period of 14.4 μm. In the experiment the grating was oriented to produce two nearly collinear beams of comparable intensity from a single beam incident on it near the Bragg angle. These beams were coupled into the waveguide and subsequently resolved by the geodesic lens, as seen in Fig. IV-12b. The 0.38-mm separation of the focal spots shows that the two waveguided beams propagated at an angle of 27.6-mrad relative to each other. The interference pattern formed by the

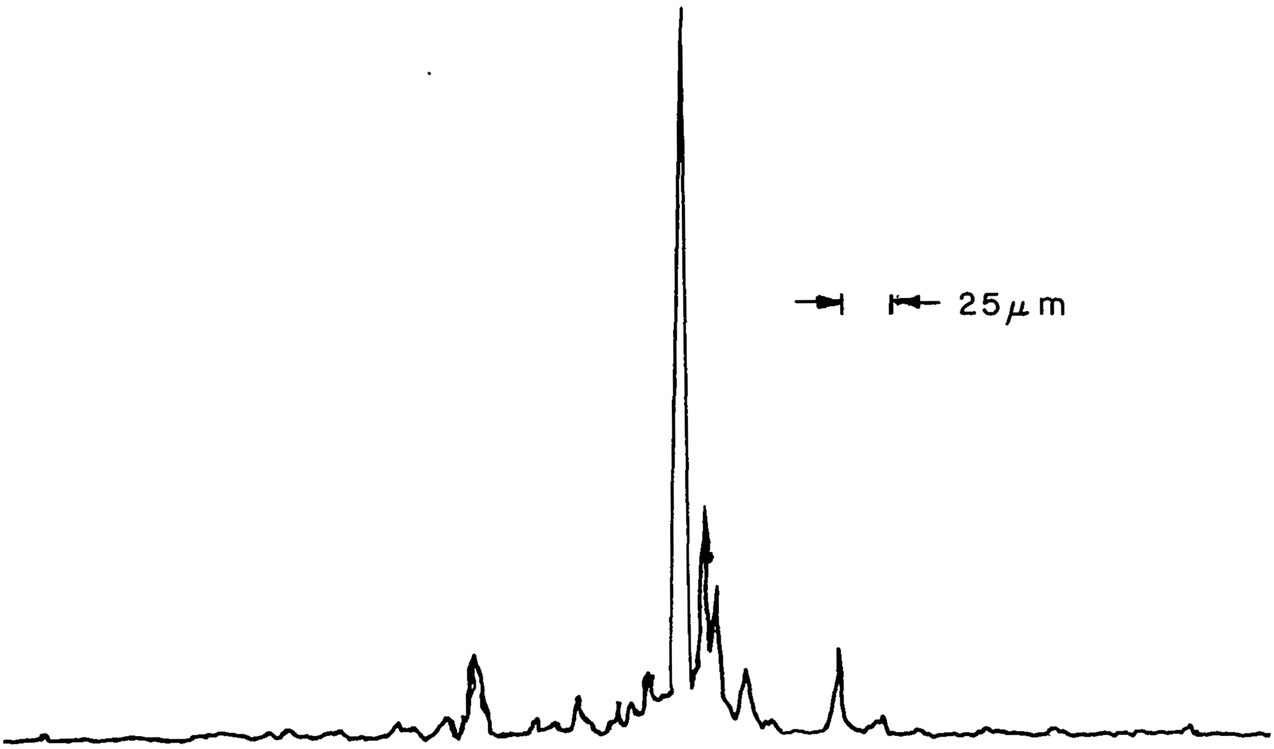

FIGURE IV-11. FOCAL SCAN FOR WAVEGUIDE LENS L4 FABRICATED IN PHOTOBROWN™ GLASS.

(a) SIMPLE FOCUSING

(b) RESOLUTION OF TWO GUIDED BEAMS HAVING AN ANGULAR SEPARATION OF 27.5 MILLIRADIANS

FIGURE IV-12. RESOLUTION TEST OF PYREX LENS L2 (LENS DIAMETER: 9.0 mm) guided beams before they enter the lens has a corresponding spatial frequency $K = 441\ \text{mm}^{-1}$ and periodicity $\Lambda = 2\pi/K = 15.3\ \mu\text{m}$. This periodicity is larger than that of the grating used to produce the two beams presumably because a slightly magnified image of the grating was projected onto the coupling spot.

Waveguide lenses will be more useful for optical processing as they are able to resolve smaller spatial frequencies. As a further test of the capabilities of lens L2, we placed a 7.9 line/mm Ronchi ruling into the laser beam prior to coupling it into the guide. The ruling generates number of diffracted beams that propagate at an angle of 5 mrad with respect to each other. When these are coupled into the Pyrex waveguide of index 1.49, their angular separation is reduced to 3.3 mrad, and the minimum spatial frequency associated with their interference pattern is $49.5\ \text{mm}^{-1}$, corresponding to a periodicity $\Lambda = 127\ \mu\text{m}$. Equation III-(12) suggests that a lens with the spherical aberrations measured in L2 should be able to resolve these beams if the input aperture is reduced to 3.5 mm; however, this was not found to be the case. While the intensity distribution of light in the focal plane of the lens clearly changed when the Ronchi ruling was placed in the beam, it was not possible to resolve individual focal spots corresponding to various orders of diffraction.

This suggests that the resolving power of lens L2 is limited by scattering. In the case of similar lens L3, we found that scattering-induced windows in the front focal plane had a characteristic width $\delta = 37.5\ \mu\text{m}$. Since this value is less than the 127 μm periodicity of the Ronchi ruling, and since the windows are randomly oriented, their overall effect is to scramble the spatial information processed by the lens. Consequently, discrete focal spots for the various beams generated by diffraction at the Ronchi ruling were not observed.

Better success with this experiment was obtained using the geodesic lens fabricated in Photobrown$^{\text{TM}}$ glass. Figure IV-13 shows the intensity distribution in the back focal plane of this lens when the 7.9 line/mm Ronchi ruling is placed before the input coupling prism. Thirteen diffracted orders and the zero order are resolved. The tallest peak corresponds to the zero order. Relative heights of the peaks are not significant

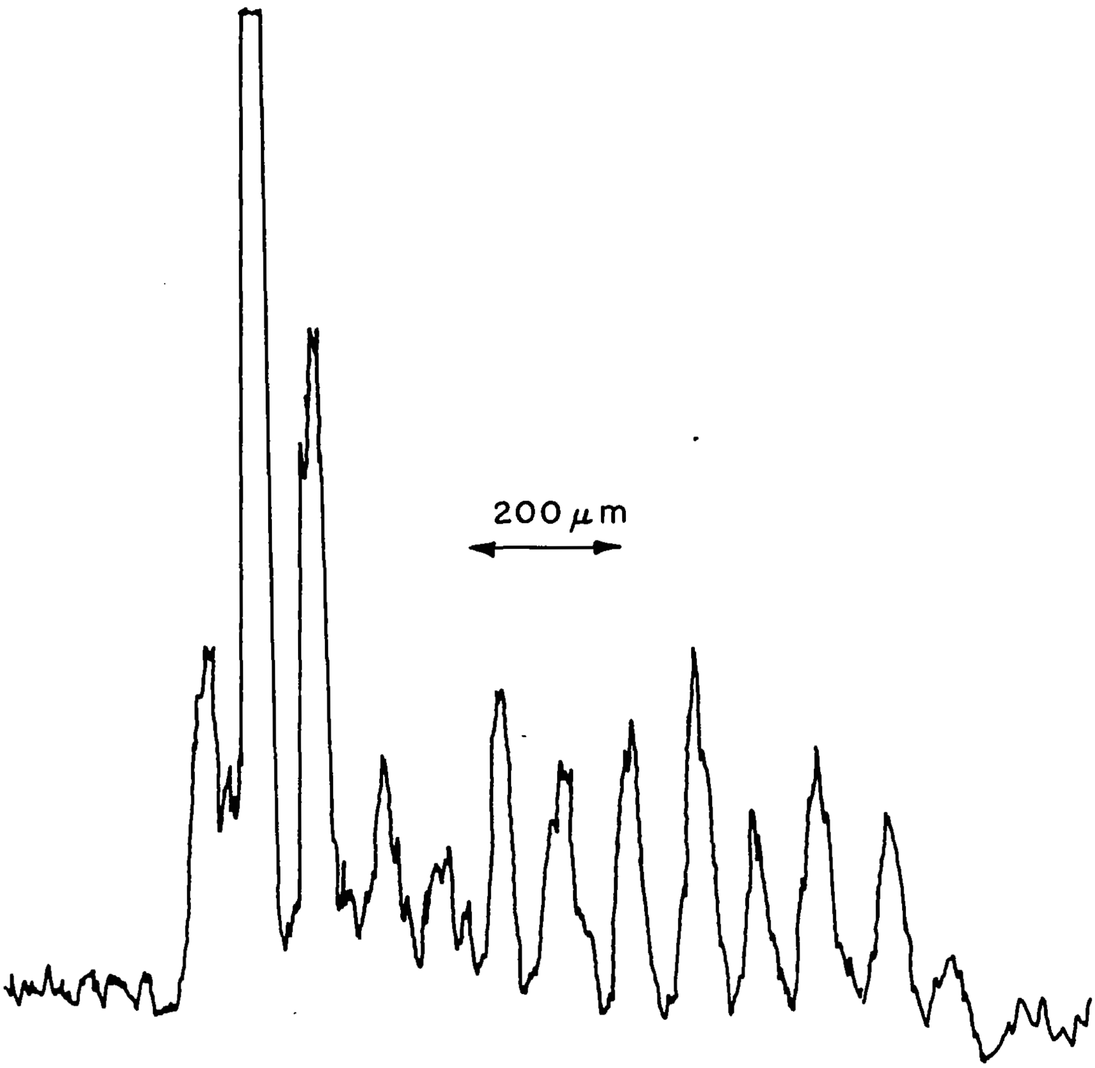

FIGURE IV-13. RESOLUTION OF 13 DIFFRACTED BEAMS BY PHOTOBROWN™ LENS L4. BEAMS WERE DIFFRACTED AT A 7.9 line/mm RONCHI RULING AND PROPAGATED AT A RELATIVE ANGLE OF 3.3 mrad. LENS FOCAL LENGTH IS 28 mm.

because different orders are coupled into the guide with different efficiencies. The widths of the peaks were limited by the 37.5-μm resolution of the detection system. This resolution was determined by the 0.6-mm-slit width of the aperture placed over the fiber bundle in this particular experiment. The success we experienced in resolving the Ronchi-ruling transform using the Photobrown™ lens is consistent with the high quality of this lens shown by the focal scan of Fig. IV-11.

THEORETICAL STUDIES OF GEODESIC WAVEGUIDE LENSES

Two theoretical studies of the properties of geodesic waveguide lenses were undertaken as part of this program. These studies were both motivated by the experimental observation that the focal lengths of our lenses were different than predicted by the conventional theory,(30) which ignores rounding of the lens rim and assumes that the shape of the lens depression is spherical. We investigated the influence of both aspherical shaping and rim rounding on the focal charactreristics of geodesic waveguide lenses. The results are contained in Ref. (33) and in Ref. (40), respectively. The principal conclusions are the following:

(1) The small amount of rim rounding required for effective waveguide-to-lens coupling increases the lens focal parameters f_0 and f_1 by a few tenths of a percent.

(2) One-percent deviations of a geodesic lens depression from sphericity can result in ten-percent deviations in the paraxial focal length f_0 and one-hundred-percent deviations in the third-order spherical-aberration coefficient f_1.

(3) Shaping a lens depression in the form of an oblate spheroid is a technique that may be used to eliminate third-order spherical aberrations in geodesic lenses.

(4) The waveguide thickness in the region of an oblate spheroidal lens may be adjusted to eliminate both third- and fifth-order spherical aberrations, thus producing a waveguide lens with diffraction-limited performance over apertures as large as a centimeter.

These results should significantly influence further development of geodesic lens technology.

V. INTEGRATED OPTICAL DATA PROCESSORS FOR NASA APPLICATIONS

As space missions and earth resource surveillance techniques become more sophisticated, NASA is finding itself in the position of being able to take more data than can be conveniently transmitted, to transmit more data than can be stored, and to store more data than can be processed in a reasonable length of time. It is evident that any form of on-board data processing which can reduce the amount of transmitted data without causing a loss of significant information is the key to alleviating all of these problems. With this in mind meetings were held with NASA personnel in which several specific systems were discussed. From these discussions, we conceived two distinct types of integrated optical data processors. The first was a Fourier-transform device which is well suited for handling data with a characteristic periodicity. This was suggested by discussions of COPE, the Carbon Monoxide Pollution Experiment.(2) The second concept, upon which significantly more effort was expended, was for a holographic-subtraction device which is capable of preprocessing the output of a multichannel scanning system such as the MOCS.(1) Both these concepts will be discussed in this section. Although the motivation for these concepts originated with specific NASA systems, it should be emphasized that the applicability of the concepts is not limited to these systems.

A FOURIER-TRANSFORM PROCESSOR

The purpose of the COPE experiment was to demonstrate a remote system for the measurement of the CO atmospheric burden. The CO absorption spectrum (Fig. V-1a) in the 2.3 μm to 2.4 μm region consists of two groups of quasi-periodic absorption lines. This periodicity immediately suggests that a Fourier-transform system could be used to monitor the modulation amplitude of the signal and thereby determine the atmospheric concentration of CO. Initial attempts to design an integrated-optics

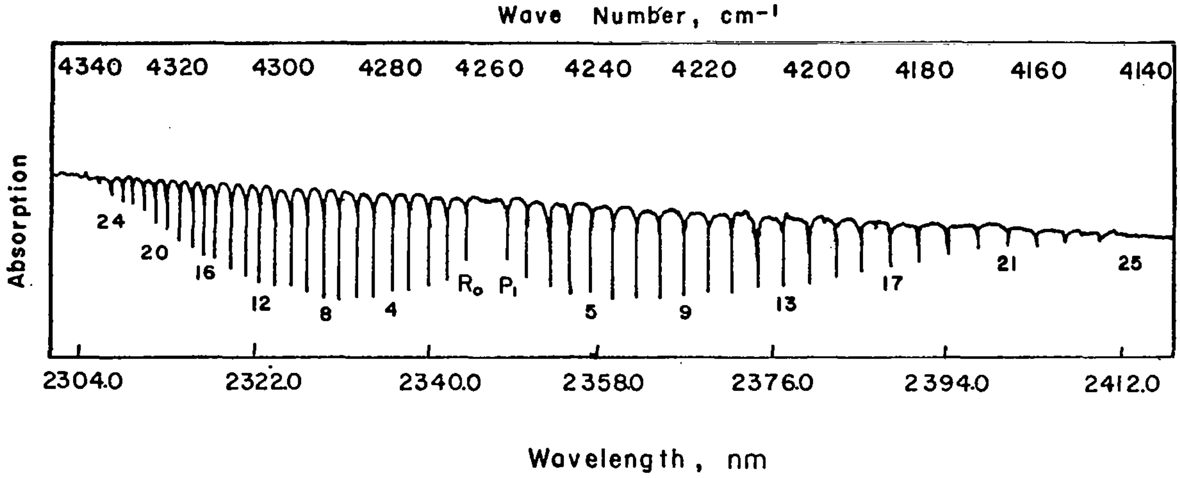

(a) THE SPECTRUM OBSERVED IN A LABORATORY EXPERIMENT

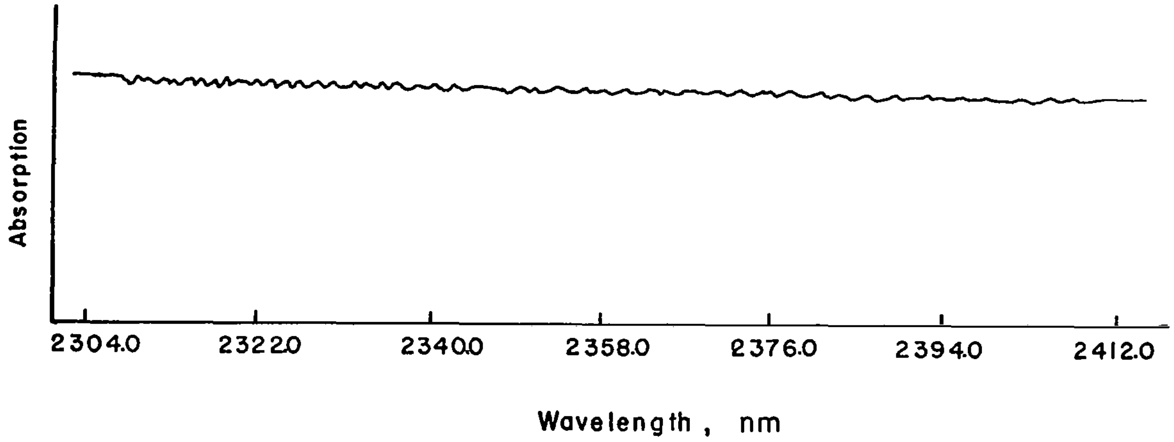

(b) THE SPECTRUM THAT MIGHT BE OBSERVED IN REFLECTED SUNLIGHT FROM A HIGH-ALTITUDE PLATFORM

FIGURE V-1. THE NEAR IR 2-0 ABSORPTION SPECTRUM OF CO.

instrument capable of performing such a measurement presupposed a mechanism whereby the periodic amplitude variation produced by spectrally dispersing light passing through CO could be converted to a phase or amplitude variation of a monochromatic guided wave.

The concept of the Fourier-transform spectrum analyzer is illustrated in Fig. V-2. The dispersed light is incident normally upon the interaction region where it imparts a periodic phase or amplitude variation to the guided wave which mimics the amplitude fluctuations of the dispersed beam. Upon traversing the waveguide lens, this periodic variation produces two side-bands which can be detected at a or b. The ratio of the signals at a or b to the zero order signal detected by c is proportional to the CO concentration.

Conceptually, the interaction region could consist of a photochromic or a photorefractive material or a photoconducting layer on an electrooptic waveguide (Fig. V-3). In fact the desired periodic signal appears only as a weak perturbation on a very large dc background (Fig. V-1b). Since the available light levels are very low, and since none of the suggested interaction mechanisms are very strong, the implementation of this concept for atmospheric pollution monitoring does not seem likely. Attempts to design a Fourier-transform device with a direct optical input have therefore been suspended in favor of the multichannel, holographic subtraction device which is discussed below.

A MULTICHANNEL HOLOGRAPHIC COMPARATOR

Motivation for the Device

We conceived the general idea for the multichannel holographic comparator as a result of discussions with NASA personnel on the Multichannel Ocean Color Sensor (MOCS) system.(1) This system, which is shown schematically in Fig. V-4, presents data in the form of 20 voltages, one for each of 20 spectral channels. The voltages representative of spectral data are presented in parallel and are updated every millisecond.

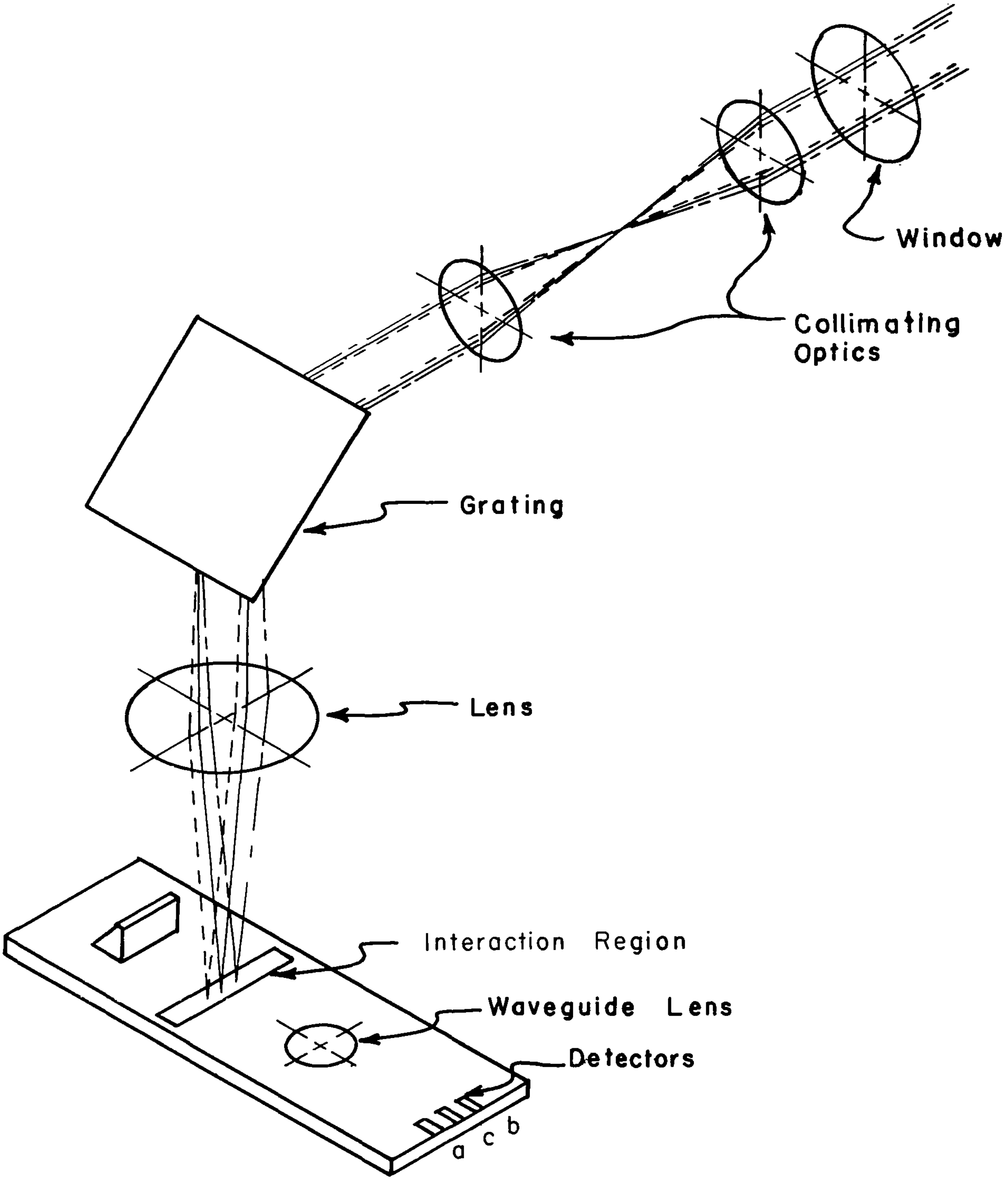

FIGURE V-2. SCHEMATIC OF AN INTEGRATED OPTICS FOURIER-TRANSFORM SYSTEM FOR MONITORING THE INTENSITY OF THE CO 2-0 ABSORPTION SPECTRUM.

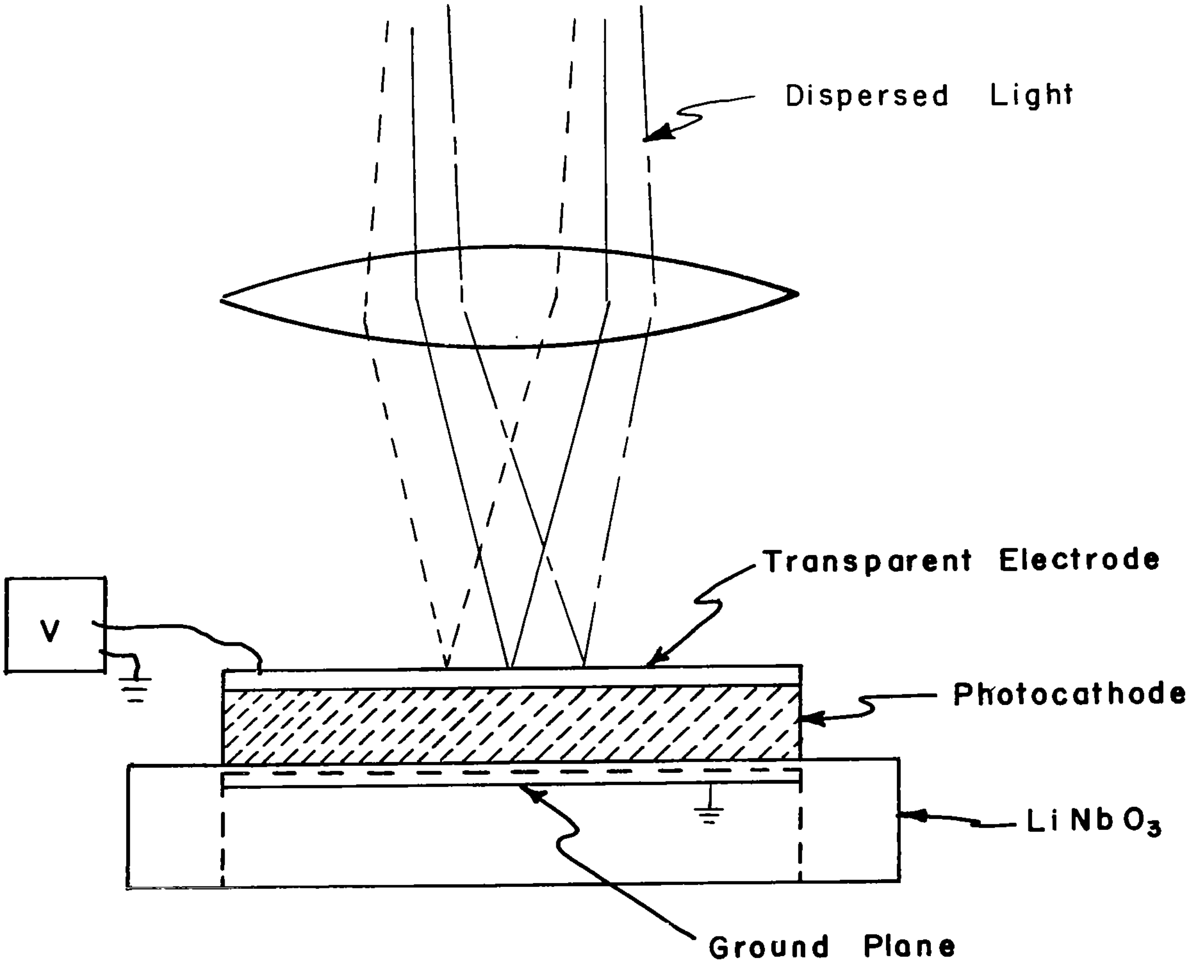

FIGURE V-3. SCHEMATIC OF INTERACTION REGION USING A PHOTOCONDUCTIVE LAYER TO CONVERT THE AMPLITUDE DISTRIBUTION IN THE INPUT BEAM TO AN INDEX VARIATION IN THE ELECTROOPTIC WAVEGUIDE. AVAILABLE SIGNAL LEVELS ARE TOO SMALL FOR THIS SCHEME TO BE PRACTICAL.

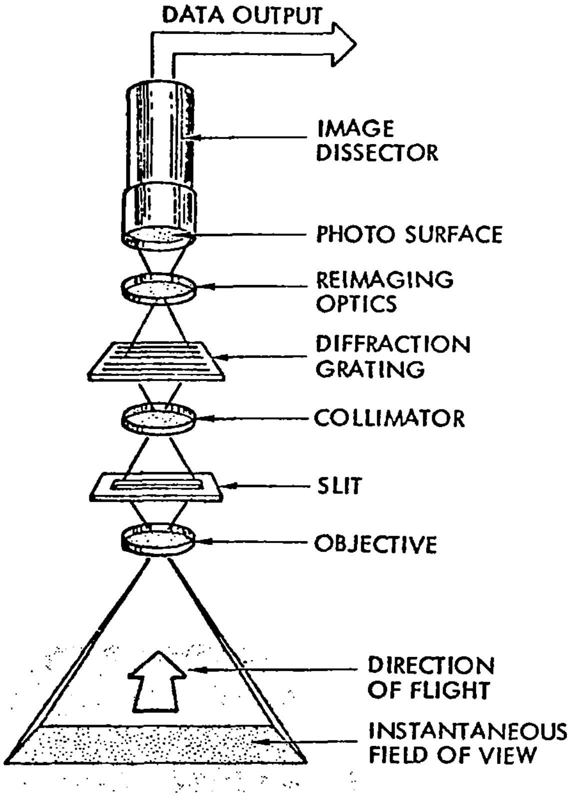

FIGURE V-4. SCHEMATIC OF THE MULTICHANNEL OCEAN COLOR SENSOR. THE OUTPUT IS A SET OF 20 VOLTAGES, ONE FOR EACH SPECTRAL CHANNEL.

The purpose of the MOCS is to record the spectral characteristics of the light reflected from the ocean surface. From these spectral data information about the concentration of plankton, pollutants or other impurities in the water can be derived. The majority of the data, however, is indicative of essentially pure water and is therefore uninteresting. The purpose of the multichannel comparator is to flag the data indicative of pure water so that it can immediately be discarded. Thus, only the interesting data will be transmitted and subsequently processed. A modification of the basic comparator may allow the real-time comparison of the MOCS data with a large reference library and thereby provide identification of the impurity signal in addition to the simple indication of departure from the pure-water signal.

Technical Background

In order to describe the operation of the integrated optical holographic comparator, brief discussions on three subjects will be necessary. These subjects are holographic subtraction,(6) electrooptic introduction of information, and photorefractivity.(21) Following the discussions of these three subjects the integrated optics device will be described.

Holographic Subtraction

Optical subtraction is possible because of the fact that the amplitudes of two superimposed, mutually polarized coherent beams add algebraically. Thus, if the amplitudes of two beams are equal in magnitude but differ by $(2n + 1)\pi$ in relative phase, there will be a local cancellation. This is, for example, the cause of the central dark spot in a well-aligned Michelson interferometer when the path length variations between the arms differ by $(2n + 1)\lambda/2$.

Consider now a hologram produced in the conventional manner depicted in Fig. V-5a. As shown in Fig. V-5b, reconstruction of this hologram enables a viewer to see a virtual image of the object in its original position.

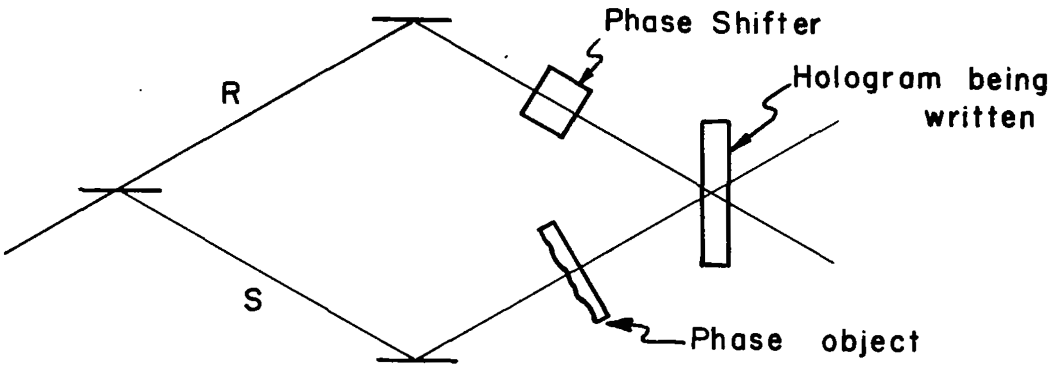

(a) THE FORMATION OF THE HOLOGRAM OF A PHASE OBJECT

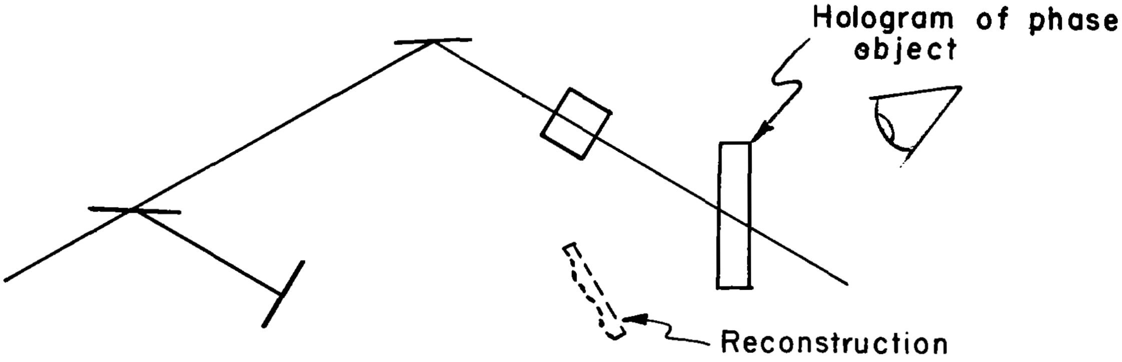

(b) RECONSTRUCTION OF OBJECT WITH SIGNAL BEAM BLOCKED

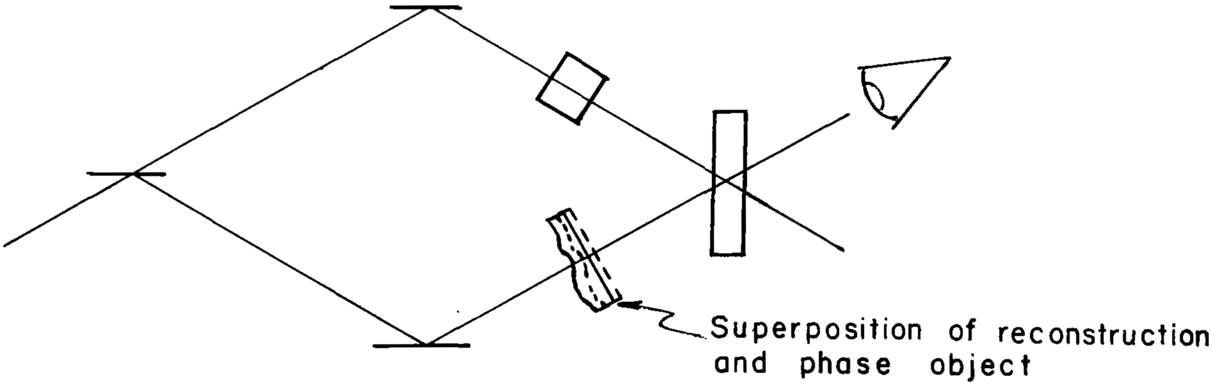

(c) SUPERPOSITION OF OBJECT AND IMAGE. AN APPROPRIATE PHASE SHIFT WILL RESULT IN THE OBSERVER SEEING A DARK FIELD

FIGURE V-5. THE HOLOGRAPHIC SUBTRACTION PROCESS.

In the third part of the figure, the shutter has been removed from the signal beam so that the viewer sees both the virtual object and, by looking through the hologram, the real object illuminated by the signal beam. If there has been no change in the object or in the optical system between the hologram formation and this viewing, the observer will see an object which is brighter than that which is seen with either R or S beam blocked. However, if a phase shift is introduced into one of the beams, the brightness will change, passing through one minimum and one maximum as the introduced phase shift goes from 0 to 2π. In the simplest case, where both the direct and the holographically reconstructed beams are plane waves of equal intensity, the brightness can be made to pass through zero. This is referred to as holographic subtraction. Any region of the object which has changed between the hologram formation and the subtraction process will distort the wavefront and will produce a bright spot on the dark background.(6)

Electrooptic Information Input

A convenient way to introduce information into the hologram shown in Fig. V-5 is to control the index of refraction of selected regions of the "phase object". Thus an electrode configuration such as that shown in Fig. V-6 is capable of introducing 10 channels of analog phase information when it is established on a slab of electrooptic material like $LiNbO_3$. Assume that a hologram of this phase object was made with voltages $V_1 \ldots V_{10}$ on the electrodes. If the holographic subtraction process of Fig. V-5 were now performed, any deviation of the voltages from the original set would introduce a phase change so that the subtraction would no longer be complete and a bright spot or a series of bright spots would appear on the dark field.

Photorefractivity

In order to record a hologram in either a three dimensional or a waveguide configuration, a photosensitive material is required. Ideally,

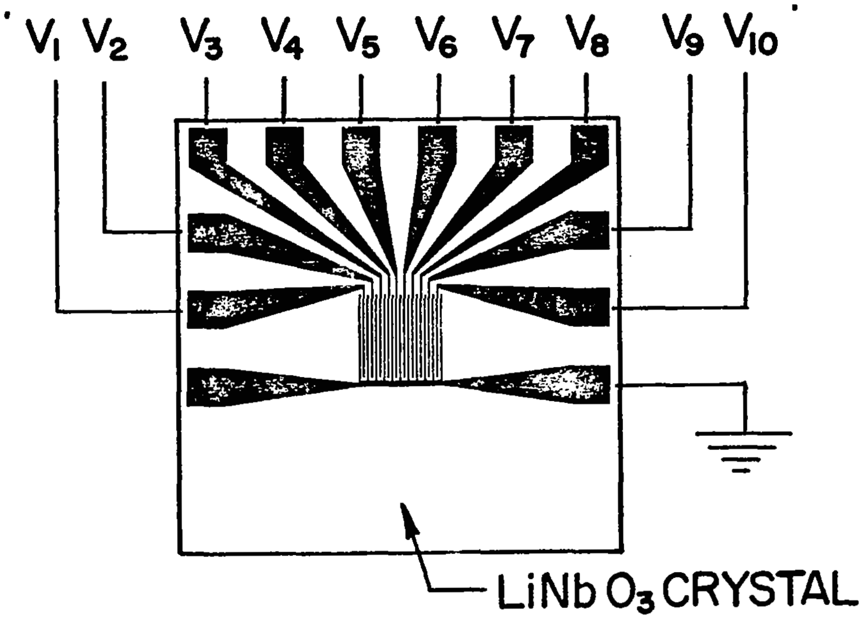

FIGURE V-6. ELECTROOPTIC INFORMATION INPUT DEVICE. VOLTAGES APPLIED TO ELECTRODES PERTURB THE PHASE OF A LIGHT BEAM PASSING THROUGH THE CENTER OF THE ELECTROOPTIC CRYSTAL.

this material should undergo an index-of-refraction change rather than an optical density change as the result of optical irradiation, so that holograms with high diffraction efficiencies can be written. A material which exhibits very low scattering is also desirable. In addition, for an integrated optics device, the material must be capable of existing in or on the waveguide, or ideally, actually be the waveguiding material.

Crystalline $LiNbO_3$ satisfies all of the above criteria. The photorefractive process by which holograms can be written in $LiNbO_3$ is unique to pyroelectric materials. Since the process has been discussed at length in the literature,(21-23) it will only be described quite briefly here.

The photorefractive process in $LiNbO_3$ is initiated by the absorption of a photon which promotes an electron from a shallow trap into the conduction band. Once in the conduction band, the electron moves, generally in the direction of the positive c-axis, until it is retrapped. By a sequence of successive excitation/drift/retrapping events, a space-charge distribution evolves corresponding to an excess of electrons in dark regions of the crystal. This produces an internal field which, via the electrooptic effect, produces the desired modulation of the index of refraction.

For the purposes of this discussion, the following facts about writing holograms by the photorefractive effect in $LiNbO_3$ are important.(21-23)

- Holograms are best written so that the grating vector is parallel to the c-axis. This requirement affects device layout and configuration.
- The photorefractive sensitivity is a function of transition metal impurity concentration and valence state. The sensitivity can be made to increase by orders of magnitude with the introduction of iron impurities in the concentration range 10 to 1000 ppm.
- Holograms can be erased by irradiation with the writing wavelength, but are fairly stable against irradiation by long wavelength (i.e. red) radiation. Owing to the dark conductivity of the crystal,

they have a finite lifetime which ranges from minutes to days as a function of temperature and concentration and valence of impurities.

- Holograms may be fixed by appropriate thermal treatments so that they are stable for indefinite periods.
- Holograms can be written in a $LiNbO_3$ waveguide with high diffraction efficiencies.

The Integrated Optics Holographic Comparator Concept

The techniques of integrated optics will allow all of the concepts discussed in the preceding section to be utilized in a compact, rigid structure capable of comparing a multiplicity of parallel analog inputs to a standard set at exceedingly high data rates. We first present a straightforward version of this device. In the following section we will discuss some of the system considerations which will influence the final design choice.

A schematic of one configuration of the comparator is shown in Fig. V-7. The waveguide is an outdiffused layer on the surface of a Y-cut $LiNbO_3$ slab. Light is coupled in via a grating coupler, and split into two beams by a grating beam splitter. The signal beam passes under a set of electrodes which, via the electrooptic effect, impress a signal pattern upon the guided wave. The reference beam passes between two electrodes which, when energized, impart a suitable phase shift to the reference beam. The two beams then intersect in the hologram region.

In order to use the device, a set of reference voltages is applied to the data-input electrodes. In the MOCS application, these voltages would be those corresponding to the clear water spectrum. A hologram is then made using the index-of-refraction pattern induced by this set of voltages as the object. This hologram is made in such a way as to be stable over some predetermined time period. Now, an appropriate phase shift is introduced into the reference beam and voltages representative of the unknown data set are impressed upon the electrodes. If they are identical to the reference set, the holographic subtraction process

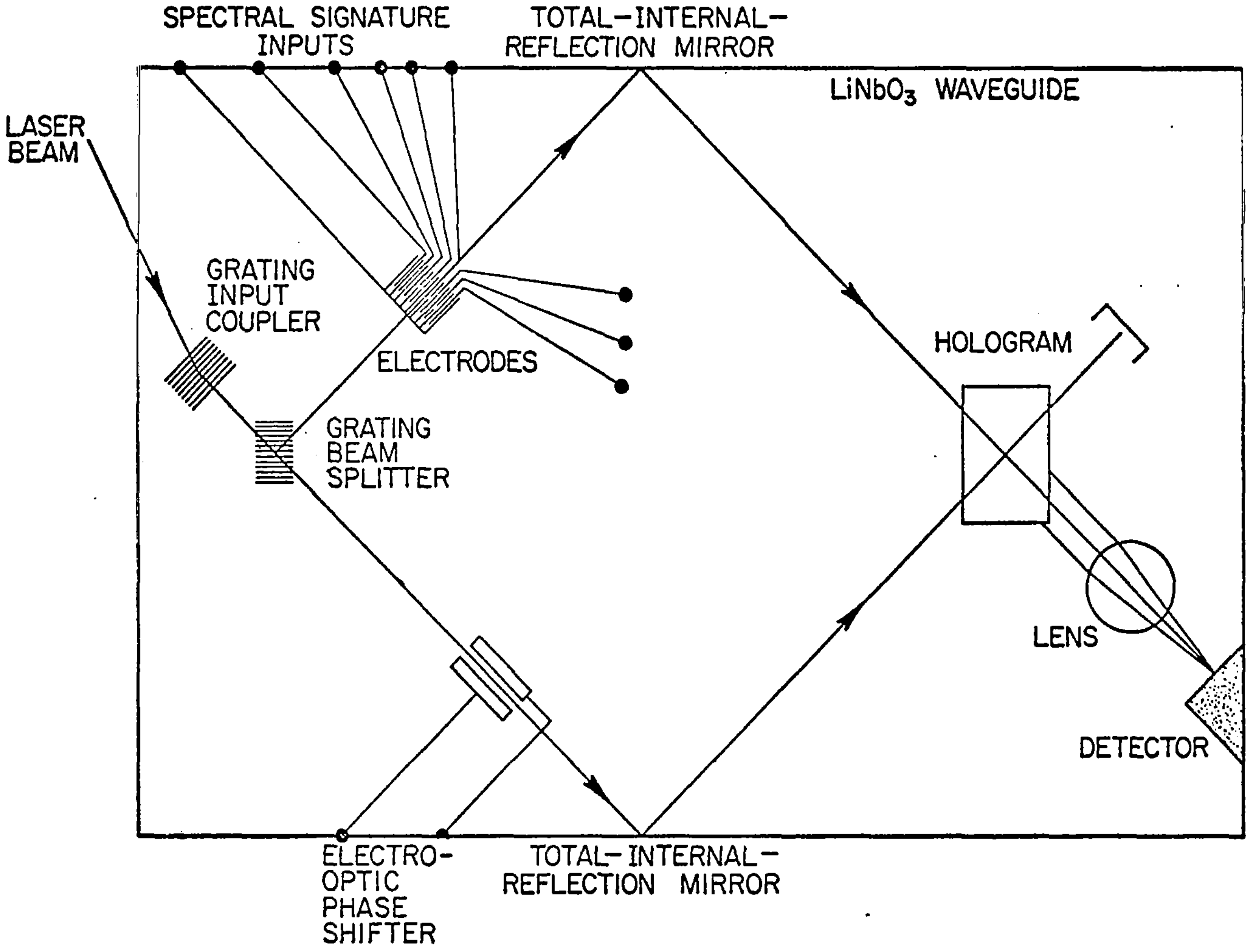

FIGURE V-7. SCHEMATIC OF ONE CONFIGURATION OF THE INTEGRATED OPTICS HOLOGRAPHIC COMPARATOR.

ensures that no light reaches the detector. If the data do not match the reference set, light arrives at the detector in proportion to the mismatch. Thus, a simple discriminator at the detector output can be set to flag data which exceed a predetermined degree of mismatch so that this data can be transmitted or stored for further analysis.

An interesting modification of the system differs from the previous design only in the addition of a second set of electrodes, identical to the first set and located over the signal beam between the first set of electrodes and the hologram region. The reference hologram is made with no voltages on any of the electrodes. It therefore contains only information about the various optical imperfections in the system. During the subtraction steps these imperfections will be compensated for since they have been written into the hologram.

To use this modification of the device, the data voltages are impressed upon the first electrode set, and a negative set of reference voltages are impressed upon the second electrode set. If the two sets are equal in magnitude but opposite in sign, there will, at least to zero order, be a complete cancellation of their respective effects upon the wave front. If a library of reference voltages exists, it should be possible to cycle through the entire library of say, 10^3 to 10^4 reference sets during 10^{-3} sec to find a best fit to the unknown set. Thus, the device has the potential of being able to identify as well as flag interesting data.

VI. PRELIMINARY STUDIES OF THE INTEGRATED OPTICS HOLOGRAPHIC SUBTRACTION SYSTEM

The basic concepts necessary to understand the operation of an integrated optics data-processing system utilizing holographic subtraction were presented in the preceding section. In this section we will first present and briefly describe a variety of configurations in which such a system may be built. In order to make an intelligent choice among these configurations, one must be able to both predict the fabrication procedures and to estimate the ultimate operating characteristics. This can be done only after the accumulation of significant experimental and theoretical background and experience. This must include knowledge of relevant material properties, theory of holography, effects of device structures upon guided wave properties, component characterization and a host of fabrication techniques.

As the ultimate utility of the holographic-subtraction technique became increasingly apparent, the motivation for accumulating this background became more compelling. In particular, two areas were selected for initial emphasis since they impact strongly upon the feasibility of the holographic-subtraction device and they have not previously been the subjects of detailed study. The first of these areas is that of the formation of waveguide holograms in an optically stable configuration. Several approaches to this problem will be discussed, two of which have yielded encouraging preliminary results. The second major area has to do with the details of the holographic-subtraction process. It includes theoretical studies of the effects of electrode structure and experimental studies of electrode fabrication and holographic subtraction in a waveguide. These are also discussed below. The details of the photolithographic techniques applied to the production of metal patterns on $LiNbO_3$ is discussed in the Appendix.

ALTERNATIVE CONFIGURATIONS FOR AN INTEGRATED OPTICAL HOLOGRAPHIC SUBTRACTION SYSTEM

A basic part of an integrated holographic-subtraction system like that shown in Fig. V-7 is a waveguide interferometer. As in the case of its three-dimensional counterpart, the interferometer divides a beam of light into two parts that propagate along distinct but intersecting optical paths. If the coherence length of the beam is sufficiently long, the variety of optical paths that may be employed for an integrated holographic-subtraction system is unlimited. However, practical considerations associated with component fabrication may severely limit those choices for which the signal-to-noise characteristics of the system are acceptable.

Figures VI-1 and VI-2 show a variety of waveguide interferometer configurations that are candidates for use with a holographic-subtraction processor. The configurations differ from each other in one or more of the following respects:

(1) The method used to split a beam into two parts.
(2) The method used to recombine beams at the hologram.
(3) The angle at which beams are recombined at the hologram.
(4) The relative lengths of the two arms of the interferometer.
(5) The amount of space available for component fabrication.

Choice of the optimum waveguide interferometer for use with a practical holographic-subtraction system must be based on experiments that address these differences and their relative effects on the sensitivity of the holographic-subtraction process.

THEORETICAL AND EXPERIMENTAL TECHNIQUES AND RESULTS

Waveguides and Photorefractive Effects

Due to the extreme sensitivity of the holographic subtraction process it is necessary that the light beams undergo no spurious phase

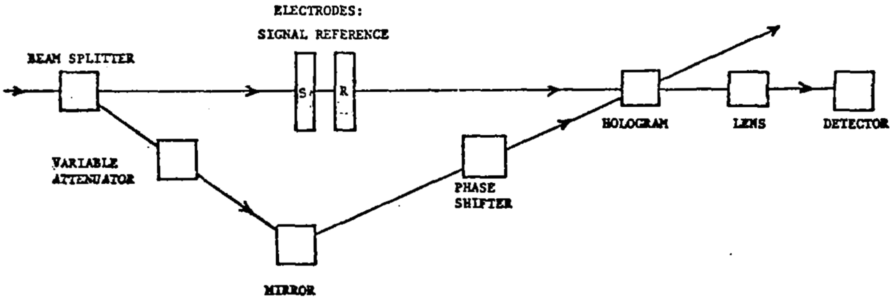

(a) TRIANGULAR INTERFEROMETER

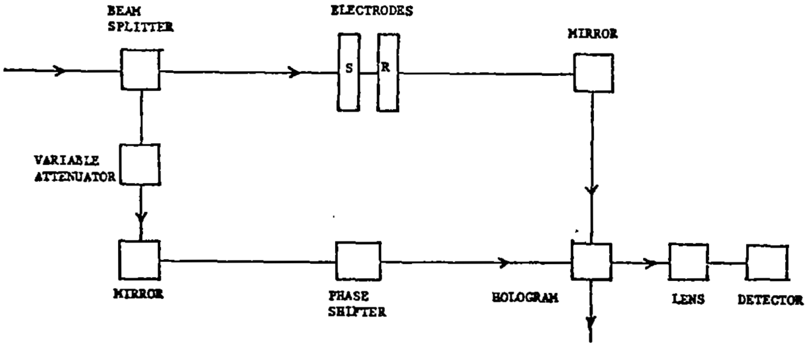

(b) MACH-ZEHNDER INTERFEROMETER

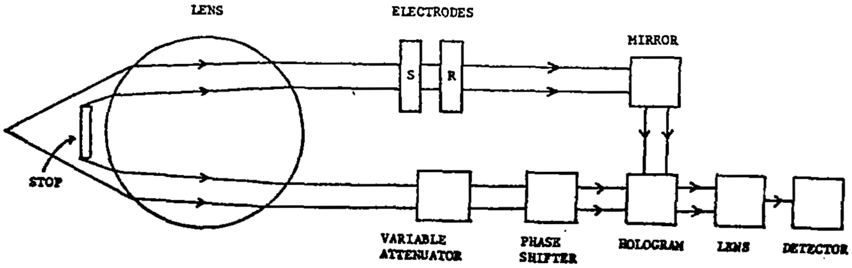

(c) MODIFIED MACH-ZEHNDER INTERFEROMETER

FIGURE VI-1. WAVEGUIDE INTERFEROMETER CONFIGURATIONS FOR A HOLOGRAPHIC-SUBTRACTION PROCESSOR.

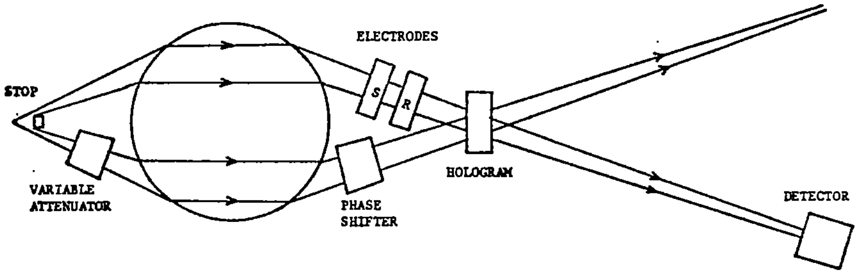

(a) LENS INTERFEROMETER

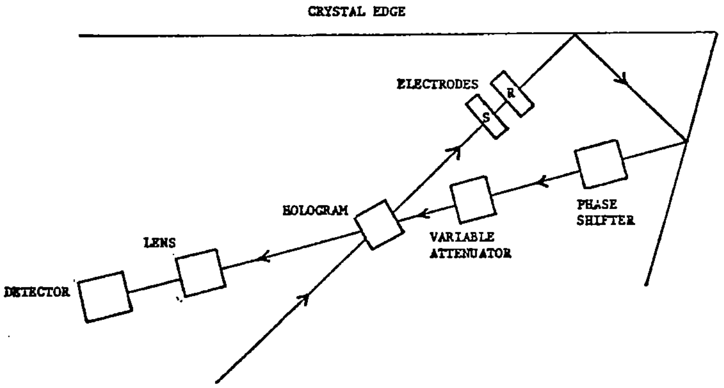

(b) TOTAL-INTERNAL-REFLECTION INTERFEROMETER

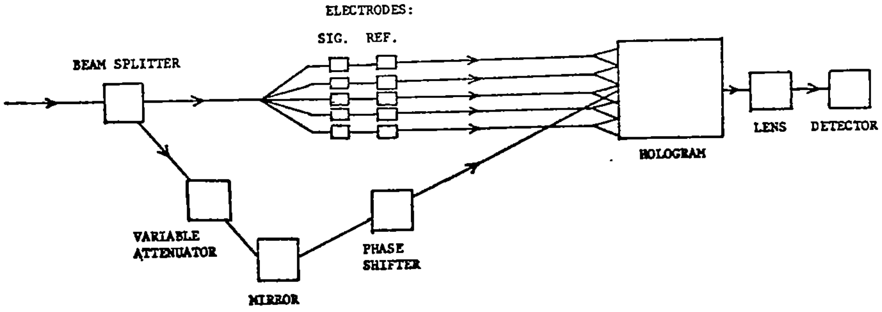

(c) CHANNEL-GUIDE CONFIGURATION

FIGURE VI-2. MORE WAVEGUIDE INTERFEROMETER CONFIGURATIONS FOR A HOLOGRAPHIC-SUBTRACTION PROCESSOR.

shifts over any portion of their paths between the beam splitter and the hologram during readout. In particular it is essential that the waveguide not exhibit detectable photorefractive effects at the optical wavelength and intensity used to operate the device. The degree of material stability required can be appreciated from the fact that, for a two centimeter optical path, an average index-of-refraction change of 1.6×10^{-6} will result in a $\pi/10$ phase shift for red light.

Initially, we wrote holographic diffraction gratings by interfering two guided waves in iron-and titanium-infused waveguides. Diffraction efficiencies and writing efficiencies were good but the diffracted beam exhibited instabilities which were due to photorefractive effects along the length of the beam in the waveguide. Three additional approaches to writing gratings in waveguides were investigated in an attempt to overcome this problem. These approaches are discussed below.

Use of an Outdiffused Waveguide

It is known that the photorefractive sensitivity of pure $LiNbO_3$ is very low. It was therefore reasoned that if one could write a grating with high intensity light, the waveguide-grating combination would be stable against optical damage by low intensity read beams. The major difficulty encountered in this approach was that only very inefficient (low diffraction efficiency) gratings could be written.

Iron Spot in an Outdiffused Waveguide

An ideal situation is one in which the grating region has a much higher photorefractive sensitivity than the rest of the waveguide. This situation was realized by diffusing a small (10 mm x 3 mm) iron spot in an outdiffused guide. This produced outstanding results in that a stable grating with diffraction efficiency of greater than 60% was written in the iron-doped region using a He-Ne laser. The grating was read out for a period of several days with no obvious degradation of grating or waveguide.

No attempt was made to fix this grating, but no difficulties are anticipated other than those associated with the mechanical problems of heating the waveguide-coupler combination. This method would therefore be very suitable for situations in which a single holographic element had to be written in a given $LiNbO_3$ slab.

Multiphoton Photorefractivity

Although the linear photorefractive process is an exceedingly useful effect, it does have certain disadvantages. The most troublesome of these are related to the formation of several holograms on a single substrate or the formation of fixed thick holograms, especially of complex objects. The latter problem stems from the fact that the material is always sensitive to the writing wavelength even if the hologram has been thermally fixed. Thus, even if low intensity beams are used, some degradation in performance may occur. Even if a stable state is achieved, the thermal fixing process is very inconvenient in a complex device since components must be formed one at a time, but local heating of $LiNbO_3$ will cause it to fracture and general heating will alter previously written structures.

What is obviously needed is a method for writing a permanent hologram which will not be damaged by subsequent light. One option is to write with a suitable short wavelength and read with a longer wavelength for which the photorefractive sensitivity is negligible. The problem here is that for any but the simplest plane-wave grating, these holograms must be read with the light having the same wavelength as the writing light.

A solution to this problem is presented by the recently discovered nonlinear photorefractive effect. In a recent paper it was demonstrated by D. von der Linde, A. M. Glass, and K. F. Rodgers(46) that is possible to use a two-photon absorption to initiate the photorefractive process in undoped $LiNbO_3$. By choosing a wavelength λ such that hc/λ is less than the bandgap but $2hc/\lambda$ exceeds the bandgap it is possible to use short intense pulses to write a grating which is essentially impervious to low-intensity continuous radiation at the writing wavelength. This is accomplished by using sufficiently high intensities (> 10^6 watts/cm^2) that the probability of a two-photon absorption becomes significant. The grating, or complex hologram, has the optical properties of a grating written with wavelength λ even though energies associated with the wavelength $\lambda/2$ are used to excite the trapped electrons. This is an important fabrication technique for several reasons:

- The hologram written with a high intensity pulse of light at 0.6328 μm from, for example, a flashlamp pumped dye laser, has the optical properties associated with 0.6328 μm even though the two photon energy which is required to excite an electron from a trap is that associated with light of half the writing wavelength, i.e., 0.3164 μm. Even a complex grating formed in this manner can be read out efficiently with a low-power He-Ne laser with no risk of further photorefractive effects.
- A localized long-lived hologram can be written on a given region of a crystal without heating or in any other way disturbing the remainder of the crystal.
- Writing efficiencies may be considerably higher than for holograms written using short-wavelength linear processes.
- Local erasure by irradiation with short wavelength light is possible.

To explore the nonlinear technique and to verify the results of Ref. 46, we performed several experiments using a Chromatix Nd:YAG laser as a source of intense coherent light pulses both at 0.53 μm, and 0.659 μm. Success at the longer wavelength was particularly relevant since it exceeds the He-Ne wavelength and therefore indicates that the two-photon writing process can be used to produce gratings usable with this laser. In Fig. VI-3 we show a log-log plot of Δn/pulse vs peak power density for a grating written in bulk $LiNbO_3$ with light of λ = 0.659 μm. The slope of this line is close to 2, confirming the two-photon process. The data are consistent with those of Ref. 46.

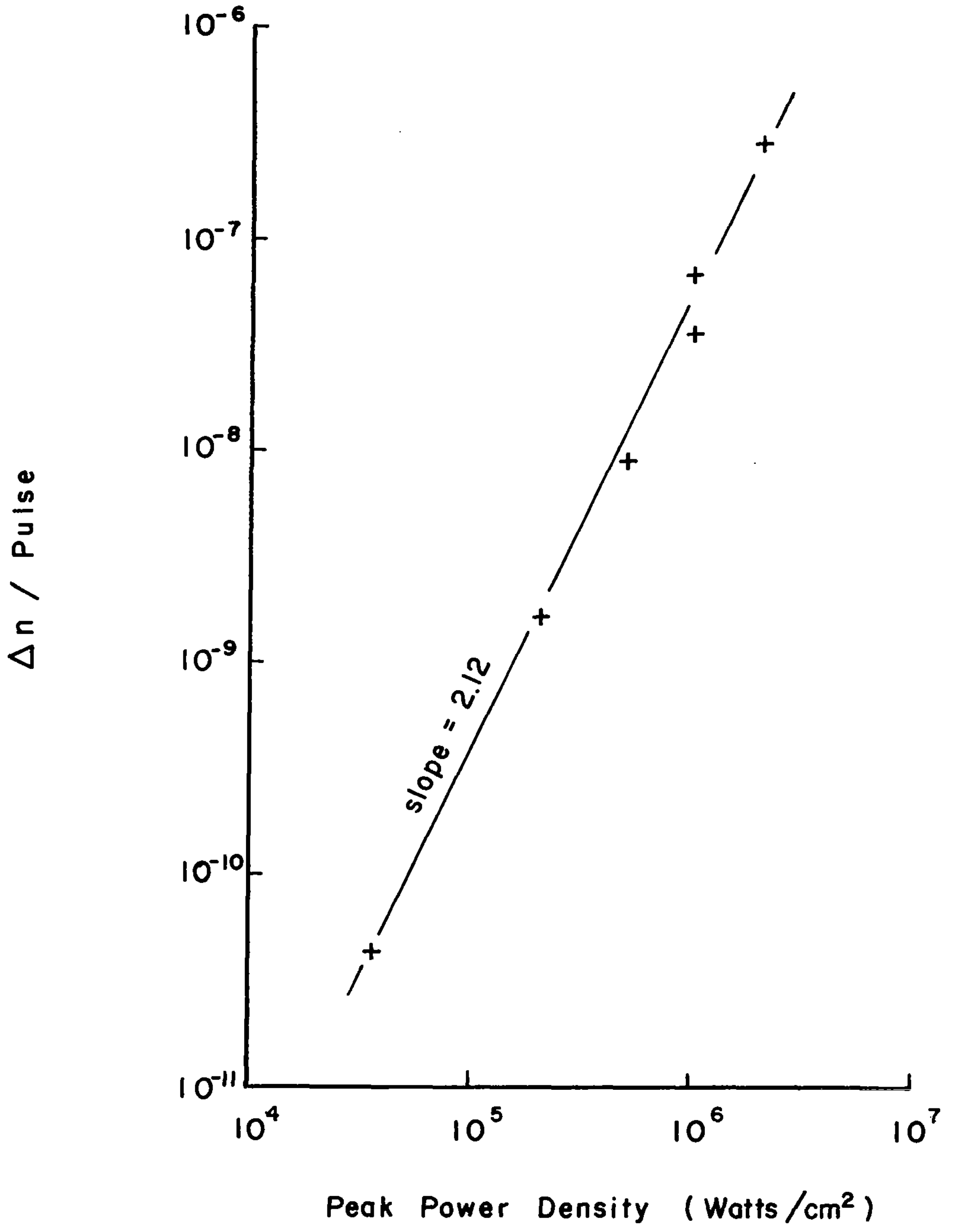

FIGURE VI-3. LOG-LOG PLOT OF THE PHOTOREFRACTIVE SENSITIVITY OF UNDOPED $LiNbO_3$ EXPRESSED IN TERMS OF Δn/PULSE VS THE PEAK POWER DENSITY OF THE WRITING LIGHT. THE WRITING WAVELENGTH IS 0.659 μm.

In addition to the bulk measurements, we have used the same laser to write gratings by interfering two guided waves in an outdiffused waveguide in undoped $LiNbO_3$. The success of these experiments gives us every reason to believe that the two-photon photorefractive effect will provide a valuable tool for the fabrication of integrated optics components in $LiNbO_3$.

Holographic Subtraction and Electrode Structures

Conventional Holographic Subtraction

Experiments on bulk holographic subtraction were initiated in order to have a convenient way to visualize the performance of various system components and configurations. The experimental arrangement is the standard holographic configuration shown in Fig. VI-4. Holograms were recorded in both high-resolution film and $LiNbO_3$ slabs.

An initial electrode design is shown in the insert of Fig. VI-4. For the preliminary experiments this pattern was transferred photolithographically onto a glass substrate. Subsequently, the pattern was transferred to a $LiNbO_3$ slab so the sensitivity of the holographic process to electrooptically induced phase shifts could be studied (see Fig. V-6). However, only very preliminary measurements have been made to date.

Holographic Subtraction in Waveguides

One of the most important results of the current work was the successful demonstration of holographic subtraction using a waveguide grating. With unfocused beams, extinction ratios of 50 to 1 were observed. This demonstrated our ability to make waveguide holograms of sufficient quality to be used in a laboratory model of the data preprocessor.

The waveguide used in the subtraction experiment was the outdiffused waveguide with the iron spot discussed above. The laboratory arrangement was that illustrated in Fig. VI-5. The holographic grating was written in the waveguide by intersecting two guided beams from a He-Ne

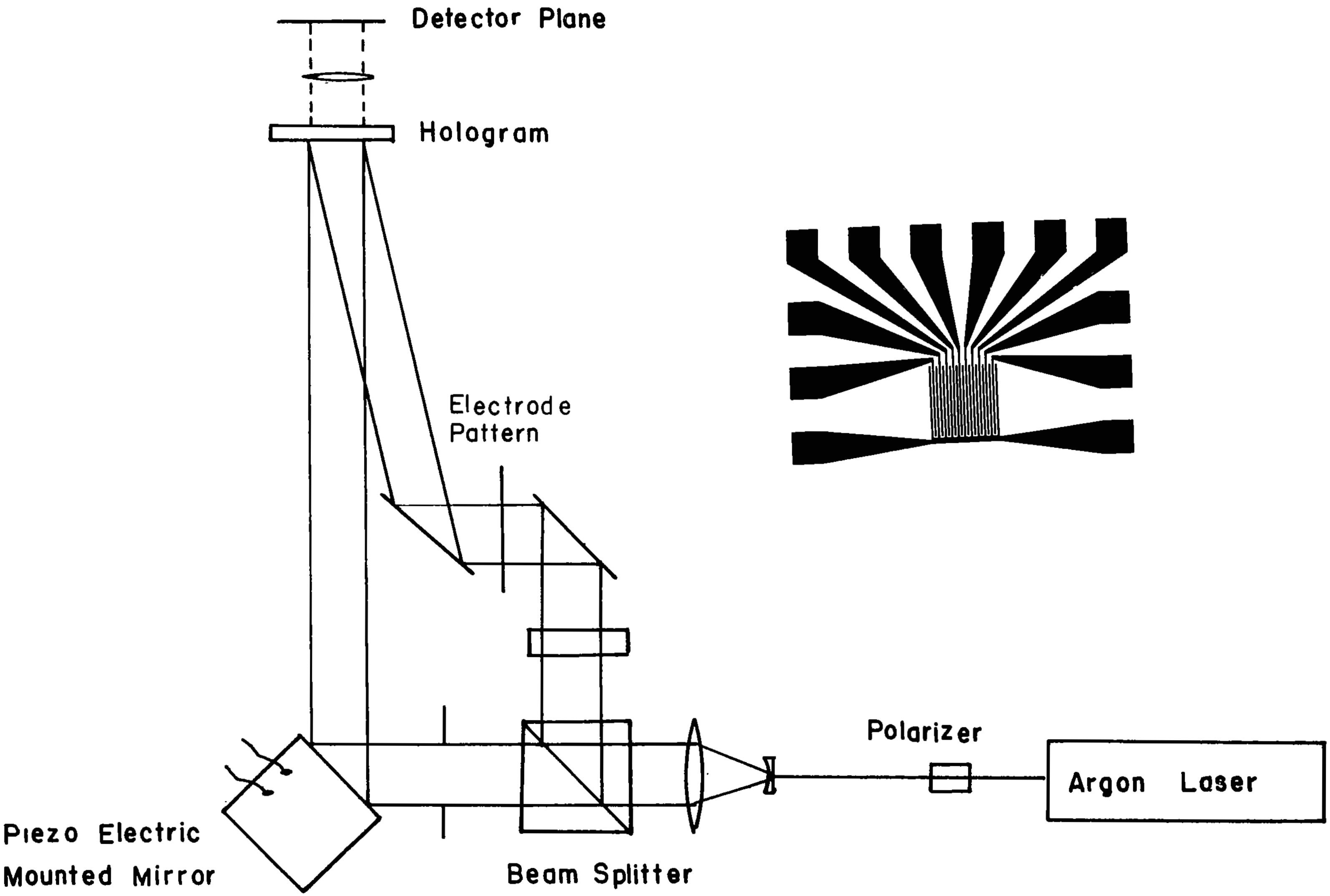

FIGURE VI-4. BLOCK DIAGRAM OF EXPERIMENTAL ARRANGEMENT FOR BULK HOLOGRAPHIC SUBTRACTION. THE INSERT IS A 2X PHOTOGRAPH OF THE ELECTRODE PATTERN.

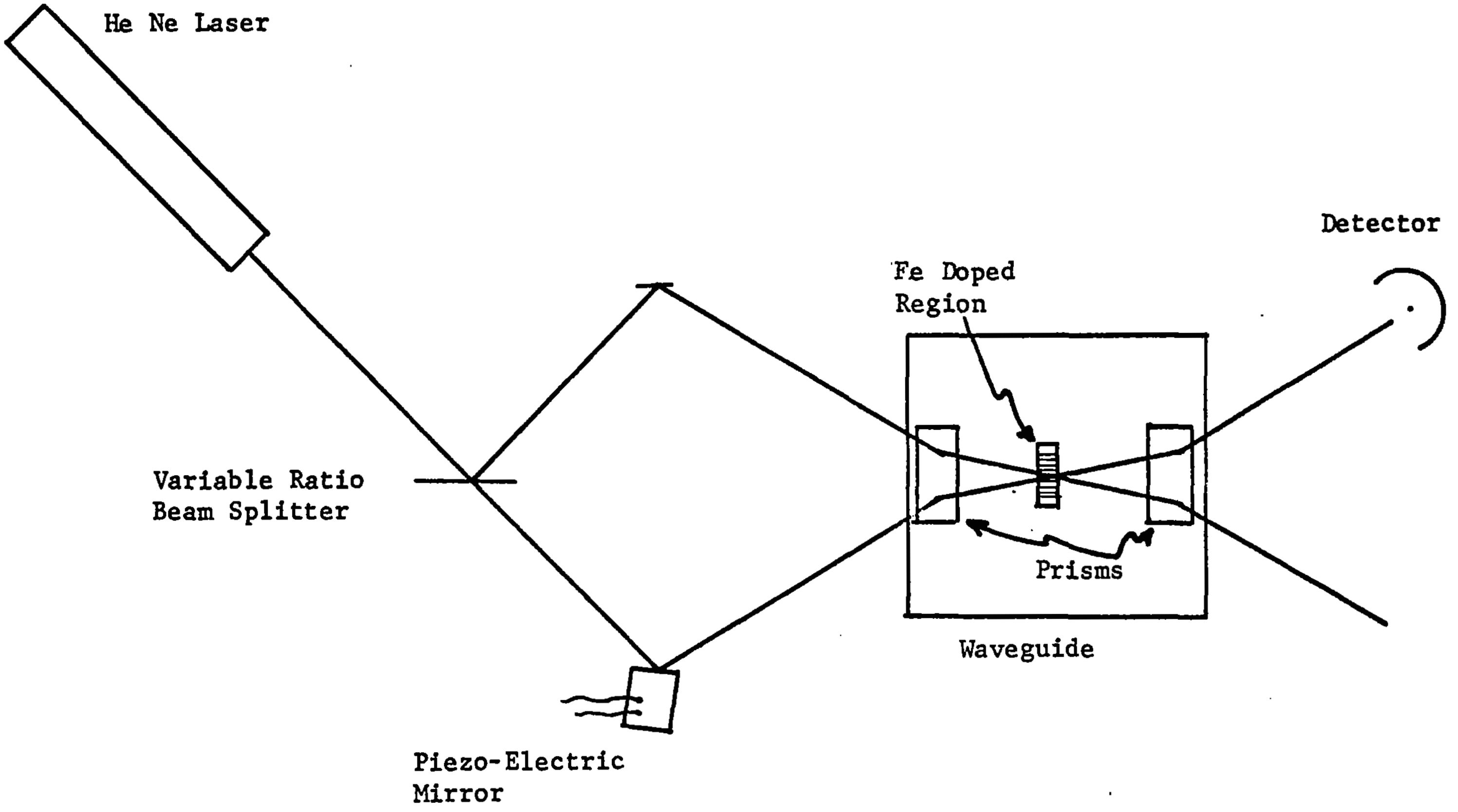

FIGURE VI-5. HOLOGRAPHIC SUBTRACTION USING A GRATING WRITTEN IN AN IRON-INFUSED SPOT IN AN OUTDIFFUSED $LiNbO_3$ WAVEGUIDE.

laser (λ = 0.633 μm). After recording the gratings, the intensity of the He-Ne beam was reduced to minimize further writing or erasing action. Holographic subtraction was observed by monitoring either one of the two coupled-out beams. The total power in each coupled-out beam was the sum of the straight-through component (zero order) and the 1st-order diffracted component from the opposite beam. To achieve holographic subtraction, a π phase difference was introduced into the straight-through beam by affecting a small change in the beam path length. This change was introduced by a small translation of the mirror mounted on the piezoelectric driver. To further optimize the extinction ratio, the straight-through beam was apertured to reduce its width to that of the 1st-order diffracted beam. The reduced size of the diffracted beam occurs because the grating was written with laser beams having nonuniform intensity distributions. As a result the diffraction efficiency of the grating varies appreciably over its full width. As previously noted, an extinction ratio of 50:1 is produced with the above approach.

Electrode Diffraction Effects

Among the most convenient methods for introducing information on a light beam in a $LiNbO_3$ waveguide are those which employ the electrooptic effect. A variety of electrode configurations may be devised which are suitable for use with digital data or with the output of a multichannel device. A knowledge and understanding of the effects of the electrode structure upon the signal beam are required for all studies of possible data-processing systems. The desired effect is the impression of a phase shift, proportional to the signal voltage for a channel, on the portion of the beam associated with the channel. Undesirable effects include attenuation of the signal beam by the electrode structure, spurious phase shifts introduced by the structure, and diffraction of light into other signal channels. The presence of some attenuation is tolerable, but any variation in attenuation from one channel to another will introduce diffraction. Constant phase shifts, although spurious, in themselves should not cause problems; however, spatial variations in these shifts will also result in diffraction. Thus, the primary undesirable effects can all be described in terms of diffraction at the electrode structure.

Light propagation in the region of the waveguide in which an electrode structure is located is altered both by the structure and by the voltages impressed upon it. The voltages impressed on the electrodes induce, via the electrooptic effect, changes in the bulk refractive index of the waveguiding medium which in turn cause changes in the effective index of refraction of the guided mode. These index changes cause phase shifts in the light beams passing through the affected regions. The phase shifts so produced are the desired effects of the electrodes—the introduction of information onto the optical beam. These phase shifts will not, in general, be of ideal form—uniform in the electrode region and zero outside of this region—because they will typically be influenced by fringing-field effects, and fringing fields are never uniform. The electrodes themselves introduce a phase shift on a light beam passing under them because the metal of the electrodes is sampled to some extent by the evanescent "tail" of the guided wave. This changes the effective refractive index of the guided-wave mode, and produces a phase shift that will be nearly ideal in the sense that it vanishes abruptly at the edge of each electrode.

These phase shifts, whatever their origin, are spatially limited in extent to widths of roughly 10-100 wavelengths. Consequently, diffraction effects will be important. These effects will influence the operation of the processor in three ways: 1) they will affect the efficiency of the electrodes in impressing the desired information on the guided beam; 2) they will affect the operation of the holographic subtraction process; 3) they will limit the extinction ratio obtainable. In the following paragraphs these effects will be discussed, and some analyses based on simple models of the complicated physical situation will be presented.

Electrode Operation. A portion of one electrode structure that may find use in an integrated optical holographical-subtraction processor is pictured schematically in Fig. VI-6. Three rays are indicated in the

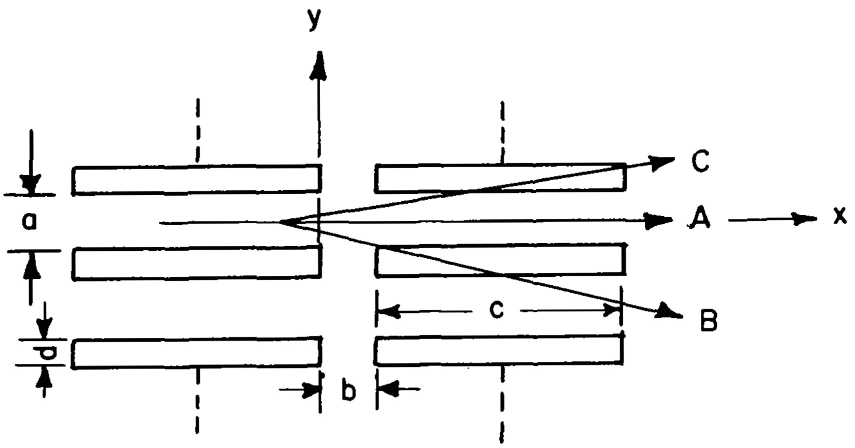

FIGURE VI-6. EFFECTS OF ELECTRODE STRUCTURE ON WAVEGUIDED LIGHT.

figure. Ray "A" passes through the right-hand set of electrodes in the same channel that it traversed the left-hand set. Hence, it contains the desired phase information. Ray "B" passes under an electrode and through part of an adjacent channel. Since it receives its modulation from two different channels, it contributes to crosstalk. Ray "C" does not pass through an adjacent channel, but because it passes under an electrode, it does not receive the full phase shift intended for it. This ray represents a contribution to "noise" which limits, for example, the extinction ratio that can be achieved in a holographic-subtraction processor.

A simple model for the analysis of the electrode system of Fig. VI-5 has been devised. In this model, we assume that the effect of each electrode pair on the left is simply to produce a spatial step-function change in phase on an otherwise perfect plane wave. The width of the step is taken to be equal to the electrode separation, a, and the magnitude of the phase shift is denoted by ϕ. Thus, taking the direction of propagation along the x-axis and letting the y-axis lie perpendicular to the structure, we can write for the disturbance at x = 0

$$U(0,y) = \exp[-ikx + i\phi\{H(y+a/2) - H(y-a/2\}], \tag{VI-1}$$

where H(x) is the Heaviside unit step function and k is the propagation constant of the incident plane wave. The propagation of the disturbance down the waveguide is best described in terms of its angular spectrum; i.e., by the Fourier decomposition of U(0,y) into plane waves propagating in various directions.(47) Angular spectra obey a simple propagation law given below; so the disturbance at any point x can be reconstructed by inverse Fourier transformation. The angular spectrum at x=0 is given by

$$\begin{aligned} A_o(\alpha/\lambda) &\equiv \int_{-\infty}^{\infty} dy U(0,y)\exp(i\alpha y/\lambda) \\ &= \delta(\alpha/\lambda) + a(e^{i\phi}-1)\ \mathrm{sinc}(a\,\alpha/\lambda), \end{aligned} \tag{VI-2}$$

where

$$\mathrm{sinc}(Z) \equiv \sin(\pi Z)/(\pi Z), \tag{VI-3}$$

λ is the wavelength of the light in the medium of the waveguide, and α is given by

$$\alpha = \sin \zeta \quad . \qquad \text{(VI-4)}$$

Here ζ is the angle between the direction of propagation of a component plane wave and the x-axis. Propagation of this angular spectrum to finite values of x is represented simply by appending a factor $\exp(-ikx\sqrt{1-\alpha^2})$.(47) Hence the disturbance at x is given by

$$U(x,y) = e^{-ikx} + a(e^{i\phi}-1) \int_{-\infty}^{\infty} \mathrm{sinc}(a\ \alpha/\lambda) e^{-ik(x\sqrt{1-\alpha^2} + y\alpha)} d(\alpha/\lambda) \qquad \text{(VI-5)}$$

The sinc function appearing above is a common function in optics. It has a central peak of width $2\lambda/a$, beyond which it oscillates with diminishing amplitude and period λ/a (see Fig. III-3a). When a is large, the peak becomes narrow and approaches the form of a Dirac delta function:

$$\lim_{a \to \infty} a\,\mathrm{sinc}(a\ \alpha/\lambda) = \delta(\alpha/\lambda) \qquad \text{(VI-6)}$$

Although the integral in Eq. VI-5 cannot be performed analytically, we note that kx is large when x is more than a few micrometers. Consequently, we can use the stationary-phase approximation to evaluate the integral to an accuracy sufficient for our purposes.(48) According to this method, we obtain

$$U(x,y) \sim e^{-ikx} + (a\ /\lambda)(e^{i\phi}-1)(x/r\lambda\sqrt{\lambda/r}\ \mathrm{sinc}(ay/\lambda r)e^{-ikr+i\pi/4} \quad , \qquad \text{(VI-7)}$$

where $r^2 = x^2 + y^2$. Using Eq. (7), we can calculate the intensity distribution of the light, $I(x,y) = |U(x,y)|^2$, from which we can, for a given electrode design, calculate the fraction of light corresponding to rays "A", "B" and "C" of Fig. VI-6.

There are several points about the calculations outlined above that should be brought out. First, the step-function phase shift assumed in the model is a worst-case choice from the viewpoint of deleterious effects of diffraction, because the abrupt phase change causes larger values for the Fourier components of the higher spatial harmonics (α/λ). Real electrodes will invariably produce more gentle phase variations.

Second, it should be noted that the effect of changing ϕ is to change the amplitude and phase of the diffracted terms but not their form. This will be important below in considering the influence of diffraction on the holographic-subtraction process; here it means that an electrode design which minimizes the diffraction effects for one value of ϕ will do so for all values of ϕ to good approximation. Finally, it should be noted that the first term of Eq. (7) represents an infinite plane wave, whereas in practice the beam will be finite in extent. The principal effect of a finite beam width is to replace the first term of Eq. (2) by a term W sinc$(W\alpha/\lambda)$, where W is the beam width. When $W \gg a$, we can ignore this refinement. Using Eq. (7), we find for the intensity distribution

$$I(x,y) = 1+2(ax/\lambda r)\sqrt{\lambda/r}\ \mathrm{sinc}(ay/\lambda r)\,\mathrm{Re}\{(e^{i\phi}-1)e^{i\pi/4}e^{-ik(r-x)}\} + (a/\lambda)^2|e^{i\phi}-1|^2(\lambda x^2/r^3)\ \mathrm{sinc}^2(ay/\lambda r). \qquad \text{(VI-8)}$$

The amount of light entering the channel at x=0 is the integral of Eq.(8) over the channel width, or simply a for a unit amplitude incident beam. The amount of light corresponding to rays "A" is the same integral evaluated at x=b+c, the length of the channel. For rays "C", we use the integral from $y = a/2$ to $y = (a/2)+d$ (d is the electrode width) and for rays "B", the integral from $y = (a/2)+d$ to $y=\infty$, both cases evaluated at x=b+c. The integrals cannot be evaluated exactly, but numerical evaluation will not be difficult. The integrals must be multiplied by 2 for rays "B" and "C" in order to account for rays diffracted both upward and downward.

<u>Holographic Subtraction</u>. Analysis of the operation of a holographic-subtraction processor in the presence of diffraction is a very complex task. The presence of the spherical waves in Eq. (5) due to diffraction makes the coupled-wave analysis(49) of holography intractable. Two approaches to the problem have been investigated. In the first, the integral in Eq. (5) is approximated by a finite sum, and the corresponding hologram becomes a superposition of plane gratings. During readout, each component of the signal beam is assumed to be diffracted by each grating of the composite hologram, but to be coupled only to the reference

beam. This approximation violates conservation of energy, but the violation is not severe if the hologram is not too efficient. Complete analysis of even this approximation is not possible, but the resulting set of equations can be programmed for computer solution. A simpler approach is to model the signal beam as three discrete beams consisting of an undiffracted main beam of amplitude $S(x)$ and two diffracted side beams of amplitude $S_+(x)$ and $S_-(x)$. To obtain the relative values of these amplitudes at the entrance to the hologram, $x=0$, it is appropriate to divide the sinc function of Eq. VI-2 into three sections: a central section having an area corresponding to $S(0)$ and two equal sections on either side of the central section having areas corresponding to $S_\pm(0)$.

If the three signal beams and a reference beam $R(0)$ are simultaneously incident on the hologram used for the subtraction process, the corresponding amplitudes at a depth x into the holograms are

$$R(x) = R(0)\cos(\Gamma x) - 1\, S(0)\sin(\Gamma x) \tag{VI-9}$$

$$S(x) = -iR(0)\sin(\Gamma x) + S(0)\cos(\Gamma x) \tag{VI-10}$$

$$\begin{aligned} U(x) &= S_+(x) + S_-(x) = 2\, S_+(x) \\ &= 2\rho\{S(0) - i[\varkappa R(0) + \nu S(0)]\sin(\Gamma x)/\Gamma + \\ &\qquad [\varkappa S(0) + \nu R(0)][\cos(\Gamma x) - 1]/\Gamma\}, \end{aligned} \tag{VI-11}$$

where $\rho = S_\pm(0)/S(0)$ and,

$$\Gamma = \varkappa/\sqrt{\cos(\theta_R)\cos(\theta_S)} \quad , \tag{VI-12}$$

with θ_R and θ_S equal to the incidence angles of the R and S beams, respectively. $\varkappa$ and ν are coupling constants for the various diffraction processes, according to the following scheme:

Coupled Beams	Coupling Constant
R-S	$\varkappa$
$R\text{-}S_\pm$	$\rho\varkappa$
$S\text{-}S_\pm$	$\rho\nu$
$S_\pm\text{-}S_-$	$\rho^2\nu$

The value of ρ is determined by angular integrations over portions of the central lobe of the sinc function: Define

$$\xi_0 = 2\int_0^{\lambda/3a} a \; \mathrm{sinc}(a\alpha/\lambda)d(\alpha/\lambda) \; ; \quad \xi_1 = \int_{\lambda/3a}^{\lambda/a} a \; \mathrm{sinc}(a\alpha/\lambda)d(\alpha/\lambda) \qquad \text{(VI-13)}$$

Then we write

$$S(0) = S_0[1 + (e^{i\phi}-1)\xi_0] \qquad \text{(VI-14)}$$

and

$$\rho = (e^{i\phi}-1)\xi_1/[1 + (e^{i\xi}-1)\xi_0] \quad . \qquad \text{(VI-15)}$$

Finally, we define the amplitude and phase of the reference beam by

$$R(0) = R_0 e^{i\psi} \quad . \qquad \text{(VI-16)}$$

The output signal beam in this model consists of three plane waves, propagating at a small angular separation ζ. These produce an interference pattern whose period increases with decreasing ζ. To optimize the efficiency of holographic subtraction, it is necessary to determine the value of ψ which minimizes the signal-beam output intensity I_{out} when φ has the value used to write the hologram, φ_W. Using this value of ψ one next determines the ratio S_0/R_0 which further minimizes I_{out}. Denote the doubly minimized value of I_{out} by I_{min}. Next allow ϕ to range over $[0,2\pi]$ and seek the maximum value, I_{max}, of I_{out}. The ratio I_{max}/I_{min} is the achievable extinction ratio for this model.

In order to determine I_{min}, we insert Eq. IV-10 and IV-11 into the expression for the output signal

$$A_{out} = S_+ e^{-i\underset{\sim}{\sigma}+ \cdot \underset{\sim}{r}} + S e^{-i\underset{\sim}{\sigma} \cdot \underset{\sim}{r}} + S_- e^{-i\underset{\sim}{\sigma}- \cdot \underset{\sim}{r}} \qquad \text{(VI-17)}$$

with

$$\underset{\sim}{\sigma} = k(\cos\theta_S, -\sin\theta_S) \quad , \qquad \text{(VI-18)}$$

$$\underset{\sim}{\sigma}_{\pm} = k\Big(\cos(\theta_S \pm \zeta), -\sin(\theta_S \pm \zeta)\Big)$$

$$\simeq \underset{\sim}{\sigma} \mp \underset{\sim}{\bar{\sigma}} \quad , \qquad \text{(VI-19)}$$

$$\underset{\sim}{\bar{\sigma}} = k\zeta(\sin\theta_S, \cos\theta_S); \; \underset{\sim}{\sigma} \cdot \underset{\sim}{\bar{\sigma}} = 0 \quad . \qquad \text{(VI-20)}$$

Since $S_+ = S_- = (1/2)U$ by symmetry, we have

$$A_{out} = e^{-i\underset{\sim}{\sigma} \cdot \underset{\sim}{r}}\,[S + U\cos(\bar{\underset{\sim}{\sigma}} \cdot \underset{\sim}{r})] \qquad \text{(VI-21)}$$

$\bar{\underset{\sim}{\sigma}}$ is the "grating vector" of the interference pattern produced in the output by the diffracted side beams. The period of this pattern is

$$\Lambda = \frac{2\pi}{|\bar{\sigma}|} = \frac{\lambda}{\zeta} = \frac{3}{2}\,a \qquad \text{(VI-22)}$$

Unless the detector dimensions are much smaller than *a* the interference pattern must be accounted for by some averaging process. Since the opposite case is envisioned, namely that *a* is much smaller than the detector dimensions, we must average over many periods of the $\cos(\bar{\underset{\sim}{\sigma}} \cdot \underset{\sim}{r})$ term. Thus, we will find for the intensity, I_{out}:

$$\begin{aligned} I_{out} &= \langle |S + U\cos\bar{\underset{\sim}{\sigma}} \cdot \underset{\sim}{r}|^2 \rangle \\ &\simeq |S|^2 + \tfrac{1}{2}|U|^2 \qquad \text{(VI-23)} \end{aligned}$$

If we now rewrite Eqs. VI-10 and VI-11 in the form

$$\begin{aligned} S &= S_R\,R_o e^{i\psi} + S_S S_o \quad , \\ U &= U_R\,R_o e^{i\psi} + U_S S_o \quad , \qquad \text{(VI-24)} \end{aligned}$$

we get for I_{out}, upon minimizing with respect to ψ,

$$\begin{aligned} I_{out} &= [\tfrac{1}{2}\,|U_S|^2 + |S_S|^2]\,S_o^{\,2} - R_o S_o\,D \\ &\quad + [\tfrac{1}{2}\,|U_R|^2 + |S_R|^2] R_o^{\,2} \quad . \qquad \text{(VI-25)} \end{aligned}$$

This is minimized with respect to S_o/R_o to give

$$I_{min} = \frac{1}{2}\,|U_R|^2 + |S_R|^2 - \frac{1}{2}\,\frac{D^2}{|U_S|^2 + 2|S_S|^2} \quad . \qquad \text{(VI-26)}$$

In these equations,

$$D^2 = [\mathrm{Re}(U_R U_S^*) + 2\mathrm{Re}(S_R S_S^*)]^2$$

$$+ [\mathrm{Im}(U_R U_S^*) + 2\mathrm{Im}(S_R S_S^*)] \quad . \qquad \text{(VI-27)}$$

When a is much larger than the detector, the averaging in Eq. VI-23 does not take place. In that event the factor cos $(\bar{\underset{\sim}{\sigma}} \cdot \underset{\sim}{r})$ can be taken as constant, and one finds $I_{min} = 0$.

Because of the complicated dependence of the parameters of this model on φ_W and φ, it is not practical to carry through the very tedious algebra required to evaluate I_{max}. Instead, numerical procedures will be implemented so that, once the electrode parameters are known, I_{max} and I_{max}/I_{min} can be determined.

While the model used here is simple, it points the way to a more realistic model which can utilize the full angular spectrum of the diffracted beam to determine a realistic estimate of the extinction ratio attainable. The model may also be extendable to more realistic phase-shift profiles and to more than the one-channel operation considered here.

Summary

Diffraction effects due to the electrode structure influence both the operation of the electrodes and the operation of the holographic subtraction process. The static diffraction effects of the electrode structure, as well as scattering of light by imperfections in the waveguide, are partially compensated by the hologram, while dynamic effects, arising from the application of voltages to the electrodes are not. The residual static diffraction effects and the dynamic diffraction effects limit the extinction ratio that can be obtained with the processor. Using simplified models of the phase shift induced by the electrodes and of the diffraction produced by them, formulae have been obtained to aid in the design of electrode structures that minimize diffraction and to estimate the limitations placed on the extinction ratio. Using the formulae developed, numerical evaluation of specific electrode structures will be possible.

VII. SUMMARY AND CONCLUSIONS

This program has involved three interrelated lines of investigation:

- A study of the problems involved in the fabrication of an integrated-optics Fourier-transform system.
- A consideration of the ways in which integrated optical data-processing techniques could be applied to solve specific NASA data-handling problems.
- The conception of and preliminary theoretical and experimental work on a new class of integrated optics data processors based upon holographic subtraction.

The Fourier-transform studies emphasized the design, fabrication, and characterization of geodesic waveguide lenses. Lenses were selected for attention because of their critical importance to any optical Fourier-transform system. Geodesic lenses were chosen because of their compatibility with a wide variety of integrated optical materials, and because of the possibilities this type of lens affords for correcting spherical aberrations.

Among the principal results of the lens study were the following: (1) production of geodesic lenses in Pyrex and photochromic glasses, (2) development of techniques for grinding depressions in crystalline $LiNbO_3$; (3) development of an accurate method for measurement of focal characteristics of waveguide lenses; and (4) development of computational methods for designing diffraction-limited lenses with useful apertures as large as 10 mm.

Consideration of the potential of integrated-optics techniques for alleviating NASA data-handling problems was undertaken jointly with NASA personnel. The cooperative effort led directly to the concept of the holographic-subtraction system for processing multichannel data. We believe that the ultimate capability of the system will be to compare simultaneously a set of several hundred input voltages to a reference set or a library of reference sets at nanosecond rates.

In the preliminary work done on the holographic-subtraction system in the present program, experimental and theoretical studies of waveguide hologram formation, electrode diffraction effects, and holographic subtraction were performed. The results support the conclusion that a device capable of handling the data output of the NASA Multichannel Ocean Color Sensor is clearly feasible. Moreover, they show no fundamental reasons why hundred-channel devices with nanosecond cycle times cannot be built.

REFERENCES

1. P. G. White, K. R. Jenkin, R. C. Ramsey, and M. Sorkin, "Development and Flight Test of the Multichannel Ocean Color Sensor (MOCS)", Final Contractor Report NASA-CR-2311, Prepared by TRW Systems Group, TRW, Inc., Oct. 1973.

2. M. H. Bortner, R. Dick, H. W. Goldstein, and R. N. Grenda, "Carbon Monoxide Pollution Experiment", Final Contractor Report NASA-CR-132717, Prepared by General Electric Co., Jan. 1975.

3. B. J. Thompson, "Coherent Optical Processing—A Tutorial Review", in Coherent Optical Processing, Proceedings of the Society of Photo-Optical Instrumentation Engineers, 52, San Diego, California, Aug. 21-22, 1974, pp 1-22.

4. H. Kogelnik, "Theory of Dielectric Waveguides", in Integrated Optics, Topics in Applied Physics, 7, T. Tamir, ed., pp 13-81 (Springer-Verlag, New York, 1975).

5. A. VanderLugt, "Coherent Optical Processing", Proc. IEEE, 62 (10), 1300-1319 (1974).

6. K. Bromley, M. A. Monahan, J. F. Bryant, and B. J. Thompson, "Holographic Subtraction", Appl. Opt., 10 (1), 174-181 (1971).

7. J. E. Goell, "Barium Silicate Films for Integrated Optical Circuits", Appl. Opt., 12 (4), 737-742 (1973).

8. D. Hall, A. Yariv, and E. Garmire, "Optical Guiding and Electrooptic Modulation in GaAs Epitaxial Layers", Opt. Commun., 1 (9), 403-405 (1970).

9. R. Ulrich and H. P. Weber, "Solution-Deposited Thin Films as Passive and Active Light Guides", Appl. Opt., 11 (2), 428-434 (1972).

10. I. P. Kaminow, "Optical Waveguide Modulators", IEEE Trans. Microwave Theory Tech., MTT-23 (1), 57-70 (1975).

11. T. G. Giallorenzi, E. J. West, R. Kirk, R. Ginther, and R. A. Andrews, "Optical Waveguides Formed by Thermal Migration of Ions in Glass", Appl. Opt., 12 (6), 1240-1245 (1973).

12. V. E. Wood, N. F. Hartman, and C. M Verber, "Characteristics of Effused Slab Waveguides in $LiNbO_3$", J. Appl. Phys., 45 (3), 1449-1451 (1974).

13. P. K. Tien, G. Smolinsky, and R. J. Martin, "Thin Organosilicon Films for Integrated Optics", Appl. Opt., 11 (3), 637-642 (1972).

14. J. M. Hammer, D. J. Channin, M. T. Duffy, and J. P. Wittke, "Low-Loss Epitaxial ZnO Optical Waveguides", Appl. Phys. Lett., 21 (8), 358-360 (1972).

15. E. Garmire, "Semiconductor Components for Monolithic Applications", in Integrated Optics, Topics in Applied Physics, 7, T. Tamir, ed., p 246 (Springer-Verlag, New York, 1975).

16. M. B. Panish, "Heterostructure Injection Lasers", IEEE Trans. Microwave Theory Tech., MTT-23 (1), 20-30 (1975).

17. B. Kim and C. S. Tsai, "High-Performance Guided-Wave Acoustooptic Scanning Device Using Multiple Surface Acoustic Waves", Proc. IEEE, 64 (5), 788-793 (1976).

18. J. Kushibiki, H Sasaki, N. Chubachi, N. Mikoshiba, and K. Shihayama, "Thickness Dependence of Acousto-Optic Diffraction Efficiency in ZnO Optical Waveguides", Appl. Phys. Lett., 26 (7), 362-364 (1975).

19. K. W. Loh, W.S.C. Chang, and R. A. Becker, "Convolution Using Guided Acousto-Optical Interaction in As_2S_3 Waveguides", Appl. Phys. Lett., 28 (3), 109-111 (1976).

20. G. B. Brandt, M. Gottlieb, and G. E. Marx, "Integration of Deflection and Detection of Guided Light on Silicon Substrates", Paper TuA6, Topical Meeting on Integrated Optics, Salt Lake City, Utah, Jan. 1976.

21. D. von der Linde and A. M. Glass, "Photorefractive Effects for Reversible Holographic Storage of Information", Appl. Phys., 8 (2), 85-100 (1975).

22. V. E. Wood, N. F. Hartman, C. M Verber, and R. P. Kenan, "Holographic Formation of Gratings in Optical Waveguiding Layers", J. Appl. Phys., 46 (3), 1214-1215 (1975).

23. D. L. Staebler, W. J. Burke, W. Phillips, and J. J. Amodei, "Multiple Storage and Erasure of Fixed Holograms in $LiNbO_3$", Appl. Phys. Lett., 26 (4), 182-184 (1975).

24. J. D. Crow, N. F. Borelli, T. P. Seward III, and J. Chudak, "Light-guiding in Photochromic Glasses", Appl. Opt., 14 (3), 580-584 (1975).

25. R. Ulrich and R. J. Martin, "Geometrical Optics in Thin-Film Light Guides", Appl. Opt., 10 (9), 2077-2085 (1971).

26. P. K. Tien, S. Riva-Sanseverino, R. J. Martin, and G. Smolinsky, "Two-Layered Construction of Integrated Optical Circuits and Formation of Thin-Film Prisms, Lenses, and Reflectors", Appl. Phys. Lett., 24 (11), 547-549 (1974).

27. F. Zernike, "Luneburg Lens for Optical Waveguide Use", Opt. Commun., 12 (4), 379-381 (1974).

28. D. B. Anderson, R. L. Davis, J. T. Boyd, R. R. August, and R. E. Eisele, "Optical Waveguide Lenses. I", Technical Report AFAL-TR-76-54, Rockwell International Report (74-1187.13/501), Nov. 1975.

29. G. C. Righini, V. Russo, S. Sottini, and G. Toraldo di Francia, "Thin-Film Geodesic Lenses", in Space Optics, Proceedings of the Ninth International Congress of the International Commission for Optics, B. J. Thompson and R. R. Shannon, eds. (National Academy of Science, Washington, 1974), pp 682-692.

30. E. Spiller and J. S. Harper, "High Resolution Lenses for Optical Waveguides", Appl. Opt., 13 (9), 2105-2108 (1974).

31. C. M. Verber, D. W. Vahey, and V. E. Wood, "Focal Properties of Geodesic Waveguide Lenses", Appl. Phys. Lett., 28 (9), 514-516 (1976).

32. P. K. Tien, R. J. Martin, and S. Riva-Sanseverino, "Novel Metal-Clad Optical Components and Method of Isolating High-Index Substrates for Forming Integrated-Optical Circuits", Appl. Phys. Lett., 27 (4), 251-253 (1975).

33. D. W. Vahey and V. E. Wood, "Focal Characteristics of Spheroidal Geodesic Lenses for Integrated Optical Processing", IEEE J. Quantum Electron. QE-13 (4), 129-134 (1977).

34. W.-T. Tsang and S. Wang, "Thin-Film Beam Splitter and Reflector for Optical Guided Waves", Appl. Phys. Lett., 27 (11), 588-560 (1975).

35. C. V. Shank and R. V. Schmidt, "Optical Technique for Producing 0.1 μ Periodic Surface Structures", Appl. Phys. Lett., 23 (3), 154-155 (1973).

36. T. Tamir, "Beam and Waveguide Couplers", in Integrated Optics, Topics in Applied Physics, 7 T. Tamir, ed., pp 83-137 (Springer-Verlag, New York, 1975).

37. J. W. Goodman, Introduction to Fourier Optics, Chapter 5, pp 77-100 (McGraw-Hill, San Francisco, 1968).

38. D. C. Champeney, Fourier Transforms and Their Physical Applications, Chapter 11, pp 138-162 (Academic Press, London, 1973).

39. F. A. Jenkins and H. E. White, Fundamentals of Optics, Third Edition, Chapter 9, pp 140-142 (McGraw-Hill, New York, 1957).

40. V. E. Wood, "Effects of Edge-Rounding on Geodesic Lenses", Appl. Opt. 15 (11), 2817-2820 (1977).

41. R. P. Kenan, "Large-Angle Switching in Planar Optical Waveguides" Final Technical Report on ONR Contract N00014-75-C-0591, Reqn. No. NR 215-236/11-29/74, Battelle Columbus Laboratories, Dec. 1975.

42. C. M. Verber, "Integrated Optics Program", Final Report to Battelle Memorial Institute on Contract B-1333-1150, Battelle Columbus Laboratories, June, 1976.

43. T. P. Sosnowski and H. P. Weber, "Thin Birefringent Polymer Films for Integrated Optics", Appl. Phys. Lett., 21 (7), 310-311 (1972).

44. J. E. Goell and R. D. Standley, "Sputtered Glass Waveguides for Integrated Optical Circuits", Bell Syst. Tech. J., 48 (10), 3445-3448 (1969).

45. L. O. Svaasand, M. Eriksrud, G. Nakken, and A. P. Grande, "Solid-Solution Range of $LiNbO_3$", J. Cryst. Growth, 22 (3), 230-232 (1974).

46. D. von der Linde, A. M. Glass, and K. F. Rodgers, "Multiphoton Photorefractive Processes for Optical Storage in $LiNbO_3$", Appl. Phys. Lett., 25 (3), 155-157 (1974).

47. J. W. Goodman, op.cit., pp 48-51.

48. A. Erdelyi, Asymptotic Expansions, Chapter 2, pp 51-56 (Dover Publications, 1956).

49. H. Kogelnik, "Coupled Wave Theory for Thick Hologram Gratings", Bell Syst. Tech. J., 48 (9), 2909-2947 (1969).

APPENDIX

FORMATION OF METAL PATTERNS ON $LiNbO_3$ BY PHOTOLITHOGRAPHIC TECHNIQUES

by

C. M. Chapman

The successful operation of the integrated optics devices described in this report requires the deposition of metal electrodes on the surface of the $LiNbO_3$ waveguides. The photolithographic techniques found to be suitable for this operation are described in this Appendix.

In those cases where a commercially made mask was not at hand, a photographic film mask was prepared at Battelle. Both positive and negative photoresists were employed. Electrical contact was made with air-dry conducting silver paint.

Mask Fabrication

The master pattern was prepared on a transparent acrylic panel (Plexiglas, Perspex) 3.2 mm thick, using 1.6 mm-wide self-sticking opaque tape for narrow lines and for outlining large areas, such as contact pads, to be covered by black craft paper. The clear panel allowed backlighting for high contrast, sharp edge definition, and uniform, high intensity illumination by a simple array of floodlamps. A one-step photoreduction of the mask onto 35-mm very-high-resolution Kodak 649GH film was made using a Konica T-2 camera with f/1.8 lens. This procedure has proven satisfactory for line and space widths at least as small as 12 μm.

In some instances it has been necessary to transfer to film a commercially made metal-on-glass pattern in order to off-center the pattern beyond the capability of the photolithographic exposure apparatus. A conventional photo-enlarger equipped with electronic flash has produced an acceptable pattern on Kodak 649GH film in which line widths and spacing were as small as 3.4 μm.

Substrate Preparation

$LiNbO_3$ substrates, nominally 3.2 mm thick, were metallized by hot-boat evaporation of aluminum in vacuum using a tungsten boat. Approximate metal thickness was 0.1 μm.

Prior to metallization, substrates were cleaned by rinsing in a mixture of equal parts of acetone, isopropanol, and trichlorethylene, followed by soaking and gentle swabbing in warm (60°C) MICRO Laboratory Cleaning Solution (basically a liquid detergent). Warm tap water was used for the first rinse; the final rinse was demineralized water at room temperature. The substrates then were baked for about 2 hours at 210°C in circulating air and transferred to the vacuum chanber as soon as they were cool enough to handle. Care was taken to minimize the possibility of damage by thermal shock by temperature cycling the oven, thus permitting the samples to be inserted and removed at near room temperature.

After metallization, samples were stored in a desiccator jar until application of photoresist.

Photolithographic Procedure

The photolithographic procedure comprised 1) spin-application of photoresist onto the metallized substrate, 2) baking the photoresist, 3) UV exposure to the pattern, 4) developing the pattern in the resist, 5) baking the remaining resist, 6) etching the pattern in the aluminum layer, and 7) removing the remaining resist. This general procedure was the same for both the positive and negative resists employed; however, the etchants were different. An alkaline etchant was used with the KTFR (Kodak Thin-Film Resist) negative resist and acidic etchant with the Shipley AZ 1350 resist. The etchant formulations for aluminum were:

Alkaline Etchant

Solution A -	deionized water	1000 μm^3 (ml)
	sodium hydroxide	500 gm
Solution B -	deionized water	3000 μm^3 (ml)
	potassium ferricyanide	1000 μm^3 (ml)

When needed, 1 part Solution A was mixed with 3 parts Solution B (by volume) and the mixture used at room temperature.

Acidic Etchant

deionized water	100 μm^3 (ml)
phosphoric acid (conc.)	800 μm^3 (ml)
acetic acid (conc.)	50 μm^3 (ml)
nitric acid (conc.)	10 μm^3 (ml)

This mixture was used at room temperature.

The KTFR negative resist was used with the BCL-made film masks and metal-on-glass masks in which the transparent regions correspond to the desired pattern. The parameters associated with the 7 procedural steps stated above were:

1) Spin-coating of resist: 5000 rpm for 30 seconds for the resist with a nominal viscosity of 100 mN s/m^2 (centipoises) as measured on a Brookfield viscometer; less viscous resists also were employed. Resist filtering was not necessary for the coarser patterns.
2) Pre-bake: 80°C in a nitrogen atmosphere for 20 minutes.
3) UV exposure: 30 to 45 seconds to a 100 W mercury arc lamp with no filter. The exposure station is a Kulicke and Soffa Model 675 with vacuum hold-down for sample and mask to effect pressure contact between mask and resist.
4) Develop: 45- to 60-second fine-spray application of KTFR rinse for 30 to 60 seconds.
5) Post-bake: 80°C in a nitrogen atmosphere for 30 minutes.
6) Etch: fine-spray application of etchant until visually complete removal of aluminum, usually 10 to 15 seconds.
7) Resist removal: substrate immersed in developer for 20 to 30 minutes, then in an equal parts mixture of acetone, isopropanol, and trichlorethylene; softened resist then peeled in sheet segments by use of a pointed wooden probe.

These procedures were employed in preparing the pattern of Fig. VI-4 on $LiNbO_3$. The resist removal by peeling was satisfactory and precluded the use of hot liquid stripping agents customarily employed for removal of exposed KTFR resist. In fabricating patterns finer than that of Fig. VI-4 sample immersion rather than spray applications of the various processing solutions was used to minimize mechanical damage to the developed protective resist.

The Shipley AZ 1350 positive resist was used with metal-on-glass masks in which the opaque regions corresponded to the desired pattern. Steps 1 through 6 were the same as described above for KTFR, except that Shipley developer was used, followed by a 20:1 dilution of developer with demineralized water for 20 seconds as a first rinse and demineralized water alone as a final rinse. Etching usually took about 60 seconds. Step 7, resist removal, was carried out simply by immersion of the sample in acetone for several seconds. Again spray droplets instead of immersion destroyed the pattern if it contained sufficiently fine detail.

In general, given the choice of the appropriate mask, the AZ 1350 positive resist is preferred to the KTFR negative resist primarily because of ease of removing the unexposed resist in Step 7. Also, the positive resist is more hydrophobic than the negative and therefore is much less subject to swelling when subjected to the various processing liquids. Since the unexposed areas of the positive resist continue to be light-sensitive after sample removal from the UV exposure equipment, the sample must be protected in nonfiltered room-light environments; this is an inconvenience rather than major deficiency for those fabrications where a second exposure is not required. Neither type of resist has been tested to the limits of its resolution capability and processing durability with the equipment and techniques at hand. Resist viscosity in the ranges employed, 40 to 100 mN s/m^2 (centipoises), has not proven to be a critical processing parameter. Some problems have been experienced with the appearance of what seems to be etching and resist dissolution products on the $LiNbO_3$ surface, especially when immersion rather than spray techniques are employed. This contamination appears to be peculiar to $LiNbO_3$ since it does not appear on glass or aluminized surfaces. It has not interfered with device performance. The problem has been encountered by others and should be solvable with further experimentation.

NASA-Langley, 1977 CR-2869